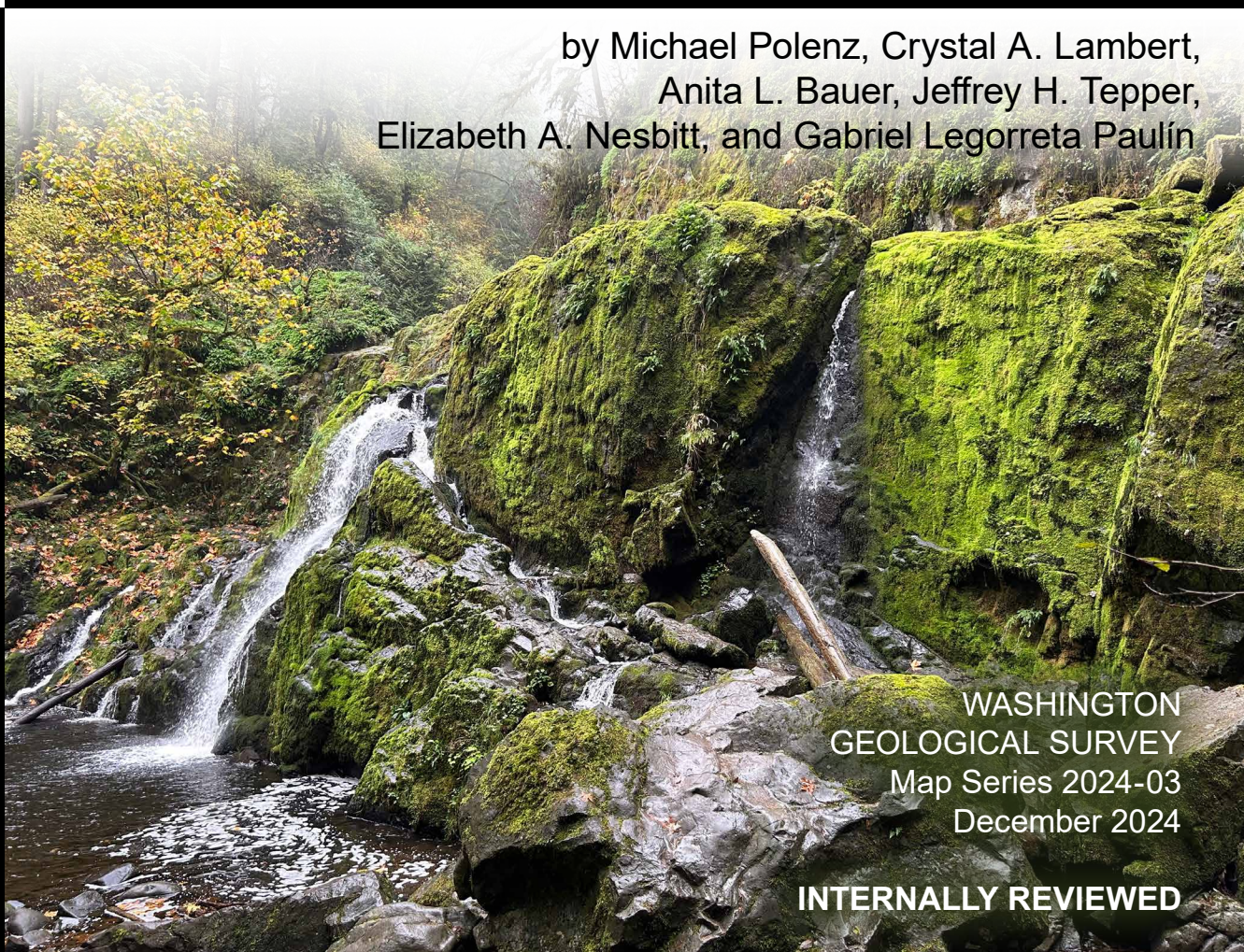


GEOLOGIC MAP OF THE EATONVILLE 7.5-MINUTE QUADRANGLE, THURSTON, PIERCE, AND LEWIS COUNTIES, WASHINGTON

by Michael Polenz, Crystal A. Lambert,
Anita L. Bauer, Jeffrey H. Tepper,
Elizabeth A. Nesbitt, and Gabriel Legorreta Paulín



WASHINGTON
GEOLOGICAL SURVEY
Map Series 2024-03
December 2024

INTERNALLY REVIEWED



WASHINGTON STATE DEPARTMENT OF
NATURAL RESOURCES
WASHINGTON GEOLOGICAL SURVEY

GEOLOGIC MAP OF THE EATONVILLE 7.5-MINUTE QUADRANGLE, THURSTON, PIERCE, AND LEWIS COUNTIES, WASHINGTON

by Michael Polenz, Crystal A. Lambert, Anita L. Bauer, Jeffrey H. Tepper,
Elizabeth A. Nesbitt, and Gabriel Legorreta Paulín

WASHINGTON
GEOLOGICAL SURVEY
Map Series 2024-03
December 2024

*This geologic map was funded in part by
the USGS National Cooperative Geologic
Mapping Program, award no. G23AC00468*

*This publication has been subject to an iterative technical review
process by at least one Survey geologist who is not an author.*

*This publication has also been subject to an iterative
review process with Survey editors and cartographers.*



WASHINGTON STATE DEPARTMENT OF
NATURAL RESOURCES
WASHINGTON GEOLOGICAL SURVEY

DISCLAIMER

Disclaimer of Warranties. No express or implied warranty of any kind is made regarding the information contained herein, including, but not limited to, the warranty of merchantability, warranty of fitness for a particular purpose, or warranties of content, completeness, accuracy, reliability, usefulness, or that use would not infringe on privately-owned rights.

Use at Your Own Risk. The information presented here is intended for use as a general screening tool in community planning or for creating awareness and understanding of geologic information and is neither intended to constitute advice nor is it to be used as a substitute for site-specific advice from a licensed professional. You use this information at your own risk and should not act (or refrain from acting) based upon the information without independently verifying the information and, as appropriate, obtaining professional advice regarding your particular facts and circumstances.

Limitation on Liability. User agrees there shall not be liability on the State of Washington, Washington Department of Natural Resources, or their officers, agents, representatives, or employees for any damages allegedly resulting from any use of or reliance on this information. Under this limitation, there shall be no liability for any damages whatsoever, including but not limited to any damages in contract or tort for compensatory, consequential, punitive, direct, indirect, or special damages such as personal injuries, property damage, loss of profits, or any other losses or expenses.

No Endorsement. Reference herein to any specific commercial product, process, or service by trade name, trademark, manufacturer, or otherwise, does not constitute or imply its endorsement, recommendation, or favoring. Further, the views and opinions of authors expressed herein do not necessarily state or reflect those of the State of Washington or any agency thereof.

INDEMNIFICATION

Research supported by the U.S. Geological Survey, National Cooperative Geologic Mapping Program, under USGS award number G23AC00468. The views and conclusions contained in this document are those of the authors and should not be interpreted as necessarily representing the official policies, either expressed or implied, of the U.S. Government.

WASHINGTON STATE DEPARTMENT OF NATURAL RESOURCES

Hilary S. Franz—*Commissioner of Public Lands*

WASHINGTON GEOLOGICAL SURVEY

Casey R. Hanell—*State Geologist*

Jessica L. Czajkowski—*Assistant State Geologist*

Ana Shafer—*Assistant State Geologist*

Alexander N. Steely—*Assistant State Geologist*

Washington State Department of Natural Resources Washington Geological Survey

Mailing Address:

1111 Washington St. SE
MS 47007

Olympia, WA 98504-7007

Street Address:

Natural Resources Bldg, Rm 148
1111 Washington St SE

Olympia, WA 98504

Phone: 360-902-1450

Fax: 360-902-1785

Email: geology@dnr.wa.gov

Website: <http://www.dnr.wa.gov/geology>



WGS Website

Publications and Maps:

[www.dnr.wa.gov/programs-and-services/geology/
publications-and-data/publications-and-maps](http://www.dnr.wa.gov/programs-and-services/geology/publications-and-data/publications-and-maps)

Washington Geology Library Searchable Catalog:

[www.dnr.wa.gov/programs-and-services/geology/
washington-geology-library](http://www.dnr.wa.gov/programs-and-services/geology/washington-geology-library)

Suggested Citation: Polenz, Michael; Lambert, C. A.; Bauer, A. L.; Tepper, J. H.; Nesbitt, E. A.; Legorreta Paulin, Gabriel, 2024, Geologic Map of the Eatonville 7.5-minute Quadrangle, Thurston, Pierce, and Lewis Counties, Washington: Washington Geological Survey Map Series 2024-03, 1 sheet, scale 1:24,000, 39 p. text. [https://www.dnr.wa.gov/publications/ger_ms2024-03_geol_map_eatonville_24k.zip]

Cover Photo: Little Mashel River Waterfalls. Photo by M. Polenz.



POLENZ, MICHAEL

Michael Polenz
December 2024

Contents

Introduction	1
Geologic Overview	2
Bedrock	2
Unlithified Deposits	3
Regional Structure	3
Methods	4
Geologic Mapping	4
Potential-Fields Geophysical Methods	4
Description of Map Units	6
Holocene to Pleistocene Postglacial Deposits	6
Late Pleistocene Glacial Deposits	7
Pliocene to Miocene Sediment of the Mashel Formation	11
Miocene to Eocene Sedimentary and Volcanic Rocks	12
Discussion	15
Reassessing the Mashel Formation	15
Summarizing the Northcraft Formation	16
Structural, Subsurface, and Geophysical Attributes of the Map Area	19
Suggestions for Further Study	21
Acknowledgments	22
Author Contributions	22
References	22
Appendix A. Geochronology	28
Appendix B. Geochemistry	34
Appendix C. Geophysics	35
Appendix D. Landsat Spectral Image Analysis	39

FIGURES

Figure 1. Regional map of the southern Puget Lowland	2
Figure 2. Radiometric ages of Northcraft Formation samples versus longitude	16
Figure 3. Total alkalis versus silica plot of Northcraft Formation samples	16
Figure 4. AFM diagram and FeOt/MgO-SiO ₂ plot of Northcraft Formation samples	17
Figure 5. Major and trace element Harker diagrams of Northcraft Formation samples	17
Figure 6. Spider diagram of Northcraft Formation samples	18
Figure 7. Spatial geochemical trends among Northcraft Formation samples	18
Figure 7. Bedrock box canyon along the Little Mashel River	19
Figure 8. Densely jointed zone along the Mashel River	19
Figure 10. Brecciated andesitic-basalt	19

TABLES

Table 1. Summary of age analyses.	5
Table 2. Lithologic assemblages that distinguish northern-sourced drift, Cascade Range-sourced sediment, and Mashel Formation	10
Table A1. Infrared-stimulated luminescence (IRSL) ages	28
Table A2. ²³⁸ U/ ²⁰⁶ Pb ages of zircons	30
Table A3. ⁴⁰ Ar/ ³⁹ Ar ages	32
Table C1. Combined averages of geophysical properties	36

MAP SHEET

Geologic Map of the Eatonville 7.5-minute Quadrangle,
Thurston, Pierce, and Lewis Counties, Washington

Figure M1. Geophysical interpretation for the map area

Geologic Map of the Eatonville 7.5-minute Quadrangle, Thurston, Pierce, and Lewis Counties, Washington

by Michael Polenz¹, Crystal A. Lambert¹, Anita L. Bauer¹, Jeffrey H. Tepper², Elizabeth A. Nesbitt³, and Gabriel Legorreta Paulín⁴

¹ Washington Geological Survey
1111 Washington St SE
MS 47007
Olympia, WA 98504-7007

² Department of Geology
University of Puget Sound
1500 N Warner St. #1048
Tacoma, WA 98416-1048

³ The Burke Museum
of Natural History
and Culture
University of Washington
4300 15th Ave NE
Seattle, WA 98108-1446

⁴ Instituto de Geografía
Universidad Nacional
Autónoma de México
Ciudad Universitaria
del Coyoacán
cp 04510, México, D.F.

ABSTRACT

We present a geologic map of the Eatonville quadrangle along the Nisqually River in Washington's southeastern Puget Lowland. The map documents ages, stratigraphy, and distribution of glacial, fluvial, and volcanic deposits.

We use geochemistry and geochronology to characterize the Eocene Northcraft Formation, which includes volcanic, volcanoclastic, and intermediate intrusive rocks that represent early Cascade arc volcanism. Analyses of 43 intrusive and extrusive Northcraft samples range from basalt to rhyolite, but andesite is predominant and ~70 percent of samples have adakite traits that point to derivation from an eclogitic source within the subducting slab or deep crust. Eight new ages range from ~38–34.5 Ma and confirm that the Northcraft Formation youngs eastward, beginning at ~46 Ma in quadrangles to the west and continuing that trend across this map area.

We found no evidence that deformation at the southern margin of the Tacoma basin occurred post-Eocene in this map area. The Tacoma basin's southeast margin is characterized by gradual gravity and aeromagnetic gradients, in contrast to sharper and higher-amplitude gradients across the southwest margin of the Tacoma basin. Analysis of existing aeromagnetic and new gravity data suggests that most aeromagnetic highs in the area are from volcanic rocks and intrusive bodies, which are Eocene where exposed and likely of similar age in the basin.

We revise the age of the Mashel Formation to Pliocene to late Miocene. New detrital zircon ages suggest that sediment near the base and near the top of the Mashel Formation type section in the Eatonville quadrangle is late Miocene, at most ~6 Ma. Outside the type section, the formation yielded a <4.1 Ma age west of the Eatonville quadrangle.

Our mapping locally refines the maximum extents of the Hayden Creek and Wingate Hill alpine glaciations and the Vashon continental glaciation. Vashon Drift includes deposits and landforms from the Tanwax flood, and possibly from other periglacial outburst floods. A new luminescence age constrains the age of the Hayden Creek ice advance to <105 ±24 ka.

INTRODUCTION

The map area is located 43 km southeast of Olympia, at the transition between the Puget Lowland and the western Cascade Range (Fig. 1). The area is used for forestry, urban and rural residences, agriculture, recreation, conservation, aggregate mining from glacial outwash and volcanic bedrock, and hydroelectric generation via two dams on the Nisqually River.

This map continues a campaign of 1:24,000-scale mapping that started west of the current quadrangle (Polenz and others, 2021, 2022, 2023), providing geologic context for private and public land-use decisions, and improved understanding of geologic hazards (earthquakes, landslides, lahars, and floods) and resources (water and quarry rock). Prior mapping in the area began in

the 20th century (Bretz, 1911, 1913; Walters, 1965; Noble and Wallace, 1966; Walters and Kimmel, 1968; Crandell and Miller, 1974; Schasse, 1987a; Walsh and others, 1987; Drost and others, 1999). This map and report provide insight into rock types, properties, ages, and the processes that formed the landscape, including: Eocene volcanism, Pleistocene glaciation and lahar deposition, and postglacial alluviation. This publication also offers new geophysical data and an updated analysis of gravity and magnetic anomalies where the Puget Lowland meets the Cascade Range.

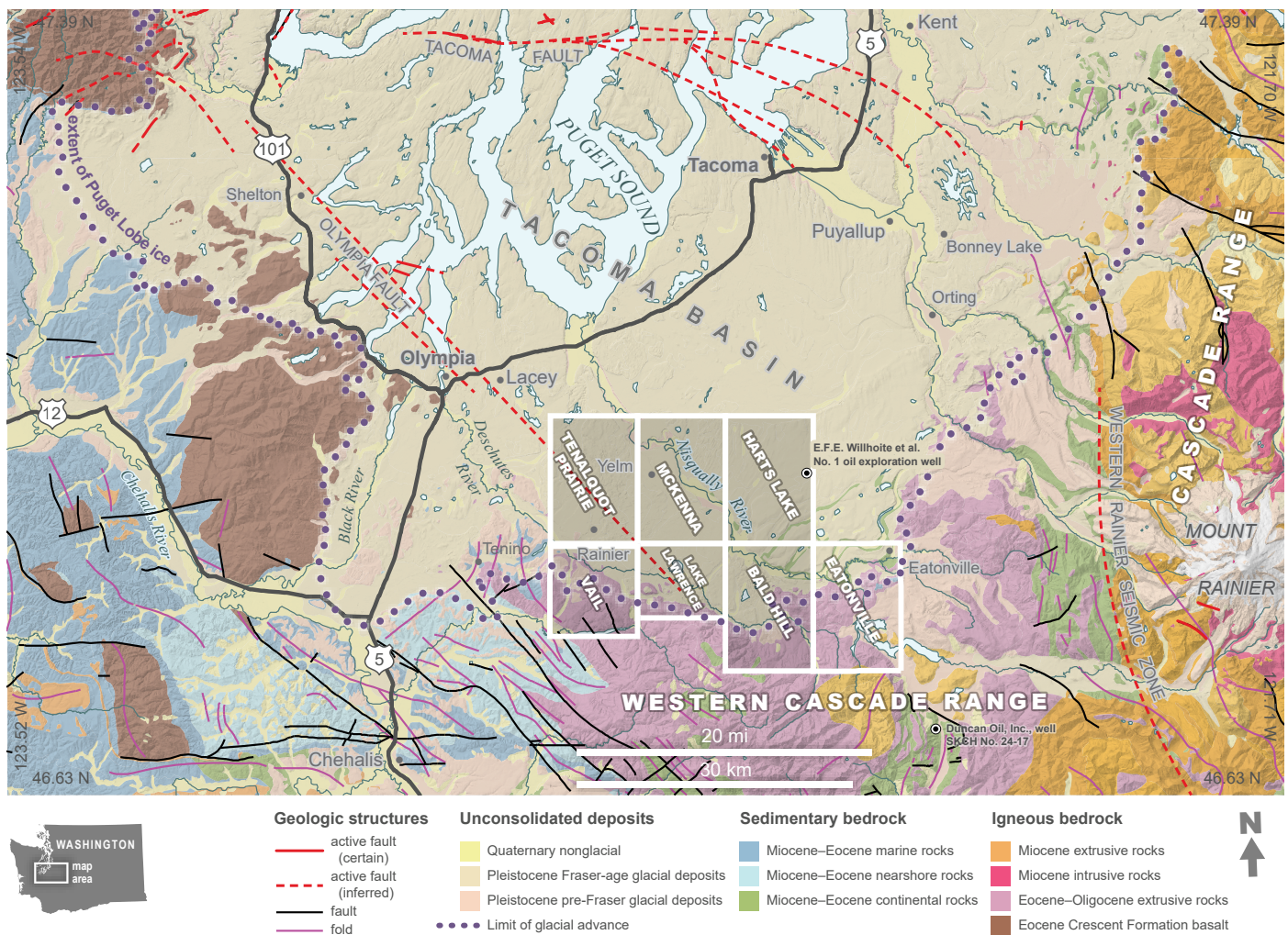


Figure 1. Regional map of the southern Puget Lowland showing simplified surface geology, tectonic structures, and place names in the vicinity of the Eatonville quadrangle. White outlines show areas mapped from 2020 to 2024; 7.5-minute quadrangle names added for geographic context.

GEOLOGIC OVERVIEW

Bedrock

The map area exposes rocks of the ancestral western Cascade Range (Fig. 1)—late to middle Eocene Northcraft Formation lava flows, pyroclastic and volcanoclastic rocks, dikes, and small intrusive bodies (Schasse, 1987a). These rocks are mostly andesite and basaltic andesite, but range from basalt (Snively and others, 1951, 1958; Hagen, 1987; Schasse, 1987a; Phillips and others, 1989) to rhyolite (Phillips and others, 1989; Polenz and others, 2021, 2022, 2023; see *Discussion*). Our previous mapping (Polenz and others, 2021, 2022, 2023) suggested that geophysically similar rocks in the Tacoma basin (Fig. 1) are also igneous and of similar age.

Gard (1968) included the Northcraft Formation in the sedimentary Puget Group based on breccia, tuff, and conglomerate 14–25 km north-northeast of the Eatonville quadrangle. That approach honors the Northcraft Formation’s stratigraphic association with upper- to middle-Eocene, terrestrial to marine sedimentary rock assemblages that represent a broad, long-lived marine delta system (Buckovic, 1979; Flores and Johnson, 1995; Sadowski and others, 2018). These sedimentary rocks

include the Carbonado and Spiketon Formations of the Puget Group north of the map area (Willis, 1898; Gard, 1968), the Puget Group to the east and south (Schasse, 1987a,b), and the McIntosh, Skookumchuck, and Cowlitz Formations to the south and west (Weaver, 1912, 1937; Snively and others, 1951, 1958, 1959; Henriksen, 1956; Pease and Hoover, 1957; Buckovic, 1979; Schasse, 1987a; Walsh and others, 1987; Flores and Johnson, 1995; Polenz and others, 2018, 2019, 2020, 2022, 2023; Sadowski and others, 2018, 2019). Geophysical data and two oil wells near the map area (Fig. 1) suggest that the Northcraft Formation is interbedded with sedimentary rocks of Puget Group age and paleoenvironmental association. However, the Northcraft Formation is primarily igneous in the map area, unlike the primarily sedimentary Puget Group. Thus, Gard’s (1968) inclusion of the Northcraft Formation in the Puget Group seems ill suited for the primarily igneous rocks in the Eatonville quadrangle.

Geophysical models (Finn, 1990; Polenz and others, 2021, 2022, 2023; Contreras and others, 2023; Anderson and others, 2024; Alex Steely, WGS, written commun. 2021) indicate that basement rocks beneath the map area include early Eocene Crescent Formation basalt of the Siletzia terrane and ultramafic

mantle rocks (dense and strongly magnetic) deeper in the subsurface (Finn, 1990).

Unlithified Deposits

Unlithified deposits in the map area include Miocene to Pleistocene volcanoclastic sediment, Pleistocene glacial sediment, and Pleistocene to Holocene alluvium. The oldest unlithified deposits in the map area are Mashel Formation—compact, pumice-rich fluvial and lacustrine sediment at its type section (Walters, 1965) and along the nearby valley walls of the Nisqually, Mashel, and Ohop rivers (Walters, 1965; Noble and Wallace, 1966; Walters and Kimmel, 1968; Schasse, 1987a). Plant fossils in the Mashel Formation were interpreted as late middle Miocene (Walters, 1965, p. A58–59). Similarity and proximity suggest that Pliocene sediment 950 m west of the Eatonville quadrangle is also Mashel Formation (see *Discussion*; Polenz and others, 2023).

Glacial sediment in the map area includes older, strongly weathered, alpine Wingate Hill Drift northeast, north, and west of Alder Lake (Crandell and Miller, 1974; Schasse, 1987a); and younger, distinctly less weathered, but otherwise similar, alpine Hayden Creek Drift farther south within the map area, both east and west of Alder Lake (Crandell and Miller, 1974; Schasse, 1987a).

Minimally weathered Vashon Drift covers the northern third of the map area with sediment derived from the Cascade Range and the Coast Mountains of British Columbia. Most of this drift was moved into the map area by Cordilleran glacial ice and meltwater during the late Wisconsinan Vashon stage of the Fraser Glaciation (marine oxygen isotope stage 2, (MIS 2))¹, the most recent of several continental ice sheet advances into the Puget Lowland (Booth and others, 2004; Troost and Booth, 2008; Polenz and others, 2013, 2015; Troost, 2016). Vashon ice reached its southern terminus in the map area (Bretz, 1911, 1913; Noble and Wallace, 1966; Walters and Kimmel, 1968; Crandell and Miller, 1974; Schasse, 1987a). Radiocarbon dates suggest a gradual Vashon ice advance followed by rapid ice collapse; the Vashon ice advance and recession in the map area both occurred between about 16 and 15.3 ka (Polenz and others, 2015, fig. 3 and discussion; Haugerud, 2021).

Landforms document glacial scour and deposition from ice and meltwater: drumlins and flutes record southwestward ice movement (Iverson and others, 2017); kettles and eskers mark where stagnant ice wasted away (Haugerud, 2009; Polenz and others, 2009); and channels and terraces document meltwater pathways (Bretz, 1913; Logan and others, 2009; Pringle and Goldstein, 2002; Futornick and others, 2008) and postglacial incision. All these landforms are readily apparent on lidar-based images.

Undivided glacial and nonglacial alluvium and lahars (units Qpc and Qpvl) locally overlie Mashel Formation north of the Vashon ice limit, and bedrock and alpine drift south of the Vashon ice limit. This undivided sediment likely includes sedimentation pulses from volcanism and Pleistocene glaciations of Mount Rainier and surrounding areas. Units Qpv and Qpvl are

sparsely exposed in the map area but are better exposed west and northwest of the map area, where samples have yielded varied late Pleistocene ages (Polenz and others, 2021, 2022; Contreras and others, 2023).

Regional Structure

The Eatonville quadrangle is situated at the southern edge of the Tacoma basin (Fig. 1) in the forearc of the active Cascadia subduction zone, between the arc-volcanic Cascade Range to the east and the Eocene accreted Black Hills, Willapa Hills, and Olympic Mountains to the west. About 23 km east of the map area, clusters of recorded seismicity (Brocher and others, 2017) indicate that the north-northwest-striking western Rainier seismic zone (Stanley and others, 1996) is active. West of the Eatonville quadrangle, the northwest-striking, northeast-down Olympia fault bounds the Tacoma basin (Fig. 1; Polenz and others, 2021, 2022) and may fit a regional framework in the Puget Lowland of basin-bounding, north-northwest-striking, dextral oblique faults such as the Rattlesnake Mountain fault zone (Dragovich and others, 2010) and east-west-striking reverse faults such as the Tacoma fault (Gower and others, 1985; Brocher and others, 2001). These faults collectively accommodate ongoing crustal shortening and plate rotation in the Cascadia forearc (Wells and McCaffrey, 2013; McCaffrey and others, 2013; Wells and others, 2014). Yet in the Eatonville quadrangle, no fault or fold has been identified (Fig. 1). Although the depth to basement (Crescent Formation) in the map area is not well-constrained, aeromagnetic and gravity anomalies suggest that depth to basement gradually but unevenly increases northwest from the map area into the Tacoma basin (Fig. M1A; Contreras and others, 2023; Polenz and others, 2023), where models estimate that the depth to basement rocks reaches 5–7 km (Daneš, 1985; Pratt and others, 1997; Brocher and others, 2001; Van Wagoner and others, 2002). This descent of depth to basement implies folding or faulting, but the southern edge of the Tacoma Basin in and west of the map area lacks the clear geophysical anomalies that mark the Olympia fault along the southwestern edge of the Tacoma basin farther west. Furthermore, whereas the Tacoma fault along the northern edge of the Tacoma basin is active (Nelson and others, 2008), no Quaternary tectonic deformation has been clearly connected to the southern edge of the Tacoma basin, including at the southern end of the Olympia fault (Polenz and others, 2021, 2022, 2023). Indeed, the entire Olympia fault's slip history, sense of slip, and potential activity remain unclear (Sherrod, 2001; Magsino and others, 2003; Walsh and Logan, 2005; Clement and others, 2010; Odum and others, 2016; Polenz and others, 2016, 2021, 2022). However, Polenz and others (2021, 2022) suggested that northeast-down offset along the Olympia fault is substantially Eocene. The same may be true at the southern edge of the Tacoma basin, because (1) compared to structures farther north, recorded seismicity is minimal in the map area and along the Olympia fault (Brocher and others, 2017); (2) mostly volcanic rocks fill the Tacoma basin northeast of the Olympia fault to <300 m below the surface (Polenz and others, 2021, 2022, 2023). The basin-filling rocks are much thicker than similar rocks southwest of the fault and are probably Eocene in age (Polenz and others, 2021, 2022, 2023; Contreras and others, 2023), which would imply that Tacoma basin deepening, and hence northeast-down offset

¹ Marine isotope composition of benthic foraminifera is a proxy for global ice volume; even-numbered stages refer to global glacial periods (Morrison, 1991; Lisiecki and Raymo, 2005).

at the southern edge of the Tacoma basin is also substantially Eocene (Polenz and others, 2021, 2022, 2023).

METHODS

Geologic Mapping

We identified units from field observations in the summer and fall of 2023. We collected field data mostly as point notes at more than 500 sites using Esri Field Maps and constructed maps using Esri ArcGIS Pro. We refined the field mapping through:

- Age analyses (Table 1, Appendix A, Data Supplement), including:
 - ◆ One infrared-stimulated luminescence age for determining depositional ages for Cascade-Range-sourced sediment.
 - ◆ Six U-Pb ages on zircon for (1) constraining depositional ages for Miocene sediment (two samples) and (2) determining crystallization ages on Eocene volcanic rocks (four samples).
 - ◆ Seven $^{40}\text{Ar}/^{39}\text{Ar}$ ages for determining eruptive or crystallization ages of igneous rocks (four samples).
- Fifty geochemical analyses (Appendix B, Data Supplement) to classify igneous rocks, test their geologic unit association, and (or) identify their volcanic source.
- Geophysical data collection and modeling (Appendix C, Data Supplement) to infer subsurface rock types and structures.
- Spectral analysis of satellite images (Appendix D) to help identify rock types where field data are sparse.
- Petrographic review of 48 thin sections to identify rock types, minerals, alteration, and microscopic structures.
- Analysis of pollen to assist paleoenvironmental interpretation.
- Surveys of clast composition and weathering to assess sediment provenance, characterize units, and assist in determining relative ages. We present one count of 50 clasts from the Mashel Formation. To separate clast assemblages associated with Cordilleran ice incursion(s) from Cascade-Range-sourced assemblages, we searched outcrops for rock types that mapping farther west had documented only in Cordilleran ice-associated assemblages (see *Vashon Drift*).
- Evaluation of 113 well and boring records to assess thickness and character of subsurface deposits.
- Consideration of prior geologic mapping and studies.
- Inspection of aerial orthophotos (true color and infrared) to help identify wetland areas or land use that may have affected surficial deposits.
- Geomorphic mapping on lidar to help infer associated geologic deposits. We used a lidar-based digital elevation model (DEM) with a 3-ft grid resolution (Washington Geological Survey, 2005, 2017, 2020a,b, 2022; Weyerhaeuser written commun., 2022) to estimate elevations and derive hillshade images and contours.

In addition, we coordinated our detrital zircon sampling at the Mashel Formation type section with Chris Schiller (paly-nologist) and Paul Kester (paleontologist) (both with the Burke Museum of Natural History and Culture) to ensure that our age data can inform their paleoenvironmental and biostratigraphic assessments.

We use the metric system—except for elevation, which we report in feet above mean sea level (ft) to facilitate comparison with topographic maps. We reference Folk (1980) for sedimentary rock classifications. We use the geologic time scale of the U.S. Geological Survey (USGS) Geologic Names Committee (2018). Where that scale lacks Epoch subdivisions, we reference Walker and Geissman (2022).

Potential-Fields Geophysical Methods

We collected 224 new gravity measurements to construct a refined isostatic gravity map with particularly dense station spacing along and near Cross Section A–A'. We then applied a quantitative algorithm to the interpolated gravity map to mark high-amplitude, linear gradients ('gravity max-spots'; Appendix C; Fig. M1A). Gravity max-spots delineate boundaries between rocks with contrasting densities, locating subsurface lithologic contacts and structures (Phillips and others, 2007). Aeromagnetic survey data (Fig. M1A) compiled from Blakely and others (1999, 2020, 2024) are used to delineate contacts between geologic units of contrasting magnetic properties. Forward-modeled isostatic gravity and aeromagnetic profiles (using GM-SYS; Geosoft Inc.) along line X–X' (Fig. M1B) developed from map-view geologic and geophysical data inform subsurface interpretations. Line X–X' in Fig. M1 is truncated at the Eatonville quadrangle boundaries; modeling extended northwest to the Willhoite well² and southeast to near the Duncan well³ (Figs. 1 and M1A). New rock density and magnetic susceptibility measurements from 67 outcrops within and beyond the map area complement rock property data from previous efforts and helped constrain geophysical models (Appendix C; Data Supplement; Alex Steely, WGS, written commun. 2021; Contreras and others, 2023; Polenz and others, 2021, 2022, 2023). Appendix C details gravity, magnetic, rock property, and modeling methods.

² E.F.E. Willhoite et al. No. 1 well, API Number: 046-053-00006 (Washington Geological Survey, 2019), hereafter referred to as the Willhoite well, drilled in 1961 by the Humble Oil & Refining Company 7.6 km northwest of the Eatonville quadrangle to a well depth of 1,744 m (5,721 ft). We accessed original files and reports from the Willhoite well (Washington Geological Survey, Oil and Gas files-WA File Number 157, 2023), supplemented by Contreras and others' (2023) assessments of magnetic susceptibility of well cuttings.

³ Duncan Oil, Inc., well SKCH No. 24-17, API Number: 046-041-00195 (Washington Geological Survey, 2019), hereafter referred to as the Duncan well, drilled in 2002, located 7.3 km south-southeast of the map area and 2.4 km southwest of our geophysical model line.

Table 1. Summary of age analyses. The Appendices and Data Supplement offer additional information about samples and analysis.

Sample ¹	Material	Map Unit	Method	Notes	Age $\pm 2\sigma^2$
GD11	sand	Qpc _{ph}	Infrared-stimulated luminescence	Luminescence age dates fluvial sand deposition 4 m below the top of a >6 m thick fluvial section of sand that is directly overlain by a 2–5 m thick Hayden Creek till.	103.4 \pm 23.2 ka (preliminary result 2024/04/22)
GD1	andesite groundmass	Eva _n	⁴⁰ Ar/ ³⁹ Ar	Mini-plateau age dates eruption. Error is internal. Sampled at Eatonville Public Library.	34.59 \pm 0.19 Ma
GD6	plagioclase from gabbro	Eli _n	⁴⁰ Ar/ ³⁹ Ar	Inverse isochron age dates plagioclase crystallization. Lab prefers this inverse isochron age to 38.04 \pm 0.13 Ma plateau age for this sample. Error is internal. Sampled from an SR7 roadcut 1.8 km south-southwest of Hugo Peak.	37.91 \pm 0.25 Ma
GD9	plagioclase from basaltic andesite dike	Eli _n	⁴⁰ Ar/ ³⁹ Ar	Mini-plateau age dates plagioclase crystallization in a dike. Groundmass yielded a 38.54 \pm 0.09 Ma total fusion age—inferior because intense ³⁹ Ar recoil suggests age exceeds true crystallization age. Error is internal. Sampled from a west-facing shore on Alder Lake (Little Nisqually finger on west side of the lake).	37.21 \pm 0.21 Ma
GD10	plagioclase from andesite	Eva _n	⁴⁰ Ar/ ³⁹ Ar	Plateau age dates plagioclase crystallization. Groundmass yielded 38.48 \pm 0.09 Ma total fusion age—inferior because intense ³⁹ Ar recoil suggests age exceeds true crystallization age; clinopyroxene yielded 29.96 \pm 2.79 Ma plateau age—for which insufficient gas prevented a good result. Error is internal. Sampled from a beach exposure along the east shore of Alder Lake.	36.87 \pm 0.12 Ma
GD2	sand	RMc _m	detrital zircon U-Pb	Maximum depositional age computed using TuffZirc from a coherent group of 5 zircons. The youngest single grain (excluded by TuffZirc) yielded a 5.2 \pm 0.3 Ma age. Sampled from Mashel Formation type section about 40 ft (12 m) below the top of the type section.	<6.1 +0.2/-0.3 Ma
GD3	sand	RMc _m	detrital zircon U-Pb	Maximum depositional age computed using TuffZirc from a coherent group of 35 detrital zircons. The youngest single grain (excluded by TuffZirc) yielded a 5.3 \pm 0.7 Ma age. Sampled stratigraphically about 0–5 m downsection of the Mashel Formation type section base—260 m downvalley of where a now-washed-out road marked the base of the type section.	<6.0 +0.1/-0.2 Ma
GD4	rhyolite tuff	Evt _n	zircon U-Pb	Zircon crystallization age computed using TuffZirc from a coherent group of 34 zircons from rhyolite tuff. The youngest single grain (excluded by TuffZirc) yielded a 35.7 \pm 1.2 Ma age. Sampled from a roadcut 1.2 km west-southwest of Hugo Peak.	37.5 \pm 0.5 Ma
GD7	rhyolite tuff	Evt _n	zircon U-Pb	Zircon crystallization age computed using TuffZirc from a coherent group of 36 zircons from rhyolite tuff. The youngest single grain (excluded by TuffZirc) yielded a 35.7 \pm 0.7 Ma age. Sampled from an SR7 road cut near the east end of Alder Lake.	37.41 \pm 0.5 Ma
GD8	diorite (?)	Eli _n	zircon U-Pb	Zircon crystallization age computed using TuffZirc from a coherent group of 33 zircons from pyroxene tonalite. The youngest single grain (excluded by TuffZirc) yielded a 35.6 \pm 0.8 Ma age. Sampled from a quarry about 1 km west of Alder Lake.	36.9 \pm 0.5 Ma
GD5	rhyolite tuff	Evt _n	zircon U-Pb	Zircon crystallization age computed using TuffZirc from a coherent group of 53 zircons from rhyolite tuff. The youngest single grain (excluded by TuffZirc) yielded a 35.6 \pm 1.3 Ma age. Sampled from an SR7 road cut 1.7 km southwest of Hugo Peak.	37.9 \pm 0.5 Ma

¹Age localities are numbered from north to south on the map and, for each technique, localities are also ordered from north to south in this table.²Error statements are 2 sigma. Maximum depositional ages from detrital samples (<#) are ages implied for the reported geologic units; for raw ages, see Appendix A and Data Supplement. U-Pb analyses by Victor Valencia (Zirchron and Washington State University); ⁴⁰Ar/³⁹Ar analyses by Dan Miggins (Oregon State University); Luminescence analyses by Sebastien Huot (Illinois State Geological Survey).

DESCRIPTION OF MAP UNITS

Holocene to Pleistocene Postglacial Deposits

af Artificial fill (Holocene)—Mixed earth materials of varied grain size and sorting, placed to raise surfaces; may contain organic material, concrete, debris, spoils, or waste rock; may be engineered; loose to compact. Excludes small or shallow fills (usually less than 1.5 m thick) such as most deposits from road construction and residential development, and fills that are commonly transient, such as in quarries.

ml Modified land (Holocene)—Mixed earth materials of varied grain sizes and sorting placed to modify topography; commonly includes excavations, some of which may expose underlying geologic deposits; may contain organic material, concrete, debris, spoils, or waste rock; may be engineered; loose to compact; typically shown where more than 1.5 m thick and (or) extensive, or where modification has sufficiently altered the original characteristics of a deposit such that it is no longer recognizable—mainly in the Eatonville city area near the northeastern map corner, where landforms suggest a patchwork of excavations and fill placement, and most observed exposures suggested that fill material was derived from surrounding Vashon Drift.

Qp Peat (Holocene to Pleistocene)—Organic and organic matter-rich sediment (peat, gyttja, muck, silt, clay, and sand) in flat-bottomed depressions or other poorly drained flat areas; loose; mostly mapped where lidar reveals landforms that suggest a lack of appreciable alluvial sedimentation and where we interpret true-color or infrared aerial photos as suggesting hydrophilic vegetation and (or) wet conditions. Thickness unassessed. North of the continental ice limit, unit Qp postdates Vashon Drift. South thereof, it postdates Hayden Creek Drift because the Hayden Creek glaciation would have eroded it or covered it with drift, and unit Qp was not found above the Hayden Creek ice limit.

Qa Alluvium (Holocene to Pleistocene)—Floodplain and channel sediment of mostly Cascade-Range-sourced andesitic pebbles, cobbles, boulders, sand, silt, clay, and peat, all in varied amounts; gray to pale gray and brown to pale brown, weathers brown, orange, red, and yellow; fresh to mildly weathered; loose; mostly well rounded and moderately to well sorted; mostly trough cross-bedded where gravelly, except in isolated, sparsely scattered, unbedded debris flow deposits; mostly planar-bedded in sandy and silty flood plain deposits. Alluvial fan deposits are included in units Qa and Qoa where map scale or crowding precluded separate mapping into units Qaf and Qoaf, typically because the deposit is less than ~30 m wide. The fan deposits tend to be more angular, less sorted, and less consistently bedded than other deposits in units Qa and Qoa. Qa and Qoa unit thickness is mostly unassessed,

but exposures and relief suggest that >3 m is common. Units Qa and Qoa form highly permeable, productive, usually unconfined aquifers that are sensitive to pollution and prone to impactful water level drops during times of drought. Unit Qa is mapped where there is evidence for geologically recent alluvial transport. Unit Qoa is mapped where similar deposits occur without evidence for alluvial deposition in the modern environment—such as where unit Qoa is dissected by a considerably deeper valley. North of the continental ice limit, both units Qa and Qoa postdate Vashon Drift. South thereof, they postdate Hayden Creek Drift because the Hayden Creek glaciation would have eroded them or covered them with drift, and units Qa and Qoa were not found above the Hayden Creek ice limit.

Qaf Alluvial fan (Holocene to late Pleistocene)—Pebble to boulder gravel and sand in varied abundances; may contain organic material; gray to brown; loose; subangular to rounded; moderately to poorly sorted; mostly poorly bedded, but ranging from unstratified to well bedded; derived from deposits upslope; 1.5–4 m thick in most exposures; mapped largely from fan-shaped landforms expressed in lidar where streams emerge from confined channels into broader and flatter topography. Units Qaf and Qoaf are mostly inferred to have been deposited by debris flows and floods. Unit Qaf is mapped where there is evidence for geologically recent alluvial deposition. Unit Qoaf is mapped where similar deposits lack evidence of deposition in the modern environment—evidenced, for instance, by dissection of unit Qoaf by a considerably deeper valley. Units Qaf and Qoaf are distinguished from other alluvium and outwash units primarily based on the presence of fan-shaped landforms, but the deposits in units Qaf and Qoaf also tend to be less sorted, less rounded, and less bedded than those in other alluvium. North of the continental ice limit, units Qaf and Qoaf postdate Vashon Drift. South thereof, they postdate Hayden Creek Drift because the Hayden Creek glaciation would have eroded them or covered them with drift, and units Qaf and Qoaf were not found above the Hayden Creek ice limit.

Qmw Colluvium (Holocene to Pleistocene)—Mixed earth materials of varied grain sizes and sorting, deposited by mass wasting—usually shallow ravel and soil creep. Landforms mostly suggest thicknesses between 1.5 and 8 m. Unit Qmw is shown where colluvium conceals underlying geology but may locally include outcrops of underlying units, in most instances Northcraft Formation. Unit Qmw is mostly identified from landforms. Unit Qmw locally includes small landslides and alluvial fans. Fan-shaped deposits in unit Qmw are typically steeper than those in unit Qaf and, based on lidar, tend to have less defined upslope feeder channels. Unit Qmw excludes areas where creeping, usually clayey soils appear to thinly mantle smooth slope surfaces that appear otherwise undisturbed—we mapped such

slopes as the underlying units. North of the continental ice limit, unit Qmw postdates Vashon Drift, whereas beyond the continental ice limit it mostly postdates Hayden Creek Drift but may be older above the alpine ice limit.

Qls **Landslide deposits (Holocene to Pleistocene)**—Mixed earth materials of varied grain sizes and sorting, derived from deposits upslope; variably weathered; particles angular to rounded; mostly loose, unsorted, and jumbled, but in some exposures including stratified colluvial aprons, slope wash, or internally stratified and (or) compact landslide blocks; highly varied in thickness; mostly mapped from landforms expressed in lidar (for example, hummocky slopes, deranged and disrupted drainages, tilted benches in hillsides, mid-slope scarps or otherwise disrupted or irregular slopes, and concave upper and convex lower slope forms). Similar landforms are common—but not necessarily indicative of landslides—on some slopes among Northcraft Formation volcanic rocks and in stagnant ice-related glacial deposits; we may therefore have failed to recognize some landslides and erroneously mapped others. Landslides along active river cutbanks are particularly common and can further impact valley floor sediment dynamics and land use by damming rivers, but these deposits tend to be quickly removed by the rivers, as historically occurred, for instance, just west of the map area (Pringle, 1990) and, in the winter of 2017–2018, 2 km downstream of La Grande Dam (Tacoma Power, written and oral communications, 2021–2024). Most landslides in Pierce County are adopted or adapted with minor modifications from Mickelson and others (2017). Most modifications accommodate base map constraints, such as shorelines. Some adjust landslide boundaries to better align with landforms expressed in lidar data or merge adjacent landslide polygons. Unit Qls is postglacial in age, but

some landslides south of the Vashon ice limit may be older. Absence of a mapped landslide does not indicate the absence of landslide hazard.

Late Pleistocene Glacial Deposits

VASHON DRIFT

We map as Vashon Drift all sediment deposited in the map area by Cordilleran ice, meltwater, and periglacial drainage in response to the Vashon ice incursion. Aside from till and glacial outwash (including lacustrine sediment), Vashon Drift may include some sediment where streams brought sediment from unglaciated areas but ice incursion caused the deposition.

Vashon Drift is distinguished from Cascade-Range-sourced sediment by the drift's more diverse clast content, which includes high-grade metamorphic and felsic intrusive rocks with orthoclase—lithologies that were transported into the map area exclusively by Cordilleran ice or meltwater from source areas in British Columbia and northwest Washington.. We refer to these lithologies as diagnostically 'northern-sourced' because they are not normally found in Washington's central or southern Cascade Range (Table 2). All Vashon map units below include such northern-sourced rocks—but usually only in trace quantities because the map area straddles the southeastern margin of the ice, where Cascade-Range-sourced rocks dilute the diagnostically northern-sourced rock types. Because northern-sourced clasts are uncommon, we typically inferred a deposit is Vashon Drift if we readily found even a few northern-sourced rocks in an outcrop.

Included in Vashon outwash, and possibly in all Vashon map units, are deposits from high-discharge glacial outburst floods and associated debris flow(s), notably the Cascade-Range-sourced periglacial Tanwax flood (Pringle and others, 2000; Pringle and Goldstein, 2002; Futornik and others, 2008; Parker and others, 2008; Polenz and others, 2018), and perhaps other meltwater floods (Troost, 2014; Polenz and others, 2021). We did not map these flood deposits as separate unit(s) because: (1) the Tanwax

Table 2. Lithologic assemblages that distinguish northern-sourced drift, Cascade-Range-sourced sediment, and Mashel Formation. Table adapted from Polenz and others (2023).

Northern-sourced drift	Cascade Range-sourced sediment	Mashel Formation
(Polenz and others, 2022, 2023)	(Polenz and others, 2022)	Based on 50 clasts from clast count site C1, about 0–5 m down-section (300 m down-valley) of type section
<p>Mostly Cascade Range-sourced (see center column), but:</p> <ul style="list-style-type: none"> Includes varied amounts (commonly only trace quantities) of schist, gneiss, bright pink garnets, epidote, and granitic rocks that contain orthoclase Lithologically diverse and rich in polycrystalline quartz (Walsh and Logan, 2005) <60% intermediate to felsic volcanic rocks >15% mafic igneous rocks (basalt and gabbro) 	<ul style="list-style-type: none"> >60% intermediate to felsic volcanic rocks, mostly porphyritic andesite; less abundant dacite, felsic to intermediate intrusive rocks, and basalt Other rock types absent or rare Usually less basalt, sedimentary rocks, and according to Noble and Wallace (1966), less granodiorite than in northern-sourced drift Less lithological diversity and less polycrystalline quartz than in northern-sourced assemblages of Walsh and Logan (2005) Large quantities of hypersthene in rocks from Mount Rainier (Noble and Wallace, 1966) A faintly lavender hue in gray sand exposures 	<ul style="list-style-type: none"> 74% intermediate to felsic volcanic rocks 12% intermediate to felsic intrusive rocks 8% quartz 6% metamorphic rocks

flood produced both debris flow diamicton that can resemble till (Futornik and others, 2008; Parker and others, 2008; Pringle and Goldstein written commun., 2018, and oral commun., 2023) and fluvial gravel that can resemble glacial outwash and erratic boulders; (2) both Vashon Drift and Tanwax flood deposits are mostly andesite in the map area (Table 2) and their clast content and sedimentary structures are so similar that even field review of some exposures (Barry Goldstein and Pat Pringle, oral commun., 2023) left room for debate about origin; (3) the Tanwax flood may have inundated nearly the entire Vashon-glaciated part of the map area (Pringle and others, 2000) and flood bedforms may include elongate channel bars that resemble drumlins (Goldstein and Pringle, oral commun., 2023).

Periglacial discharge carved broad channels across the Vashon-glaciated northernmost 5.5 km of the Eatonville quadrangle, the most prominent being the several hundred meters-wide Ohop Valley, wherein the modern Ohop Creek is clearly underfit. Aside from channels, the most prominent evidence cited for the flood(s) are rounded, andesitic boulders that rest on the surface within the inferred flood pathway (not limited to channels) (Pringle and others, 2000; Pringle and Goldstein, oral commun., 2023). Such boulders may be found on the surface amid all Vashon map units in this map—as can boulders that dropped out of melting ice (erratics), which also include rounded andesitic boulders. Percussion marks on flood-deposited boulders offer one avenue for distinction, however.

The timing of the Vashon ice incursion—and by implication the age of Vashon Drift—was discussed earlier (see *Geologic Overview*).

Qgo Uncompacted outwash, undivided (late Pleistocene)—Gravel, pebbly sand, or sand, all in varied amounts, with pebble gravel more abundant than cobble and boulder gravel; contains northern-sourced clasts (Table 2); may include loose diamicton that lacks diagnostic northern-sourced clasts and may have been deposited by outburst flood-associated debris flow(s) (see Vashon Drift above), such as 80 m north of the map area along SR161 at the northern edge of Ohop Valley; gray to pale gray, or mildly weathered to pale brown, brown, or variegated with iron stains; uncompacted and commonly cohesionless; well rounded to subrounded; moderately sorted to well sorted; clast supported where gravel, locally with matrix and interbeds of silt and sand; elsewhere unstratified. Unit Qgo tends to form flat to gently sloping terraces with relict, typically flat-bottomed channels. Unit thickness is commonly >6 m and may locally exceed 15 m, based on relief within terraces and terrace risers. Unit Qgo and its subunit are found within the Vashon-glaciated, northern 5.5 km of the map area. Undivided unit Qgo is mapped where outwash is either fine grained or grain size is uncertain. Unit Qgo was deposited proglacially, is generally of Vashon recessional age, and most likely includes glacial outburst flood deposits (see *Vashon Drift* above), especially where andesite boulders with percussion marks (Pringle and Goldstein, 2002) rest on the surface of unit Qgo and subunit Qgog. Unit Qgo stratigraphically overlies

Vashon till (including end moraines) and most ice-contact deposits. Unconformable contacts with underlying bedrock and Mashel Formation also appear common. Along the southern ice margin, it may locally be coeval with nearby deposition of units Qgt, Qgic, and Qgim. Locally subdivided into:

Qgog Uncompacted outwash gravel (late Pleistocene)—Pebbles, cobbles, and boulders, all in varied amounts, commonly with sandy matrix and minor sand lenses or interbeds; likely contains debris flow deposits from outburst floods (see Vashon Drift above); contains northern-sourced clasts (Table 2); tan to gray; loose; variably sorted; mostly well rounded. Unit thickness is mostly unconstrained, but terrace risers and terrace-internal relief suggest unit thicknesses of 1.5–10 m. A narrow polygon of unit Qgog is shown along a ridge top at 960 ft altitude 830 m northwest of age site GD1 because Zoe Futornik interpreted andesite boulders (unit Qgog?) as Tanwax flood high water mark (Barry Goldstein and Pat Pringle, oral commun., 2023). The unit is queried here because, although scattered andesite boulders remain, development subsequent to Futornik's field work prevented us from confirming or rejecting her interpretation. On the north side of Ohop Valley, matrix-free, well-sorted, well-rounded, bouldery andesite cobble gravel perched 5–6 m above the valley floor 280 m northeast of geochemistry sites G5–7 (line unit Qgog?) offers previously undocumented evidence for high velocity discharge in the Eatonville quadrangle segment of the Ohop Valley.

Qgoi Recessional ice-contact outwash (late Pleistocene)—Cobble gravel, pebble gravel, and less commonly sand, deposited in ice-contact braid plains or channels; also sand or mixed sand and gravel in sidewalls of kettles (closed depressions that formed where melting of buried glacial ice led to surface collapse), sand or silt in kettle bottoms; likely includes small, isolated exposures of moraine (diamicton, gravel, and sand), mainly in kettle walls; tan to gray; loose; moderately to well rounded and sorted; typically gently cross-bedded, but commonly with bedding locally oversteepened and (or) chaotic and disrupted; may range to planar-bedded; contains northern-sourced clasts (Table 2). Swales and kettle depths suggest unit Qgoi is more than 12 m thick just north of the Mashel River valley 1.7 km northeast of Cross Section A–A'. The unit may be only a few meters thick just north of the Nisqually River between 1 and 2 km southwest of the cross section (the only other mapped patch of

unit Qgoi). We infer from kettles in unit Qgoi that the unit was deposited partly on Vashon glacial ice and moraine deposits. We associate gentle cross bedding in the unit with deposition in outwash channels and braid plains, and over-steepened, chaotic or disrupted bedding with subsequent kettle collapse. Although kettles are a defining element of both units Qgoi and Qgimo, unit Qgoi forms a more continuous drape of outwash with less exposure of underlying moraine.

Qgim End moraine (late Pleistocene)—Diamicton, pebbles, sand, cobbles, silt, clay, and boulders, all in varied amounts; isolated peat deposits in some flat kettle bottoms; gray, tan, and reddish brown; loose to compact; unbedded but locally banded in diamicton, unstratified to stratified in gravel, sand and fines within the unit; contains northern-sourced clasts (Table 2). Relief suggests that unit thickness commonly exceeds 5 m. Thickness may locally exceed 30 m, based on the depth of a drainage that dissected a kame terrace within unit Qgim but likely did not erode much of the underlying bedrock 600 m east-northeast of geochemistry site G20. Unit Qgim is identified only south of the Mashel and Nisqually Rivers. The unit comprises the southernmost Vashon Drift across most of the Eatonville quadrangle and we interpret unit Qgim as end moraine at the southern margin of the Vashon ice. Diamicton within unit Qgim is mostly ablation till that dropped out of melting, stagnant ice. Less commonly, diamicton in unit Qgim includes patches of lodgment till and flow till. Some sand and gravel within unit Qgim also dropped out of melting, stagnant ice, elsewhere both were fluvially deposited by meltwater. Sand and silt, and clay in kettles, is commonly lacustrine. Boulders commonly rest on the surface of unit Qgim. We mostly identified unit Qgim based on landforms that range from smooth to hummocky, with some kettles. Surfaces in unit Qgim tend to be slightly more hummocky and contain more kame terracing than in unit Qgic. Hummocky parts of unit Qgim can resemble landslides, but unit Qgim tends to be more permeable than unit Qls, commonly with more orderly drainage incision. Compared to units Qgic and Qgt, unit Qgim tends to form slightly less streamlined surfaces with lesser development of drumlins and flutes. Most exposures of unit Qgim are less compact than unit Qgt. Unit Qgim is locally subdivided into:

Qgimo End moraine draped with outwash (late Pleistocene)—Glacial outwash pebbles, sand, cobbles, and boulders, all in varied amounts, resting as discontinuous patches on an end moraine consisting of till, pebbles, sand, cobbles, silt, clay, and boulders, all in varied amounts (as described in unit Qgim); gray, tan, and reddish brown; loose in outwash, loose to compact in moraine; moderately to well-sorted in outwash, unsorted in till; unstratified to

stratified in outwash, unbedded but locally banded in till; contains northern-sourced clasts (Table 2). The surficial outwash in unit Qgimo smooths out surface irregularities from the underlying moraine deposits. The contact between the surficial outwash and the underlying moraine is a patchwork of conformable deposition and erosional unconformities. Qgimo unit thickness is mostly unknown, but we suspect that the surficial outwash is commonly less than 3 m thick whereas the underlying moraine is generally much thicker. Relief in an aggregate pit 25–300 m southwest of Cross Section A–A' suggests >10 m total unit thickness. Unit Qgimo is identified only south of the Mashel and Nisqually Rivers. Unit Qgimo is distinguished from unit Qgim by systematic but patchy presence in unit Qgimo of surficial outwash deposited in ice-contact channel surfaces that are now fragmented by kettles. Unit Qgimo is distinguished from unit Qgoi by more pervasive presence and exposure in unit Qgimo of moraine deposits from stratigraphically beneath the outwash. Exposures of moraine in unit Qgimo are more pervasive than those in unit Qgoi, and the outwash drape is less continuous

Qgic Ice contact deposits, undivided (late Pleistocene)—Diamicton, and less abundantly pebble gravel (locally cobbly) sand, and boulders all in varied amounts; contains northern-sourced clasts (Table 2); pale gray to brown and reddish brown; mildly weathered; ranges from loose to compact in diamicton, mostly loose in gravel, sand, and fines. Rounding and sorting are varied. Diamicton is unstratified but commonly banded. Gravel, sand, and fines range from unstratified to trough cross-bedded and planar bedded. Well records and exposures in road cuts and stream cuts suggest that the unit is typically 1.5–10 m thick and may locally exceed 15 m.

We interpret diamicton in unit Qgic, and thus most of the unit, as a patchwork of lodgment and ablation till. We interpret gravel, sand, and fines as a mix of ice-contact or ice-proximal outwash and, less commonly, meltout deposits. Cobbles to medium sand comprise most of the volume in unit Qgic, with finer particles common mainly in till matrix. Boulders are commonly dispersed on the surface and locally present in till. They are less common in outwash. Deposits in unit Qgic tend to be less compact, more permeable, and more friable than in unit Qgt, and diamicton in unit Qgic commonly grades laterally from compact to loose. Compared to unit Qgt, unit Qgic is generally marked by more kettles, hummocks, and drainage channels established by meltwater and now commonly relict. Drumlin and flute surfaces in unit Qgic are less common and tend to be more disrupted (by drainages, knobs, hillocks, and troughs) than those in unit Qgt. We interpret these

all above listed landforms as signs of stagnant ice and used them to help map unit **Qgic** in this context.

Qgt Ice contact deposits (late Pleistocene)—Diamicton containing boulders, cobbles, pebbles, and sand, with an unsorted or poorly sorted matrix of sand- to clay-sized particles, all in varied amounts; matrix-supported in nearly all exposures; gray to pale reddish brown; mildly to moderately weathered near the surface and minimally weathered to fresh deeper down in compact lodgment till; mostly compact, with low permeability (acting as an aquitard—more so than unit **Qgic**); not usually penetrated by roots; clasts well rounded to faceted or angular, and in some cases striated; matrix mostly angular; unsorted; unbedded but in some exposures banded (resembling bedding); contains northern-sourced clasts (Table 2); thickness not apparent in most exposures; likely to pinch out locally, based on exposures elsewhere in the Puget Lowland. Unit **Qgt** was deposited directly by glacial ice and usually includes a loose, surficial cover of 0.5–3 m of ablation till and (or) outwash clay, silt, sand, and gravel, and dispersed boulders on the surface. We interpret the loose cover material as the main parent material for soil—the underlying compact lodgment till tends to be mostly unaffected by soil development.

Unit **Qgt** tends to be associated with south- to west-oriented drumlins and flutes that are most strongly developed between the Ohop Valley and the northwestern corner of the map, and we used these landforms to help identify the unit. However, such landforms in the Eatonville area have alternatively been interpreted as Tanwax flood channel bars (Barry Goldstein and Pat Pringle, oral commun., 2023). Limited exposure, access, and scope preempted evaluation of that hypothesis in most locations, but we note that one drumlinoid hill offers exceptional exposure of 4-m-thick lodgment till within 2 m of the surface where SR 7 enters the north side of Ohop Valley (and map area). The matrix in unit **Qgt** tends to include more fine sand, silt, and clay than the matrix in diamicton of unit **Qgic**, and partly due to that, unit **Qgt** tends to be less friable. Compared to unit **Qgic**, unit **Qgt** tends to form taller, smoother, more distinct flutes and drumlins, and the surface atop unit **Qgt** tends to contain fewer landforms commonly associated with stagnant ice, such as meltwater channels, kettles, and eskers. We used these landforms to help delineate unit boundaries between unit **Qgic** and unit **Qgt**. Unit **Qgt** appears to mostly rest on unit **RMcm** and, south of Eatonville, Northcraft Formation.

PRE-VASHON SEDIMENT

Pre-Vashon Alpine Drift

Qaph Hayden Creek Drift, undivided (late Pleistocene)—Diamicton, pebble gravel, and sand; diamicton mostly clast rich but matrix supported, with clay-rich, sandy matrix; locally includes small black plant fragments; pale gray where dry, dark olive where moist; weathers tan to

medium brown, reddish brown, orange, and pale yellow, commonly forming a mostly tan, 1–3-m-thick, clayey soil; clast weathering rinds in diamicton typically 1–3 mm thick 0.5–2.5 m below the surface, with common to pervasive interior weathered faces; loose to compact; clast lithologies Cascade-Range-sourced (Table 2).

Diamicton in unit **Qaph** includes till and lahar deposits. We interpret plant fragments as common in lahar deposits but rare in till. We further interpret that clasts tend to be well rounded to subangular in lahar deposits but mostly well rounded in till. Crandell and Miller (1974) asserted that clasts are more diverse in till—noting that (a) 80 percent of all clasts in debris flows are from Mount Rainier, whereas in till, less than 20 percent are, and (b) 30 percent of pebbles in till are andesite from Mount Rainier, six percent granodiorite, and the rest “from the Ohanapeosh and Stevens Ridge Formations and fine-grained intrusive rocks.”

Hayden Creek Drift includes surficial deposits of diamicton (till and debris flows), and bedded pebble gravel and sand. Both facies, diamicton and fluvial sediment, are spectacularly exposed, with soil development typical of this drift, along an Alder Lake shore cliff 1–1.5 km southwest of luminescence age site GD11.

Hayden Creek Drift is also well exposed in cliffs above Alder Lake, such as 4 m upsection of age site GD11, farther northwest along the same shore, and southwest across the lake, where Hayden Creek lodgment till and alluvium overlie a lower, thicker till of unknown age.

Diamicton at 2,100 ft elevation 1.26 km southwest of geochemistry site G44 suggests Hayden Creek ice reached the western map edge. Diamicton at 1,725 ft elevation on a north-facing slope 1.35 km northwest of Alder Dam suggests Hayden Creek ice overtopped the 1,800-ft-high ridge between that site and Alder Lake. We queried an alpine ice limit north of that ridge because we saw no indication of Hayden Creek ice farther north; Crandell and Miller (1974) estimated that Hayden Creek ice descended to 300 m (980 ft) elevation.

The age of Hayden Creek Drift appears to be between ~85 and ~105 ka. Crandell and Miller (1974) estimated it at 40–50 ka. Overlying tephra at Mount Rainier suggests the drift age exceeds 85 ± 6 ka (Sisson and others, 2019). Age site GD11 constrains the age of the till to <105 ± 24 ka (Table 1, Appendix A, Data Supplement). In the Cowlitz River valley south of the map area, Dethier and Bethel (1981) divided Hayden Creek outwash into younger and older subunits.

Qapw Wingate Hill Drift, undivided (late Pleistocene)—Diamicton, pebble gravel, and sand; diamicton mostly clast rich but matrix supported, with clay-rich, sandy matrix; mostly pale gray to pale yellow, with some ironstaining, from 0–5 m below the surface; matrix in upper 3–4 m weathered to mostly clay, with mud cracking common in dry exposures; clast weathering “at least twice as strongly developed as that on the Hayden Creek Drift,” with some gravel deposits “oxidized to a

depth of...10 m” (Crandell and Miller, 1974, p. 18–19); clasts mostly well rounded; loose to compact; clast lithologies Cascade Range sourced (Table 2).

Undivided pre-Vashon sediment

Qpvl Pre-Vashon lahar deposits (late(?) Pleistocene)—Clast-supported diamicton of pebbles, cobbles, boulders, and matrix of silt, sand, and clay; near base includes rounded rip-up clasts (some >1 m) of mostly fine-grained deposits that we interpret as Mashel Formation; moderately weathered. We observed unit Qpvl only in a single, mostly inaccessible exposure, resting unconformably on the Mashel Formation type section 1 km north of the confluence of the Mashel and Nisqually Rivers. Here, matrix mostly fills void spaces between clasts, and the deposit appears potentially loose—but overlying Vashon Drift implies that it underwent compressive stress from ice loading. Unit thickness is at least 6–8 m but may be up to 38 m based on the upland surface elevation upslope, where we were unable to observe the contact with the overlying Vashon Drift. We tentatively mapped the diamicton as lahar because we interpreted it as a debris flow deposit and observed only clasts consistent with a volcanic Cascade Range provenance (Table 2). The age of unit Qpvl is late(?) Pleistocene based on its stratigraphic position between Mashel Formation and Vashon Drift and because moderate weathering suggests that it is no older than similar-looking debris flow deposits mapped by Polenz and others (2022, 2023) in a stratigraphically similar position west of the Eatonville quadrangle.

Qpc Pre-Vashon, Cascade-Range-sourced sediment, undivided (late Pleistocene)—Pebbles, cobbles, bouldery gravel and diamicton, sand, silt, clay, and peat, all in varied amounts; olive gray to pale gray, pale yellowish gray, pale brownish gray, light brown, reddish brown, and pinkish brown; distinctly more weathered than Vashon Drift—sand mildly to moderately weathered; clast weathering mostly moderate to mild but ranges to rotten; compact; poorly sorted; bedding typically gently trough cross-bedded to planar, ranging from distinct to faint and locally absent; Cascade-Range-sourced (see Table 2); sand rich in plagioclase and tends to include andesitic, commonly glassy volcanic lithic fragments and smaller amounts of quartz and (or) K-feldspar, and usually distinctly less abundant opaque minerals, pyroxene, biotite, and other minerals.

The unit description above is partly based on Polenz and others’ (2023) observations of the unit west of the Eatonville quadrangle because we tentatively map unit Qpc in the Eatonville quadrangle in only two areas. One of these is inaccessible (mid-cliff) at the upper end of the Nisqually River valley walls near the western map edge. We query the unit there based on our review of drone footage and prior mapping of the unit in a similar position farther west (Polenz and others, 2023). Pebbly sand with about 20% magnetite sand grains and mostly rotten clasts on a north-facing slope at 1,040 ft altitude

915 m southwest of age site GD5 is mapped as unit Qpc because its stratigraphic position relative to Hayden Creek Drift is unconstrained, although the exposure resembles Cascade-Range-sourced unit Qpcph at the eastern map edge. It is queried because we cannot exclude northern provenance in this location. The late Pleistocene age of unit Qpc is based on its moderate weathering and stratigraphic position beneath Vashon Drift. Locally subdivided into:

Qpcph Pre-Hayden Creek, Cascade-Range-sourced sediment, undivided (late Pleistocene)—Pebbles, cobbles, and boulders in gravel and diamicton, with sand, silt, and clay, all in varied amounts; mostly gray but also brown, orange, yellow, white, and variegated; mildly to strongly weathered, with an exceptionally good and probably representative exposure along a north-facing cliff 1–1.5 km southwest of age site GD11, revealing a 1–3-m-thick, mostly buff-colored, clayey soil with few clasts and up to 2-m-thick prismatic structure; well rounded to angular; well sorted to poorly sorted; cross to planar bedded, locally ranging to unstratified; Cascade-Range-sourced (Table 2), with up to 93 percent lithic fragments observed in sand (at age site GD11). The thickness of this unit is varied in well logs, ranging up to at least 30 m.

Unit Qpcph is discontinuously exposed along the Alder Lake shore up to 1 km west and 3.5 km northwest of age site GD11. We queried the unit (as a geologic unit line) beneath the uppermost till along the north-facing Alder Lake shore 1–1.5 km southwest of age site GD11 because fluvial sediment and a second, lower till all may be either Hayden Creek age or older. The unit is inferred along the southeastern 5 km of Cross Section A–A’, where well records document sediment between underlying bedrock and surficial Hayden Creek Drift. Unit Qpcph underlies Hayden Creek till and includes glacial and nonglacial, mostly undated deposits that may range from Hayden Creek advance outwash to sediment older than Wingate Hill Drift. Sand within unit Qpcph at age site GD11 (105 ±24 ka) may be either Hayden Creek advance outwash or older sediment.

Pliocene to Miocene Sediment of the Mashel Formation

RMcm Continental sediments (Pliocene to late Miocene)—Sand and silt with clayey matrix; pumice clasts in some exposures, in some instances abundant; sections, lenses and interbeds of pebble gravel; tephra layers, clay, muck, peat, and plant fragments and imprints, all in varied amounts; compact and stiff but unlithified. Walters (1965) defined the formation as containing an upper part

of mostly clay and sand and a lower part of mostly gravel, based on a type section in the Eatonville quadrangle.

Sand and finer sediment are pale yellow, pale gray, white, less commonly orange, reddish brown, medium gray, and red, moderately to strongly weathered, sand mostly medium to coarse grained, ranging to very fine grained, angular to subrounded, mostly poorly sorted, and distinctly trough cross-bedded or planar-bedded. Sand contains: intermediate volcanic lithic fragments (<80%), pumiceous glass or pumice ($\leq 60\%$), quartz (1–30%), chlorite ($\leq 20\%$), plagioclase (3–35%), hornblende (trace to 10%), pyroxene (0–7%), and other opaque minerals (0–3%). These estimates are based on thin sections at the type section (thin section site TS7), elsewhere in the Eatonville quadrangle (TS11–12), and west of the quadrangle (Polenz and others, 2023). Dacite pumice clasts are vitrophyric; compositions at thin section sites TS2–5 are 75–78% glass, 10–15% plagioclase, 5% pyroxene, 3–5% hornblende, 1–2% opaque minerals, and 1% chlorite (TS5 only).

Mashel Formation gravel is locally cobbly but mostly consists of medium to very coarse andesite pebbles (Table 2; Data Supplement), with abundant matrix of clay to clayey sand. The gravel is pale brown to reddish brown, red, orange, buff, pale gray, and pale yellow. At a freshly exposed river cutbank ~0–5 m downsection of the type section, most clasts had weathering rinds >2 mm thick or were rotten (clast count site C1, Data Supplement). Clasts are well rounded and moderately oblate to spheroid, moderately sorted, poorly to moderately bedded, and commonly imbricated.

Unit thickness exceeds 75 m and may exceed 150 m. It is described as 46 m at the type section (in the Eatonville quadrangle) (Walters, 1965). It appears to be about 75(?) m in a cliff along the Nisqually River 600 m southeast of the type section, where the unit resembles Walter’s gravelly “lower part” of the type section. Farther north in the Eatonville quadrangle, unit thickness may exceed 150 m, based on 120–150-m-high Ohop Valley walls with exposures that resemble Walters’ (1965) mostly fine-grained “upper part” of the type section. However, all of these thicknesses are minimum estimates because the base of the unit is unexposed. Unit thickness is poorly constrained in Cross Section A–A’ (see unit **MOC** and *Discussion*).

Bedding dips gently west-southwest (225/8) at the type section and northeast (333/8) 1.75 km southwest of the northeastern quadrangle corner. These dipping beds originate from post-depositional deformation because peat, lacustrine, and planar floodplain beds have similar dips. Compared to unit **Qpc**, Mashel Formation is more compact, tends to be more weathered, and more commonly contains pumice clasts, scoria, volcanic glass, tephra, muck, peat, and common to locally abundant plant macrofossils. We observed pumice clasts and scoria mainly in gravelly and sandy sections that we interpret as lahar deposits. Sandy and finer-grained sections of Mashel Formation tend to be pale yellow, pale gray, and

white—whereas Quaternary Puget Lowland sand and fines (unit **Qpc**) tends to present more pale gray to reddish brown and orange. Geochemistry, palynology, and revised unit age are discussed below (see *Discussion*).

Miocene to Eocene Sedimentary and Volcanic Rocks

MIOCENE TO OLIGOCENE SEDIMENTARY ROCKS

MOC Sedimentary rocks (Miocene to Oligocene) (cross section only)—Sediment and sedimentary rocks, likely mostly fine-grained and volcanoclastic; inferred between units **RMC_m** and **Env** in the northern third of Cross Section A–A’ based mainly on fine-grained sediment and sedimentary rocks at 519–1,037 ft well depth in the Willhoite well along our geophysical model line (Fig. M1A—model line shown only within Eatonville quadrangle). Unit **MOC** is slightly denser than Mashel Formation, based on unit **MOC**’s greater age and burial depth and the Willhoite well log’s mention of some lithified deposits. The 120–260 m thickness of unit **MOC** is inferred from combined geophysical model thicknesses of unit **MOC** and the overlying Mashel Formation—and the decision to limit the Mashel Formation thickness in Cross Section A–A’ to what is supported by cliff exposures and our interpretation of nearby water well records. We combined unit **MOC** and Mashel Formation in our 2D-forward modeling of gravity and aeromagnetism because we expect similar geophysical properties, except for slight density increases with depth. The lower contact with underlying unit **Env** is based on the depth of the transition in the Willhoite well from fine-grained sedimentary rocks (unit **MOC**) to interbedded Eocene (?) lavas and volcanoclastics (unit **Env**). The thickness of unit **MOC** is only a crude estimate because both the upper and lower contact elevations are only poorly constrained by our modeling.

EOCENE SEDIMENTARY ROCKS

En Continental to nearshore sedimentary rocks, undivided (early? to middle Eocene) (cross section only)—Sedimentary rocks. Whereas our upsection unit **Env** is mostly volcanic and at least partly correlative with Northcraft Formation, in the deeper subsurface our 2D-forward modeling of gravity and aeromagnetism needs denser rocks with low magnetic susceptibility—parameters satisfied by well-compacted ($\rho = 2,600 \text{ kg/m}^3$) sedimentary rocks. Unit **En** may interfinger near its top with Northcraft Formation (?) volcanics and near its base with basaltic basement of the early to middle Eocene Crescent Formation. We envision unit **En** to resemble sandstone and siltstone from the lower parts of the McIntosh and Skookumchuck Formations in the Chehalis basin southwest of the Eatonville quadrangle (Snively and others, 1951, 1958, 1959;

Pease and Hoover, 1957; Buckovic, 1979; Polenz and others, 2018, 2019, 2020; Sadowski and others, 2018, 2019). West of the Eatonville quadrangle, evidence for sedimentary rocks below Northcraft Formation and above Crescent Formation includes that (1) McIntosh Formation upsection of Crescent Formation 54 km west of the Eatonville quadrangle has yielded a 47.4 ± 0.2 Ma (middle Eocene) zircon U-Pb age (Polenz and others, 2017)—older than the earliest Northcraft Formation age (45.80 ± 0.07 Ma, Polenz and others, 2021); (2) Pease and Hoover's (1957) "lower McIntosh" Formation interfingers with Crescent Formation; (3) Polenz and others (2018) found evidence that McIntosh Formation in the Bannse No. 1 well 42 km west of the Eatonville quadrangle ranges to middle Eocene age (underlying Northcraft (?) igneous rocks are probably intrusive).

UNDIVIDED EOCENE VOLCANIC AND SEDIMENTARY ROCKS

Env Interbedded volcanic and continental to nearshore sedimentary rocks, undivided (late (to middle?) Eocene?) (cross section only)—Andesitic lava, tuff, volcanoclastic deposits, and interbedded sedimentary rocks; may include some intrusive rock. We base unit Env mainly on a section of mostly volcanic rocks and less voluminous sedimentary rocks at 1,037–5,721 ft well depth in the 5,721-ft-deep Willhoite well (Figs. 1 and M1A). Some of unit Env may be more sedimentary than the Willhoite well section, as suggested by a correlative(?) 3,238-ft-thick section of mostly sedimentary Cowlitz Formation alternating with igneous rocks in the Duncan well (Figs. 1 and M1A; Washington Geological Survey, 2019). Alternatively, the more sedimentary section there may be stratigraphically lower, equivalent to unit En. Unit Env satisfies the need in our 2D-forward modeling for rocks at this depth that are intermediate in density and magnetic susceptibility between overlying sediment and underlying volcanics (Fig. M1B).

We suggest a late (to middle?) Eocene age for unit Env because (1) the unit is laterally adjacent to Northcraft Formation in the center of Cross Section A–A'; (2) Cowlitz Formation in the Duncan well is at least partly of similar age (Weaver, 1912, 1937; Henricksen, 1956); (3) the late- to middle-Eocene Skookumchuck and McIntosh Formations are stratigraphically associated with Northcraft Formation southeast, south, southwest, and west of the map area (Snively and others, 1951, 1958, 1959; Buckovic, 1979; Schasse, 1987a; Flores and Johnson, 1995; Polenz and others, 2018, 2020, 2022, 2023; Sadowski and others, 2018, 2019), as are Puget Group sedimentary rocks north of the Eatonville quadrangle (Gard, 1968). An absence of age control for Tacoma Basin fill implies that unit Env may include post-Eocene rocks.

LATE TO MIDDLE EOCENE VOLCANIC AND INTRUSIVE ROCKS OF THE NORTHCRAFT FORMATION (PUGET GROUP)

Env_n Undivided igneous and volcanoclastic rocks (late (to middle?) Eocene)—Mostly dark gray to medium gray, intermediate flows, ranging from basalt to dacite; banded to variegated, pinkish brown to lilac and pale gray rhyolite tuff; interbeds of pale gray to pale brown flow breccia and other volcanoclastic rocks; intruded by intermediate dikes, sills, and stocks; in many exposures hydrothermally altered, resulting mainly in chlorite and epidote, both of which tend to add some green to the otherwise gray rocks. Many altered rocks include trace amounts of pyrite. Undivided unit Env_n is mapped where map crowding or the presence of rocks other than andesite flows combined with a paucity of observed exposures prevented separate mapping of Northcraft Formation subunits. Where we saw contact orientations or bedding in the Northcraft Formation (including all subunits), we concluded that the orientations need not have been originally horizontal, or the exposures revealed only apparent dip. Schasse (1987) similarly reported only a single bedding dip in the Eatonville quadrangle ($313^\circ/33^\circ$ NE), and we are left with no clear sense of orientations, much less deformation. The Northcraft Formation spans more than 11 million years (Polenz and others, 2020, 2021, 2022), but all eight ages from the Eatonville quadrangle are late Eocene, between ~ 34.5 Ma and ~ 38 Ma (Table 1). Locally subdivided into:

Evan Andesite and basaltic andesite flows (late (to middle?) Eocene)—Andesite, basaltic andesite, and rarely trachyandesite and basalt; locally includes minor interbedded volcanoclastic rocks; dark to pale gray, commonly bluish gray or greenish gray where altered; dense (Fig. M1B; Table A3 in Appendix C); commonly glassy with up to 55 percent glass, and nearly everywhere porphyritic with plagioclase phenocrysts in most exposures up to 1 or 2 mm in length, and rarely more than 3 mm. Thin sections revealed 30–68% plagioclase (thin section sites TS25 and TS14). Textures are commonly autoclastic and (or) hyalopilitic, often with glomerocrysts, and occasionally poikilitic, pilotaxitic, ophitic, or subophitic. Unit Evan is so widely exposed that we mapped other Northcraft Formation units only where we had specific reason to think that andesite flows are not the main constituent. Exposures of dikes and intrusive bodies are not especially common and we found both only in a few areas with relatively good exposure. Mild to moderate propylitic or hydrothermal alteration is widespread, expressed mostly by bluish gray and greenish gray color due to silicification, chloritization, or epidotization,

commonly with trace quantities of pyrite. Unit Eva_n near the southwestern map corner includes strongly altered rocks that may be intrusive (unit Eii_n ?) but are altered beyond clear recognition. Two new $^{40}Ar/^{39}Ar$ ages from andesite in unit Eva_n are 34.59 ± 0.19 Ma at the Eatonville public library (GD1) and 36.87 ± 0.12 Ma from the east shore of Alder Lake (GD10) (Tables 1 and A3).

Eii_n

Intermediate intrusions (late (to middle?) Eocene)—Dikes and small intrusions of andesite, basaltic andesite, gabbro, diorite, and tonalite; pale to dark gray and greenish to blueish gray. We describe most exposures of unit Eii_n as dikes but note that some transition to sills within the same outcrop.

Well-exposed quarry walls at geochemistry site G36 near the western map edge reveal three generations of porphyritic basaltic-andesite dikes: a steeply east-northeast-dipping dike (G37) is cut by a steeply northeast-dipping dike (G38) that is in turn cut by near-vertical, east–west-striking dike (G38). Nearby, a porphyritic basaltic andesite dike dips south–southeast (G32) and a near-vertical andesite dike strikes northeast (G30). Several well-exposed, near-vertical dikes strike east-northeast along the Alder Lake shore 1.3–2.6 km south-southwest of Alder dam. Among these, a porphyritic basaltic andesite dike (geochemistry site G41) intruded a lithologically similar, more weathered, similarly oriented dike that itself intruded even more weathered porphyritic basaltic andesite. Other near-vertical dikes in this area strike southeast to south.

Pyroxene tonalite with <3 mm crystals is well exposed at geochemistry site G35. Gabbro is exposed along SR7 (geochemistry site G25), where most crystals are <2 mm but some range to 7 mm long. Intrusive rocks near the southwest map corner may be from the same stock as diorite farther west (unit Eig_n of Polenz and others, 2023). The southwestern intrusive rocks include strongly altered diorite at the southwestern map corner, and 2.5 km farther east-northeast, possibly diorite(?) in a strongly weathered exposure.

We suspect that unit Eii_n is more widespread than mapped: accessible exposures are sparse but gravity and aeromagnetic data suggest more voluminous subsurface intrusions (Cross Section A–A'; Fig M1), and widespread, mild to moderate propylitic or hydrothermal alteration of volcanic rocks may be a byproduct of more extensive intrusions.

Unit Eii_n yielded two $^{40}Ar/^{39}Ar$ ages: 37.91 ± 0.25 Ma on gabbro 300 m north-east of La Grande Dam (age site GD6),

and 37.21 ± 0.21 Ma on a basaltic andesite dike 1.3 km south-southwest of Alder dam (GD9). Tonalite west of Alder Lake yielded a 36.9 ± 0.5 Ma zircon U–Pb age (GD8).

Evc_n

Volcaniclastic deposits (late (to middle?)

Eocene)—Pyroclastic flows, lahars, tuffs, and fluvial conglomerate; clasts mostly pebble-sized but range to boulders; clast lithologies mostly basaltic-andesitic to andesitic, but also include basalt, dacite, rhyolite, and sandstone; medium to pale gray; where hydrothermally altered, ranging to greenish gray, green, and bluish gray; weathers pale to medium brown, pale gray, orange, yellow, orange brown, and variegated; well rounded to angular.

Observed exposures of unit Evc_n are small and sparsely scattered, and unit thickness is therefore poorly constrained. It exceeds 10 m in quarries 560 m south of geochemistry site G16 and north of age site GD8. We observed unit Evc_n only in the west half of the Eatonville quadrangle. The unit is queried 2 km north of the southwestern map corner because exposures there are so strongly weathered that we are unsure if they were ever lithified, and lack of contact exposures implies the possibility that they are more recent sediment deposits. We further note that some altered or strongly weathered exposures of unit Evc_n are difficult to distinguish from autoclastic flows of unit Eva_n .

Evd_n

Dacite (late (to middle?) Eocene)—Sparsely to strongly porphyritic dacite flows; medium to pale gray, ranges to pale greenish gray where hydrothermally altered, such as at geochemistry site G45; weathers reddish gray to reddish brown; locally platy. Unit thickness may exceed 80 m near the western map edge, based on elevations of geochemistry site G33 and an observation site 815 m farther northwest. Near the south end of Alder Lake, the height of a ridge above geochemistry site G45 suggests >55 m unit thickness. Upper and lower contacts were not observed in either area, and we did not see the unit elsewhere. We did not directly date Evd_n in the Eatonville quadrangle, but we suspect the unit age is ~37.5–40.5 Ma because rhyolite tuff from the east half of the map area yielded ages from 37.4 ± 0.5 to 37.9 ± 0.5 Ma (GD4, GD5, and GD7), dacite tuff from two age sites just west of the map area yielded ~38 Ma ages (GD7 and GD15 of Polenz and others, 2023) and dacite 7.7 km west of the map area yielded a 40.5 Ma age (GD9 of Polenz and others, 2023).

Evt_n **Felsic tuff (late (to middle?) Eocene)**—Ash flow to lapilli tuff, varies from crystal to vitric; rhyolitic in composition (geochemistry sites G17–19, G23, G26, G34, G48); locally welded; locally includes intercalated rhyolite, such as at thin section site TS47, and dikes(?), such as at TS18; gray to tan, pale green, pale yellow to lavender, orange, pink, and in some weathered exposures carmine red or maroon; commonly variegated and banded; commonly altered with epidotization, some chlorite, and localized silicification such as at thin section site TS22. We attribute more mafic geochemistry in samples G9 and G11 to extreme weathering. Unit Evt_n is usually porphyritic, with phenocrysts of mainly plagioclase (typically ~1% but ranging to 20%). Minor phenocrysts include pyroxene and other minerals. Some tuffs within unit Evt_n contain chlorite partings and (or) banded perlite texture, for instance, at thin section site TS13. Common features include widespread deformed or undeformed glass shards, in rare instances with curvilinear pieces, as well as tube pumice, flamme, cryptocrystalline-filled amygdules, and partially collapsed vesicles with secondary mineral infill. Primary textures within unit Evt_n are commonly obscured by alteration and weathering.

Unit Evt_n is widespread around Hugo Peak, extending from there north to the Mashel River, east to the map edge, south for at least 2.5 km, and west to the Nisqually River. It is also locally exposed farther south at age site GD7 and southwest at geochemistry site G48. Whereas unit Evt_n is consistently rhyolitic in this map area, felsic tuffs of the Northcraft Formation just west of the Eatonville quadrangle are dacitic (Polenz and others, 2023). Even so, geochemical traits (see *Discussion*), exposures alongside other Northcraft Formation rocks, and age all support inclusion of unit Evt_n with the Northcraft Formation. Three new zircon U-Pb ages from unit Evt_n range from ~37.4–37.9 Ma (GD4, GD5, and GD7; Table 1).

DISCUSSION

Reassessing the Mashel Formation

Walters (1965) defined the Mashel Formation as unconsolidated fluvial and lacustrine sediment with a type section in the Eatonville quadrangle. He referenced plant fossils, mostly from the Eatonville quadrangle, to assign the formation a late Miocene to late middle Miocene age. New detrital zircon ages from this study and Polenz and others' (2023) mapping of the adjacent Bald Hill quadrangle permit a late Miocene age at the type section but require a Pliocene age for at least part of the

formation elsewhere. This age reassessment has implications for Pacific Northwest paleobiogeography and paleoclimate.

AGE REVISION

Based on detrital zircon U-Pb ages from three sites in and near the map area, we revise the age of the Mashel Formation to between Pliocene and late Miocene. Two new detrital zircon U-Pb ages from this study (age sites GD2, GD3; Table 1) indicate that the type section is at most about 6 million years old (late Miocene). At both sites, the ~6 Ma age statement conservatively relies on TuffZirc, an algorithm that pools ages from multiple zircons into a statistically more robust age (see *Interpreting Our Reported Ages in Appendix A*). However, individual zircons at both sites yielded younger ages that may be accurate (Table 1; Data Supplement). Furthermore, since all ages are from detrital crystals, the sediment deposit may be still younger (see *Interpreting Our Reported Ages in Appendix A*). The type section therefore may be <5.3 Ma at the base (GD3) and <5.2 Ma at the top (GD2).

Whereas age sites GD2 and GD3 suggest a late Miocene (or younger?) age for the Mashel Formation type section, another U-Pb age from west of the map area indicates that at least part of the formation is Pliocene: 0.9 km west of the Eatonville quadrangle, Polenz and others (2023) interpreted a <4.1 Ma age (Pliocene) for sediment that they suggested may be part of the Mashel Formation. They dismissed a 4.6 Ma TuffZirc age in favor of the youngest single zircon in their sample because TuffZirc would have excluded the eight youngest zircons, which form a steady progression of slightly younger ages that Polenz and others (2023) did not feel should be collectively ignored in this detrital sample. Despite a lack of continuous exposure between the type section and their age site, we confidently interpret their site as Mashel Formation because it (1) shares all the attributes that distinguish Mashel Formation from Quaternary Puget lowland sediment (see unit RMC_m); (2) resembles no other known geologic units nearby; and (3) yielded dacite pumice clasts that, based on geochemistry, may be from the same eruption as pumice clasts from Mashel Formation in the Eatonville quadrangle (see *Implications of pumice clast geochemistry*). We infer that the Mashel Formation ranges to Pliocene age west of the map area, and if the dacite pumice clasts from west of the map area are indeed from the same eruption as those from the map area, at least part of the formation in the Eatonville quadrangle likely is also <4.1 Ma old. Since detrital deposits are younger than the zircons they contain, we also cannot rule out a Pliocene age for the type section. If the age of the type section is closer to 6 Ma (or even 5.2–5.3 Ma), present age data and lack of documented stratigraphic continuity leave room for an unconformity within the formation in the Eatonville quadrangle.

POLLEN CONTENT

Pollen counts from the Mashel Formation type section (Christopher Schiller, written commun., 2024) and fossil site F1 of Polenz and others (2023) (0.9 km west of the Eatonville quadrangle) share an abundance of early successional riparian taxa (especially alder and willow; Christopher Schiller, written commun., 2024). Their presence is consistent with volcanic disturbance suggested by the formation's high content of volcanic glass, tephra, lahar

runout sands, and pumice. Low pollen concentrations (<3,600 palynomorphs/g sediment) contributed to Polenz and others' (2023) suggested interpretation of high sedimentation in a proximally volcanoclastic environment (at their fossil site F1). At the type section in the Eatonville quadrangle, pollen concentrations can be higher (up to 33,200 palynomorphs/g sediment), but range to nearly barren (Christopher Schiller, written commun., 2024).

IMPLICATIONS OF PUMICE CLAST GEOCHEMISTRY

Whole-rock analyses of 10 Mashel Formation pumice clasts indicate all are calc alkaline. Nine are dacite (G2–4 from Eatonville, G5–7 from the Ohop Valley, and three dacites from just west of the map area; Polenz and others, 2023). One is andesite (G12 from a Nisqually River cutbank). Based on their chemical traits these clasts were sourced from a single (as yet unidentified) volcanic center in the Cascade Range. Indeed, the compositional similarity of the dacites (64.7–67.6 wt % SiO_2 , 1.6–2.1 wt % MgO , 124–162 ppm Zr, and 20.7–27.3 ppm Rb) leads us to suggest they could all be from a single eruption. If so, their three sample sites in Eatonville, the Ohop Valley, and the Nisqually Valley west of the map area likely share the same age, and that age may differ from the age of the type section, where pumice clast geochemistry remains unassessed (see *Age Revision*). Notably, all samples also classify as adakites (Defant and Drummond, 1990) based on having $\text{Sr} > 400$ ppm, $\text{Sr}/\text{Y} > 20$, $\text{Yb} < 1.8$ ppm, and $\text{La}/\text{Yb} > 10$. Adakites suggest derivation from melting of a garnet-bearing mafic rock, usually assumed to be either a subducting plate or deep arc crust (Defant and Drummond, 1990).

Summarizing the Northcraft Formation

We interpret all observed bedrock in the map area as Northcraft Formation. The Eatonville quadrangle is the latest of four adjacent 1:24,000-scale mapping projects with extensive Northcraft Formation exposures. From east to west, the 7.5-minute quadrangles include Eatonville, Bald Hill, and the northern parts of the Lake Lawrence and Vail quadrangles (Fig 1; Polenz and others, 2021, 2022, 2023, and this map). Over 150 whole-rock chemical analyses and 31 ages from the recent mapping characterize the Northcraft Formation in greater detail than any other early Washington Cascades formation in terms of chemistry and age. Observed characteristics, ages, and geochemical traits revealed no breaks that would suggest classifying these rocks as other than Northcraft Formation.

AGES

Eight new Northcraft Formation ages in the Eatonville quadrangle span 37.9–34.6 Ma (age sites GD6 and GD1; Table 1). These ages represent the young end of an ~11 m.y. age range (45.8–34.6 Ma) documented by 31 Northcraft Formation ages from the Eatonville, Bald Hill, Lake Lawrence, and Vail quadrangles (Fig. 2; Table 1; Polenz and others, 2021, 2022, 2023). These ages confirm an eastward-younging trend suggested by Polenz and others (2022, 2023) and clearly seen on Figure 2. A 32.7 ± 1.5 Ma age that Hagen (1987) attributed to Northcraft Formation 2.6 km east of the Eatonville quadrangle suggests this trend

may continue eastward and, if accurate, expands the Northcraft Formation age range to about 13 m.y. (45.8–32.7 Ma). A 23.2 ± 1.7 Ma age that Hagen reported as Northcraft Formation 5.8 km south of the Eatonville quadrangle is suspect according to Phillips and others (1986). The cause of the eastward-younging trend is not known but conceivable reasons include shallowing over time of the dip of the subducting slab (causing arc magma formation to migrate east) and (or) block rotation within the North American plate moving the map area westward relative to the magmatic source.

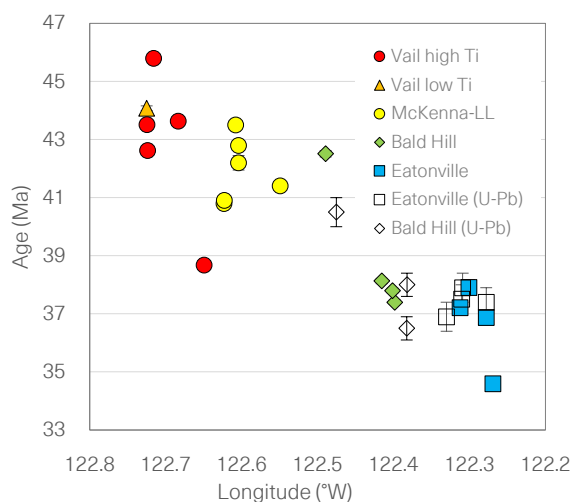


Figure 2. Radiometric ages of Northcraft Formation samples versus longitude. Ages are $^{40}\text{Ar}/^{39}\text{Ar}$ except for seven U-Pb ages (open symbols). Age error bars (vertical axis) are 2-sigma analytical (internal) error for $^{40}\text{Ar}/^{39}\text{Ar}$ ages and 2-sigma absolute (external) error for U-Pb ages. Plot includes new data for this quadrangle with previously published data from adjacent 7.5-minute quadrangles: Vail=Tenalquot Prairie-Vail (Polenz and others, 2021); McKenna-LL=McKenna-Lake Lawrence (Polenz and others, 2022); and Bald Hill (Polenz and others, 2023); same abbreviations and data sources apply to Figs. 3–7.

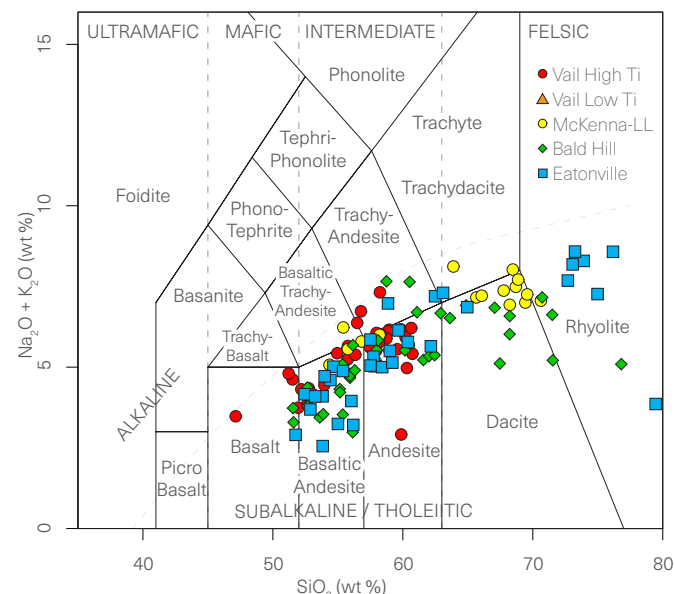


Figure 3. Total alkalis versus silica plot (Le Bas and others, 1986) for Northcraft Formation samples. The plot illustrates that the formation is mostly intermediate igneous but compositions range from basalt to rhyolite.

GEOCHEMICAL TRAITS AND EVOLUTION

The geochemical traits of the Northcraft Formation are consistent with the early arc setting implied by the age of the unit. The Northcraft Formation ranges from basalt to rhyolite (47.1–76.8 wt % SiO_2 , 0.1–10.1 wt % MgO) but basaltic andesite and andesite dominate (66% of samples; Fig. 3). Most samples classify as

calc alkaline on an AFM diagram (Fig. 4a) but tholeiitic on an FeO/MgO plot (Fig. 4b). On major oxide variation diagrams the samples define trends usually seen in subduction-related suites: as SiO_2 increases, $\text{Fe}_2\text{O}_3\text{t}$ decreases (Fig. 5), as do Al_2O_3 , MgO, MnO, and CaO, whereas K_2O increases; TiO_2 shows a hump pattern (Fig. 5), as do Na_2O , and P_2O_5 . In general, data from all four quadrangles overlap on these plots (Fig. 5), except

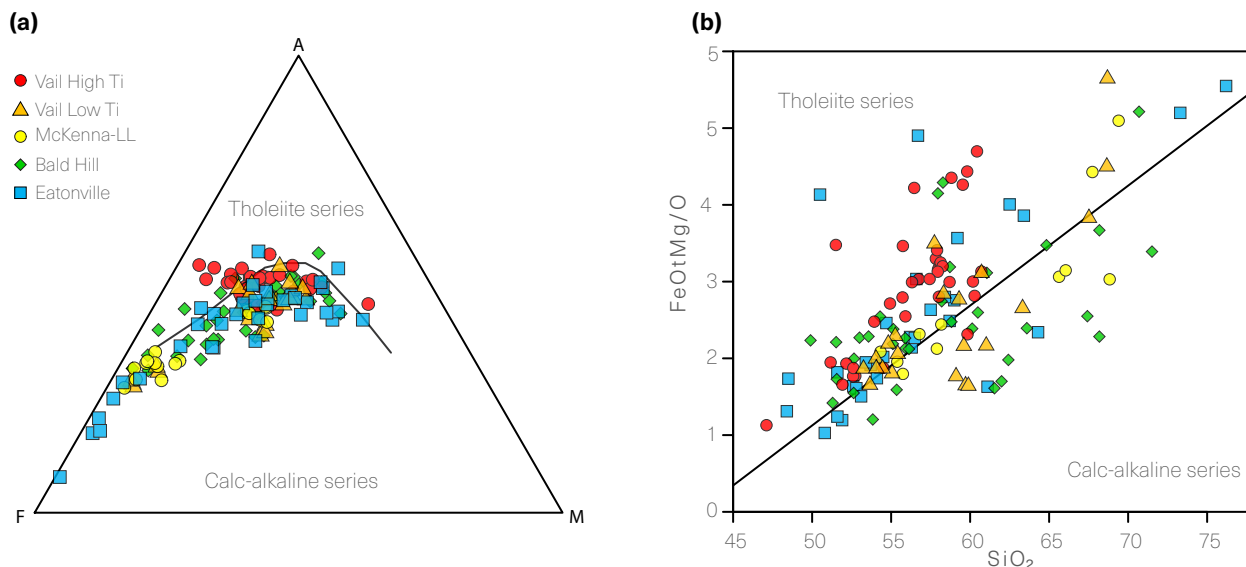


Figure 4. (a) AFM diagram plotting relative abundances of oxides of alkalis (A: $\text{Na}_2\text{O}+\text{K}_2\text{O}$), total iron (F: FeO and Fe_2O_3 —presented as $\text{Fe}_2\text{O}_3\text{t}$ in the Data Supplement and FeOt in the plot on the right) and magnesium (M: MgO) (Irvine and Baragar, 1971). The plot shows that most Northcraft samples classify as calc-alkaline. (b) FeOt/MgO- SiO_2 plot (Miyashiro, 1974) in which most samples classify as tholeiitic. In both diagrams the high TiO_2 samples have the strongest tholeiitic affinities.

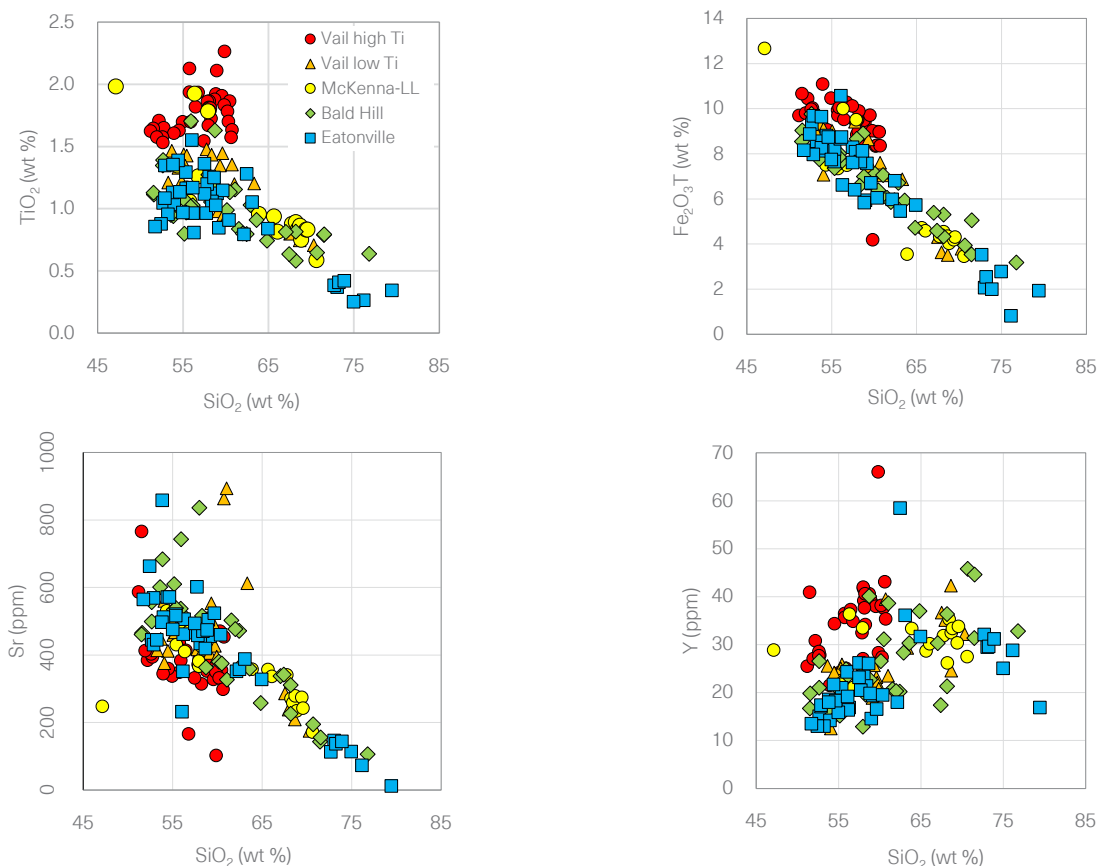


Figure 5. Representative major and trace element Harker variation diagrams. Note that data from all four quadrangles generally overlap, with the exception of the high- TiO_2 samples from Vail, which are distinguished from the rest by higher Y, TiO_2 , and $\text{Fe}_2\text{O}_3\text{t}$ (where “t” indicates total iron content), and by lower Sr.

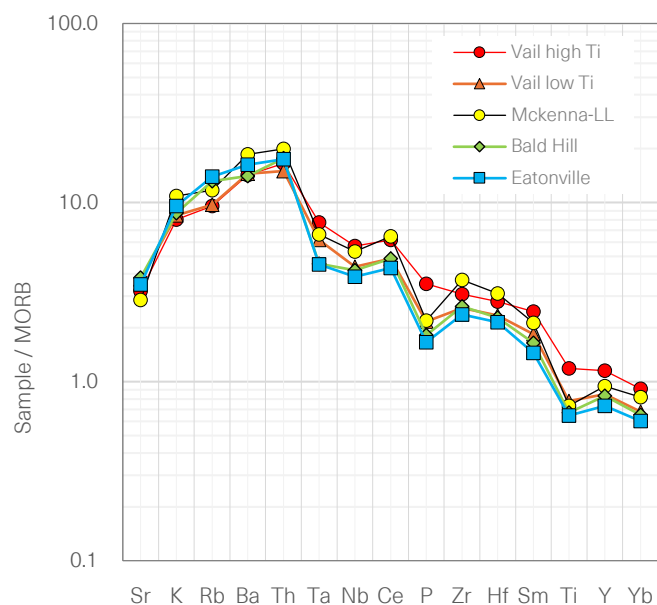


Figure 6. Mid-ocean-ridge basalt (MORB)-normalized spider diagram showing K-Rb-Ba-Th enrichments and Ta-Nb depletions characteristic of subduction-related magmas. Plotted values are averages for each quadrangle. Note that both subduction traits tend to become more pronounced from west to east (Vail to Eatonville). Depletions in P and Ti reflect fractionation of apatite and ilmenite in some samples. Data normalized to the MORB values of Sun and McDonough (1989).

for a subset of samples, mainly from the Vail quadrangle, that differ in having higher TiO_2 and Fe_2O_3 (Fig. 5), higher P_2O_5 , and lower Al_2O_3 .

Northcraft Formation trace element characteristics are also indicative of subduction-related magmatism (Winter, 2010). These characteristics include enrichments in large ion lithophile elements (Rb, Sr, Ba) and depletions in high field strength elements (Ta, Nb) on spidergrams (Fig. 6), and moderate light rare earth element enrichment, with average $\text{La}/\text{Yb} = 6.6\text{--}7.3$. One third of the Northcraft basaltic andesites and andesites have traits of adakites ($\text{Sr} > 400$ ppm, $\text{Yb} < 1.8$ ppm, $\text{Sr}/\text{Y} > 20$), a rock produced by melting of a garnet-bearing source, generally assumed to be eclogite within a subducting slab or mafic lower crust (Defant and Drummond, 1990). Adakite abundance increases eastward from 4 percent in Vail to 70 percent in Eatonville. None of the high TiO_2 samples from Vail are adakites, and these rocks also differ from other Northcraft samples in having higher average REE contents and lower Sr and Ba/Nb—for instance, Ba/Nb averages 14.4 in the high TiO_2 group versus 19.2 in the other samples, whereas >20 is typical of arc settings (Wilson, 1989).

The eastward younging of Northcraft Formation ages (Fig. 2) corresponds to a magmatic migration rate of 3–4 mm/yr (based on the distance between the oldest and youngest dated samples divided by the difference in their ages). Dated samples have revealed no discernible chemical trends over time except that the oldest rocks (>43 Ma) belong almost exclusively to the high TiO_2 group. Other chemical traits of the high TiO_2 group, including its tholeiitic affinity and low Ba/Nb, indicate an immature arc setting (Winter, 2010) consistent with being the earliest manifestation of the Cascade arc. Across the ~ 35 km geographic extent of recently mapped Northcraft rocks (this study; Polenz and others, 2021,

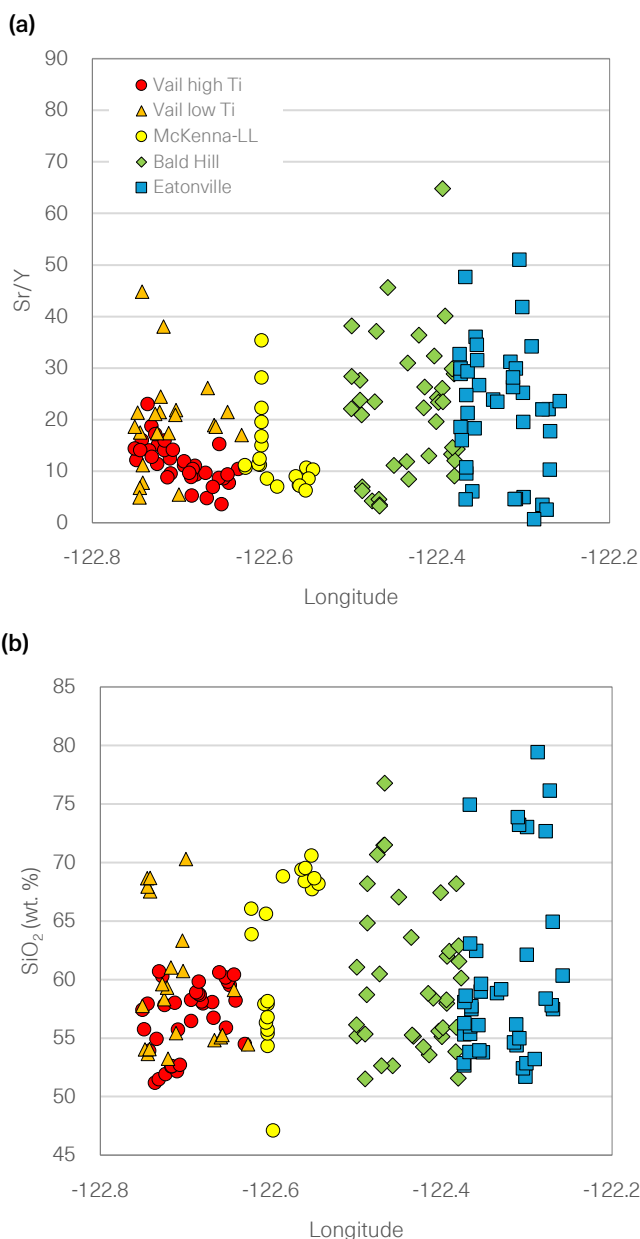


Figure 7. Examples of spatial geochemical trends among Northcraft Formation samples. (a) Eastward increase in the abundance of rhyolites and thus also lithologic diversity. Note that the SiO_2 content of the most mafic lavas remains strikingly uniform across the formation. (b) Eastward increase in the abundance of adakites ($\text{Sr}/\text{Y} > 20$), which suggests an increase in the depth of melting across the formation.

2022, 2023) there is an eastward increase in lithologic diversity, as rhyolites grow from <1 percent to 17 percent of the samples, and adakites become more common (Fig. 7b). Most other spatial trace element patterns arise from the high- TiO_2 samples being restricted to the western portion of the four map areas. Higher proportions of felsic rocks and adakites may reflect an eastward (or temporal) increase in crustal thickness, which would promote deeper crustal melting and slower magma ascent, allowing for more magma differentiation.

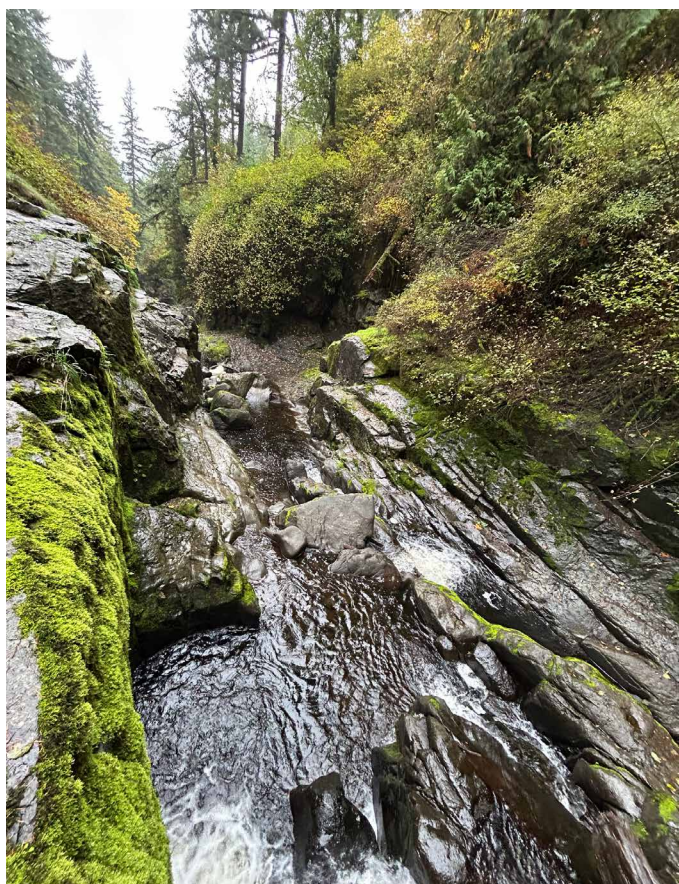


Figure 8. Bedrock box canyon along the Little Mashel River exposes and parallels near-vertical joints in the Northcraft Formation.

Structural, Subsurface, and Geophysical Attributes of the Map Area

FAULTS AND JOINTS

Although we observed several fault exposures in the Eatonville quadrangle, none could be traced beyond individual outcrops, and none coincided with notable geophysical lineaments. All are therefore probably minor. A few fault sets may nonetheless be locally notable.

Northeast-striking, near-vertical faults and fault-parallel dikes are exposed in quarries at geochemistry sites G29–G30 and G32–G33. Faint slickenlines at both sites mainly suggest strike-slip, but with unresolved sense of offset. At G32–G33, cataclasite thickness locally approaches 3 m, with less prominent gouge mostly concentrated in approximately fault-parallel seams that are 1s to 10s of cm thick. Near these faults, straight drainage reaches and lineaments, individually up to 2 km long, are similarly northeast oriented. A left-lateral fault west of the Eatonville quadrangle (2.3 km west-southwest of G32–G33; Polenz and others, 2023) appears to strike within 20 degrees of the above-noted faults. Together, these features suggest a ~6-km-long, ~4-km-wide zone with northeast-striking, steeply dipping strike-slip faults; no lineaments (topographic or geophysical) apparently extend southwest beyond Polenz and others' (2023) fault exposure or northeast beyond the Nisqually River valley—beyond which Vashon glacial deposits mostly obscure underlying structures.



Figure 9. Densely jointed zone along the west-flowing Mashel River.

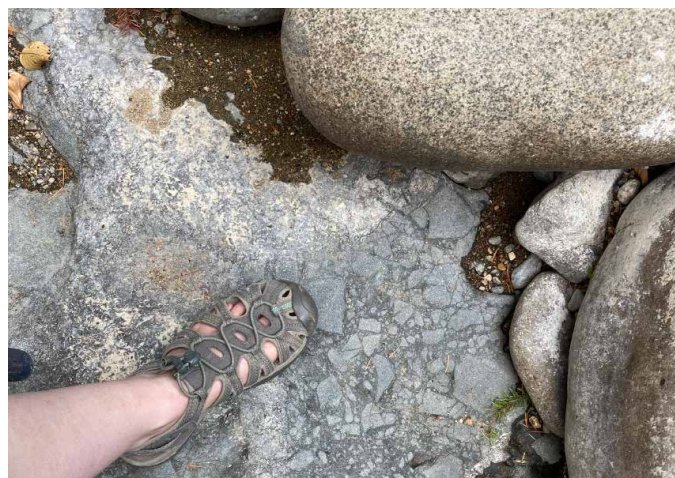


Figure 10. Brecciated andesitic basalt, bracketed by joint sets (not pictured).

Bedrock box canyons along the Mashel and Little Mashel Rivers expose north-northwest-striking, mostly steeply dipping joint sets. Whereas the Little Mashel canyon follows the joints (Fig. 8), the west-flowing Mashel River crosses densely jointed zones, each <20 m wide (Fig. 9). Some (or all?) zones include joint-parallel faults with mm- to cm-thick gouge. Gouge and slicken surface exposures are subtle, perhaps due to river scour. At least one joint set brackets brecciated basaltic andesite (Fig. 10). Together, these joint sets and faults suggest a locally dominant, north-northwest-oriented structural fabric in this part of the Eatonville quadrangle.

BEDDING ORIENTATIONS IN THE MASHEL FORMATION

Widespread, gentle, westward apparent dips in the Mashel Formation west of Eatonville may reflect sediment compaction and (or) subsidence in the Tacoma basin. In contrast, a gentle eastward dip observed in a single exposure in the City of Eatonville (in a single exposure 80 m SSE of age site GD1) may be related to subsidence and (or) compaction in a possible basin centered to the northeast of the quadrangle, the existence of which is suggested by a gravity low (EGL on Fig. M1A). Intermittent Mashel Formation exposures west of the Eatonville quadrangle and within the quadrangle in cliffs along the Ohop Valley and along the valleys of the Mashel and Nisqually Rivers reveal westward apparent dips of 1–4 degrees (Polenz and others, 2023). A gently northwest-dipping bed in the Mashel Formation type section (225°/8° NW) suggests that the above-mentioned apparent dips may understate northwesterly dips in the northwestern part of the Eatonville quadrangle. In contrast, a bed 1.75 km southwest of the northeastern quadrangle corner dips gently northeast (333°/8° NE)—and is located at the western edge of a mild gravity low ('EGL' in Fig. M1A—approximately –10 mGal relative to the center of the quadrangle). The northeasterly dip here may signal beds dipping into a small basin (or sub-basin within the Tacoma basin?) near the northeastern quadrangle corner.

The westward dip of the Mashel Formation west of Eatonville suggests westward thickening of the Mashel Formation on Cross Section A–A'. This thickening may be accommodated by unit M0C in fact being partly Mashel Formation.

GEOPHYSICAL ANALYSES

We present a combined isostatic gravity and aeromagnetic geophysical anomaly map (Fig. M1A) and a geophysical model (Fig. M1B) that support our interpretations in the geologic map and cross section. The geophysical model is a 2D forward modeling of aeromagnetic and gravity data along line X–X' (Fig. M1A) colocated with the geologic Cross Section A–A'. Model unit properties are obtained from measured field samples (Fig. M1B and Table C1), published data, and WGS records. By understanding gravity and aeromagnetic anomalies in both the map view and model in conjunction with geologic observations from the surface, we interpret the attributes of Northcraft Formation volcanics, deposits in the Tacoma Basin, deeper subsurface lithologies and the geometry of the Tacoma basin edge.

AEROMAGNETIC ATTRIBUTES OF NORTHCRAFT FORMATION VOLCANIC AND INTRUSIVE ROCKS

Geophysical map Figure M1A illustrates several high-amplitude (≥ 450 nT) aeromagnetic highs (MNV and MV in Fig. M1A, B). We attribute the moderate-wavelength (4–5 km) aeromagnetic highs (MNV in Fig. M1A) to near-surface magnetic rocks such as Northcraft Formation andesite, basaltic andesite, and dacite (units Ev_{an} and Ev_{dn}) (Fig. M1B and Table C1). We similarly interpret several high-amplitude, shorter-wavelength (1–2 km) aeromagnetic anomalies as volcanic centers or intrusive bodies (MV in Fig. M1A, B; unit E_{lin}).

In order to fit the highest amplitude magnetic high along model line X–X' (MV in Fig. M1A, B), our model requires a

tall, narrow, strongly magnetic body. This magnetic body is best explained by intrusion of material similar to unit E_{lin} which is strongly magnetic (Table C1) and exposed nearby.

Our model accommodates an aeromagnetic low southeast of the modeled intrusion (ML in Fig. M1A, B) with an ~800-m-thick, moderately dense, non-magnetic rhyolite tuff (unit Ev_{tn}) (Fig. M1B and Table C1). Rhyolite tuff exposures dominate the more than 370 m of relief northeast to northwest of La Grande, consistent with thick tuff below the surface. We therefore favor a model with thick tuff compared to alternative unit combinations with similarly good geophysical data fit. Alternative models included (1) thick deposits of non-magnetic andesite (wherein hydrothermal alteration lowered the magnetic susceptibility), or (2) thick and dense, non-magnetic sedimentary material closer to the surface.

In the southern third of the model cross section X–X' and in the map area, we observe a gradual, relatively muted, broad (about 2 km), moderate-wavelength, and positive aeromagnetic anomaly (100 to 350 nT) (IV in Fig. M1A, B). Glacial deposits mostly cover the surface, and we interpret the aeromagnetic high as volcanoclastic rocks and lava flows interfingering with tuffs and sedimentary deposits. The presence of geographically coincident aeromagnetic and gravity highs both east and west of the model line suggests that these lava flows and volcanoclastics may be sourced from multiple directions (IV, MV, and MNV in Fig. M1A; units Ev_{an}, Ev_{tn}, Ev_{cn}, and Env).

Moderately high amplitude (>100 nT), moderate wavelength (4–5 km) aeromagnetic anomalies such as TBV in Fig. M1A suggest buried, strongly magnetic flows or vents within the Tacoma basin, as previously inferred northwest and west of the Eatonville quadrangle (Polenz and others 2021, 2022, 2023; Contreras and others, 2023).

GEOPHYSICAL ATTRIBUTES OF ROCKS AND SEDIMENT IN THE TACOMA BASIN

We interpret rocks and sediment in the Tacoma basin as a combination of volcanic rocks, sedimentary rocks, and sediment, all of which we collectively consider to be basin fill, with the caveat that some of the older sedimentary and volcanic rocks may predate basin development. We infer rock types and corresponding geologic units primarily from our 2D-forward modeling (Fig. M1B). This section discusses our model units and constraints, in order of increasing depth:

We observed sediment with low density ($\rho = 1,920$ – $2,210$ kg/m³) and low magnetic susceptibility ($\chi = 0$ – 0.6×10^{-3} SI) (units Q and R0C in Fig. M1B and Table C1) at the surface and used its gravity and aeromagnetic properties to model near-surface sediment in our 2D-forward modeling. The ~300 m (1,000 ft) combined thickness of near-surface sediment in the northern half of the Eatonville quadrangle (units Q and R0C in Fig. M1B) is based on the observed section in the Willhoite well. This is because in geophysical models, the thickness of the near-surface sediments is difficult to define and can to some extent be traded against that of underlying units. In two shallow segments within model unit R0C (separated by dashed lines in Fig. M1B) we imposed lower magnetic susceptibility (0 instead of 0.6×10^{-3} SI 1.9 km from model end point X) and density (1,950 instead of 2,210 kg/m³, 2.6 km from model end point X) to fit short-wavelength anomalies in the aeromagnetic and gravity data (BFA in Fig. M1B). We

attribute these short wavelength anomalies to local variations in lithology within the unit that may be caused by contacts with glacial sediments, paleo topography, or variations in thickness of flow deposits. These variations are too high resolution for us to fully resolve with currently available data, physical properties, and geologic field observations.

Below units Q and R0c we model Tacoma basin fill ~0–0.5 km below mean sea level as Eocene interfingering volcanic and sedimentary deposits (model unit Env in Fig M1B; see also geologic unit Env). This unit is similar to Tacoma basin model units in previous WGS models (Contreras and others, 2023; Polenz and others, 2021, 2022, 2023) and is supported by the Willhoite well log. Conceptually this unit combines volcanic and sedimentary deposits that have been slightly compacted with depth. For this unit we thus assume a density similar to that of Northcraft Formation volcanoclastic deposits ($\rho = 2,380 \text{ kg/m}^3$). We also assume a slightly higher magnetic susceptibility than that of volcanoclastics or sedimentary deposits ($25 \times 10^{-3} \text{ SI}$) because of the presence of buried, strongly magnetic flows or vents within the Tacoma basin. Although the unit is necessary to the model, the thickness is difficult to constrain and can be traded against underlying or overlying units.

Eocene Sediment Below the Northcraft Formation

Geophysical modeling can be used to interpret units of rock deeper in the subsurface that may be causing broad trends in gravity. Gravity values gradually increase from the northwest corner of the Eatonville quadrangle (–13 mGal) to the southwest (>10 mGal south of the Bald Hill quadrangle) and the contours form a somewhat curvilinear map pattern (CLG in Fig. M1A). Our model attributes this gravity increase to a southward rise in elevation of the Crescent Formation basement, as did prior modeling west of the Eatonville quadrangle (Polenz and others, 2023). Our modeling along line X–X' (Fig. M1A) further infers dense, non-magnetic ($\rho = 2,600 \text{ kg/m}^3$, $\chi = 0 \times 10^{-3} \text{ SI}$) Eocene sedimentary rock (unit En) that overlies Crescent Formation, underlies Northcraft Formation, and continues laterally across the entire model (Fig. M1B). Our model's inference of unit En agrees with inferences by magnetotelluric modelers who interpret Eocene sedimentary rocks 1–10 km below the surface in and near our map area (Stanley and others, 1994). Eocene sedimentary rocks of potentially similar age are exposed 10.5 km south-southeast of the model line (and nearer the map area farther west), but their exact depth and extent beneath the map area are constrained only by modeling. Unit En causes our model to increase the depth to Crescent Formation basement. This is needed to accommodate overlying moderately dense and strongly magnetic rocks such as the Northcraft Formation, which is exposed along parts of the model line (Fig. M1B, units Ev_n, Ev_t, Ev_c and Env).

Geophysical Attributes and Geometry of the Tacoma Basin Edge

West of the Eatonville quadrangle, the southwestern margin of the Tacoma basin is clearly delineated by the Olympia fault (Brocher and others, 2001; Polenz and others, 2021, 2022; Fig. 1). In the Bald Hill quadrangle between the Olympia fault and the Eatonville quadrangle, Polenz and others (2023) favored

north-down normal faulting along the southern edge of the Tacoma basin. Within the Eatonville quadrangle, the Tacoma basin edge is less distinct and may or may not be fault bounded. Gravity and magnetic values decrease gradually from the center of the quadrangle to the east, north, and west, with the greatest overall decrease trending north-northwest into the center of the Tacoma basin (TB in Fig. M1A). Strong, linear gradients that would suggest a faulted basin edge are not apparent (Fig. M1A). Because of the gradual gravity decreases and the presence of moderate gravity lows (–11 mGal or less) east of the quadrangle (EGL in Fig. M1A), it is unclear if the Tacoma basin ends near the northwestern quadrangle corner or extends farther south into the quadrangle and (or) east of the quadrangle.

Our 2D-forward modeling cannot resolve if the southern margin of the Tacoma basin is faulted or folded. The model in Fig. M1B combines a geologically reasonable and relatively simple interpretation with best-fit gravity and magnetic data—and does not require faults or folds. Models that add fault(s) with small (approx. 250 m) north-down offset or folding with similar north-down basin lowering just north of the quadrangle can fit the data similarly well. The fault(s) can be vertical or dip south or north. Separately, at or just south of the intrusion at the center of section X–X' (MV in Fig. M1A, B), models can fit the data well with a basement anticline or vertical fault with about 400 m south-down offset. Our geologic mapping provides no evidence for—nor precludes—faults at either of the model-driven possible locations (near the center of section X–X' or near the northern map edge). We chose to present a non-faulted model in Fig. M1B because the Eatonville quadrangle lacks strong, linear anomalies in both aeromagnetics and gravity (which would likely accompany a regionally significant dip-slip fault), and because faulting does not improve model fit. However, west of section X–X' (approximately at the latitude of La Grande Reservoir), we and Polenz and others (2023) observed northeast-striking strike-slip faults and northeast-trending topographic lineaments (see *Faults and Joints*) that would project faulting across section X–X' between the above-mentioned fault model locations. Although the locations of geologically observed faulting and geophysically modeled possible faulting do not coincide, all of the above geologic and geophysical evidence could be explained by a northeast-striking, strike-slip fault system that would not require a strong geophysical footprint.

Suggestions for Further Study

- Acquire more bedding orientations from the Mashel Formation to explore if those presented here are representative and can be explained by basin fill compaction or require other explanations.
- Acquire additional ages from the Mashel Formation to establish whether the unit includes an unconformity and whether its age range extends to younger than 4.1 Ma.
- Luminescence dating and systematic assessments of weathering, lithologies (clasts and matrix), and soil development offer potential to refine mapping of alpine drift and alluvium (thicknesses, geographic distribution, and alpine ice limits—especially maximum northern extents near the eastern map edge and along and west of the Nisqually River). Detrital

U-Pb age analysis may help separate some strongly weathered sediment from Northcraft Formation.

- Review well records and well-water arsenic content, and where possible observe (and test?) drill cuttings to link geologic unit(s) to aquifer(s) with elevated arsenic content—building on efforts of Tacoma-Pierce County Health Department (2023), Contreras and others (2023), Polenz and others (2023), and Walters and Kimmel's (1968) note on geographic distribution of wells with elevated bicarbonate content.
- Collect and analyze additional gravity data north and east of the map area to better understand the extent and edge of the Tacoma basin.

ACKNOWLEDGMENTS

We thank: Christopher Schiller (Burke Museum) for sampling and analysis of fossil pollen; Pat Pringle (WGS retired) and Barry Goldstein (University of Puget Sound retired) mainly for insights into Quaternary debris flow and flood deposits; Frank Hladky (WGS retired) for advice, reviews, and correspondences; Tim Walsh (WGS retired) for context and conversations; Paul Kester (Burke Museum) for collaboratively sampling plant macrofossils for assessment and addition to Burke Museum collections; Michael Nesbitt for assistance with fossil sampling; Megan Anderson and Todd Lau (both WGS) for guidance on geophysical data collection, modeling, and interpretation; Kiersten Wilbur and Todd Lau (WGS) for geophysical data collection; Lowell Dickson (DNR) for captaining our boat on Alder Lake; Sheelagh McCarthy (DNR) and Mac McKay (WGS retired) for assistance with field work; all WGS staff who provided suggestions, edits, and guidance; Weyerhaeuser Company, Manke Lumber Company, the Pack Forest, the city of Tacoma, the Nisqually Land Trust, Washington State Parks, and many other landowners for access, local knowledge, historical context, well records, and other information. Research within Nisqually State Park was conducted under Washington State Parks and Recreation Commission Scientific Research Permit 230704.

AUTHOR CONTRIBUTIONS

C. Lambert and M. Polenz performed geological field work. C. Lambert performed petrography. A. Bauer collected, processed, and modeled geophysical data, prepared the geophysical figures, appendix, and data supplement, and drafted geophysics-centered text. G. Legorreta Paulín provided Landsat data analysis. E. Nesbitt participated in fossil sampling, examined samples for microfossils, and contributed expertise mainly for regional stratigraphic context. M. Polenz functioned as project lead, drafted GIS features and the overall report, and led geologic fieldwork. J. Tepper analyzed geochemistry, prepared the geochemical data supplement, and drafted the geochemical discussion.

REFERENCES

- Ali, A. E.; El Khidir, S. O.; Babikir, I. A. A.; Abdelrahman, E. M., 2012, Landsat ETM+ 7 digital image processing techniques for lithological and structural lineament enhancement: Case study around Abidiya Area, Sudan: *The Open Remote Sensing Journal*, v. 5, p. 83–89. [<https://doi.org/10.2174/1875413901205010083>]
- Anderson, M. L.; Blakely, R. J.; Wells, R. E.; Dragovich, J. D., 2024, Deep structure of Siletzia in the Puget Lowland: Imaging an obducted plateau and accretionary thrust belt with potential fields: *Tectonics*, v. 43, no. 2, article e2022TC007720. [<https://doi.org/10.1029/2022TC007720>]<https://doi.org/10.1029/2022TC007720>
- Barnes, D. F.; Oliver, H. W.; Robbins, S. L., 1969, Standardization of gravimeter calibrations in the geological survey: *Eos Transactions*, v. 50, no. 10, p. 626–627. [<https://doi.org/10.1029/EO050i010p00526>]
- Black, L. P.; Kamo, S. L.; Allen, C. M.; Davis, D. W.; Aleinikoff, J. N.; Valley, J. W.; Mundil, Roland; Campbell, I. H.; Korsch, R. J.; Williams, I. S.; Foudoulis, Chris, 2004, Improved $^{206}\text{Pb}/^{238}\text{U}$ microprobe geochronology by the monitoring of a trace-element-related matrix effect; SHRIMP, ID-TIMS, ELA-ICP-MS and oxygen isotope documentation for a series of zircon standards: *Chemical Geology*, v. 205, no. 1–2, p. 115–140. [<https://doi.org/10.1016/j.chemgeo.2004.01.003>]
- Blakely, R. J., 1995, *Potential theory in gravity and magnetic applications*. Cambridge University Press. [<https://doi.org/10.1017/CBO9780511549816>]
- Blakely, R. J.; Wells, R. E.; Weaver, C. S., 1999, Puget Sound aeromagnetic maps and data: U.S. Geological Survey Open-File Report 99-514, version 1.0. [<http://geopubs.wr.usgs.gov/open-file/of99-514/>]
- Blakely, R. J.; Sherrod, B. L.; Weaver, C. S., 2020, High-resolution aeromagnetic survey of the Centralia area, southwest Washington: U.S. Geological Survey data release. [<https://doi.org/10.5066/P9T4UC6W>]
- Blakely, R. J.; Bennett, S. E. K.; Staisch, L. M.; Wells, R. E.; O'Connor, J. E., 2024, High-resolution aeromagnetic survey over Packwood, Washington, and surrounding areas: U.S. Geological Survey data release. [<https://doi.org/10.5066/P9UJHQU1>]
- Booth, D. B.; Troost, K. G.; Clague, J. J.; Waitt, R. B., 2004, The Cordilleran ice sheet. In Gillespie, A. R.; Porter, S. C.; Atwater, B. F., editors, *The Quaternary period in the United States*: Elsevier, p. 17–43. [[https://doi.org/10.1016/S1571-0866\(03\)01002-9](https://doi.org/10.1016/S1571-0866(03)01002-9)]
- Bretz, JH, 1911, The terminal moraine of the Puget Sound glacier: *Journal of Geology*, v. 19, no. 2, p. 161–174. [<https://doi.org/10.1086/621826>]
- Bretz, JH, 1913, Glaciation of the Puget Sound region: Washington Geological Survey Bulletin 8, 244 p., 3 plates. [http://www.dnr.wa.gov/publications/ger_b8_glaciation_pugetsound.pdf]
- Brocher, T. M.; Parsons, T. E.; Blakely, R. J.; Christensen, N. I.; Fisher, M. A.; Wells, R. E.; SHIPS Working Group, 2001, Upper crustal structure in Puget Lowland, Washington: Results from the 1998 Seismic Hazards Investigations in Puget Sound: *Journal of Geophysical Research Solid Earth*, v. 106, no. B7, p. 13,541–13,564. [<https://doi.org/10.1029/2001JB000154>]
- Brocher, T. M.; Wells, R. E.; Lamb, A. P.; Weaver, C. S., 2017, Evidence for distributed clockwise rotation of the crust in the northwestern United States from fault geometries and focal mechanisms. *Tectonics*, v. 36, no. 5, p. 787–818, [<https://doi.org/10.1002/2016TC004223>].
- Brown, Olivia; Harris, J. R.; Utting, Daniel; Little, E. C., 2007, Remote predictive mapping of surficial materials on northern Baffin Island: developing and testing techniques using Landsat TM and digital elevation data: Geological Survey of Canada Current Research 2007-B1, 12 p. [http://epe.lac-bac.gc.ca/100/200/301/nrcan-rncan/gsc-cgc/current_research-c/2007/2007-B1/M44-2007-B1E.pdf]

- Buckovic, W. A., 1979, The Eocene deltaic system of west-central Washington. *In* Armentrout, J. M.; Cole, M. R.; Ter Best, Harry, Jr., editors, *Cenozoic paleogeography of the western United States*: Society of Economic Paleontologists and Mineralogists Pacific Section, Pacific Coast Paleogeography Symposium 3, p. 147–163. [https://archives.datapages.com/data/pac_sepm/024/024001/pdfs/147.htm]
- Chang, Zhaoshan; Vervoort, J. D.; McClelland, W. C.; Knaack, Charles, 2006, U-Pb dating of zircon by LA-ICP-MS: *Geochemistry, Geophysics, Geosystems*, v. 7, no. 5, p. 1–14. [<https://doi.org/10.1029/2005GC001100>]
- Clement, C. R.; Pratt, T. L.; Holmes, M. L.; Sherrod, B. L., 2010, High-resolution seismic reflection imaging of growth folding and shallow faults beneath the southern Puget Lowland, Washington State: *Bulletin of the Seismological Society of America*, v. 100, no. 4, p. 1710–1723. [<https://doi.org/10.1785/0120080306>]
- Contreras, T. A.; Goughnour, R. L.; Lau, T. R., 2023, *Geologic map of the Harts Lake 7.5-minute quadrangle, Pierce and Thurston Counties, Washington*: Washington Geological Survey Map Series 2023-04, 1 sheet, scale 1:24,000, with 16 p. text. [https://www.dnr.wa.gov/publications/ger_ms2023-04_geol_map_harts_lake_24k.zip]
- Crandell, D. R.; Miller, R. D., 1974, Quaternary stratigraphy and extent of glaciation in the Mount Rainier region, Washington: U.S. Geological Survey Professional Paper 847, 59 p., 2 plates. [<https://doi.org/10.3133/pp847>]
- Daneš, Z. F., 1985, Sedimentary thickness in the Puget Sound area, Washington, derived from aeromagnetic data: Washington Division of Geology and Earth Resources Open File Report 85-5, 14 p. [http://www.dnr.wa.gov/publications/ger_ofr85-5_puget_sound_sediment_thickness.pdf]
- Defant, M. J.; Drummond, M. S., 1990, Derivation of some modern arc magmas by melting of young subducted lithosphere, *Nature*, v. 347, p. 662–665. [<https://doi.org/10.1038/347662a0>]
- Dethier, D. P.; Bethel, John, 1981, Surficial deposits along the Cowlitz River near Toledo, Lewis County, Washington: U.S. Geological Survey Open-File Report 81-1043. [<https://doi.org/10.3133/ofr811043>]
- Dragovich, J. D.; Anderson, M. L.; MacDonald, J. H., Jr.; Mahan, S. A.; DuFrane, S. A.; Littke, H. A.; Wessel, G. R.; Saltonstall, J. H.; Koger, C. J.; Cakir, Recep, 2010, Supplement to the geologic map of the Carnation 7.5-minute quadrangle, King County, Washington—Geochronologic, geochemical, point count, geophysical, earthquake, fault, and neotectonic data: Washington Division of Geology and Earth Resources Open File Report 2010-2, 42 p. with 8 digital appendices. [https://www.dnr.wa.gov/Publications/ger_ofr2010-2_carnation_supplement.zip]
- Drost, B. W.; Ely, D. M.; Lum, W. E., II, 1999, Conceptual model and numerical simulation of the ground-water-flow system in the unconsolidated sediments of Thurston County, Washington: U.S. Geological Survey Water-Resources Investigations Report 99-4165, 262 p. [<https://doi.org/10.3133/wri994165>]
- Finn, C. A., 1990, Geophysical constraints on Washington convergent margin structure: *Journal of Geophysical Research*, v. 95, no. B12, p. 19,533–19,546. [<https://doi.org/10.1029/JB095iB12p19533>]
- Finn, C. A.; Phillips, W. M.; Williams, D. L., 1991, Gravity anomaly and terrain maps of Washington: U.S. Geological Survey Geophysical Investigations Map GP-988, 5 sheets, scale 1:500,000. [<https://doi.org/10.3133/gp988>]
- Flores, R. M.; Johnson, S. Y., 1995, Sedimentology and lithofacies of the Eocene Skookumchuck Formation in the Centralia coal mine, southwest Washington. *In* Fritsche, A. E., editor, *Cenozoic paleogeography of the western United States—II*: Society for Sedimentary Geology (SEPM) Pacific Section Book 75, p. 274–290. [https://archives.datapages.com/data/pac_sepm/092/092001/pdfs/274.html]
- Folk, R. L., 1980, *Petrology of sedimentary rocks*: Hemphill Publishing Company, 182 p. [<https://repositories.lib.utexas.edu/bitstreams/4537855d-d386-4794-bfbc-0f24715e64dc/download>]
- Futornick, Z. O.; Goldstein, B. S.; Parker, B. L.; Pringle, P. T., 2008, Sedimentologic evidence for a glacial outburst flood and resulting debris flow—Puget Lowland, Washington State [abstract]: *Geological Society of America Abstracts with Programs*, v. 40, no. 1, p. 70. [<https://gsa.confex.com/gsa/2008CD/webprogram/Paper135462.html>]
- Gard, L. M., Jr., 1968, *Bedrock geology of the Lake Tapps quadrangle, Pierce County, Washington*: U.S. Geological Survey Professional Paper 388-B, 33 p., 2 plates. [<https://doi.org/10.3133/pp388B>]
- Gaschnig, R. M.; Vervoort, J. D.; Lewis, R. S.; McClelland, W. C., 2010, Migrating magmatism in the northern US Cordillera: in situ U–Pb geochronology of the Idaho batholith: *Contributions to Mineralogy and Petrology*, v. 159, p. 863–883. [<https://doi.org/10.1007/s00410-009-0459-5>]
- Gower, H. D.; Yount, J. C.; Crosson, R. S., 1985, *Seismotectonic map of the Puget Sound region, Washington*: U.S. Geological Survey Miscellaneous Investigations Series Map I-1613, 1 sheet, scale 1:250,000, with 15 p. text. [<https://doi.org/10.3133/i1613>]
- Hagen, R. A., 1987, *The geology and petrology of the Northcraft Formation, Lewis County, Washington*: University of Oregon Master of Science thesis, 252 p., 1 plate. [<https://search.worldcat.org/title/16928679>]
- Haugerud, R. A., 2009, Preliminary geomorphic map of the Kitsap Peninsula, Washington; version 1.0: U.S. Geological Survey Open-File Report 2009-1033, 2 sheets, scale 1:36,000. [<https://doi.org/10.3133/ofr20091033>]
- Haugerud, R. A., 2021, Deglaciation of the Puget Lowland, Washington. *In* Waitt, R. B.; Thackray, G. D.; Gillespie, A. R., editors, *Untangling the Quaternary period—a legacy of Stephen C. Porter*: Geological Society of America Special Paper 548, p. 279–298. [[https://doi.org/10.1130/2020.2548\(14\)](https://doi.org/10.1130/2020.2548(14))]
- Heiskanen, W. A.; Vening-Meinesz, F. A., 1958, *The Earth and its gravity field*: McGraw-Hill Book Company, Inc., 470 p.
- Henriksen, D. A., 1956, Eocene stratigraphy of the lower Cowlitz River-eastern Willapa Hills area, southwestern Washington: Washington Division of Mines and Geology Bulletin 43, 122 p. [http://www.dnr.wa.gov/publications/ger_b43_eocene_stratigraphy.pdf]
- International Union of Geodesy and Geophysics, 1971, *Geodetic Reference System 1967*: International Association of Geodesy Special Publication no. 3, 116 p.
- Irvine, T. N.; Baragar, W. R. A., 1971, A guide to the chemical classification of the common volcanic rocks: *Canadian Journal of Earth Sciences*, v. 8, no. 5, p. 523–548. [<https://doi.org/10.1139/e71-055>]
- Iverson, N. R.; McCracken, R. G.; Zoet, L. K.; Benediktsson, Í. Ö.; Schomacker, Anders; Johnson, M. D.; Woodard, J., 2017, A theoretical model of drumlin formation based on observations at Múlajökull, Iceland: *Journal of Geophysical Research: Earth Surface*, v. 122, no. 12, p. 2302–2323. [<https://doi.org/10.1002/2017JF004354>]
- Kettles, I. M.; Rencz, A. N.; Bauke, S. D., 2000, Integrating Landsat, geologic, and airborne gamma ray data as an aid to surficial geology mapping and mineral exploration in the Manitowadge area, Ontario: *Photogrammetric Engineering & Remote Sensing*, v. 66, no. 4, p. 437–445. [https://www.asprs.org/wp-content/uploads/pers/2000journal/april/2000_apr_437-445.pdf]
- Koppers, A. A. P., 2002, ArArCALC—Software for $^{40}\text{Ar}/^{39}\text{Ar}$ age calculations: *Computers and Geosciences*, vol. 28, no. 5, p. 605–619. [[https://doi.org/10.1016/S0098-3004\(01\)00095-4](https://doi.org/10.1016/S0098-3004(01)00095-4)]
- Koppers, A. A. P.; Staudigel, Hubert; Malcolm, S. P.; Wijbrans, J. R., 2003, Short-lived and discontinuous intraplate volcanism in the South Pacific: Hot spots or extensional volcanism?: *Geochemistry, Geophysics, Geosystems*, v. 4, no. 10. [<https://doi.org/10.1029/2003GC000533>]

- Koppers, A. A. P.; Staudigel, Hubert; Wijbrans, J. R., 2000, Dating crystalline groundmass separates of altered Cretaceous seamount basalts by the $^{40}\text{Ar}/^{39}\text{Ar}$ incremental heating technique: *Chemical Geology*, v. 166, p. 139–158. [https://doi.org/10.1016/S0009-2541(99)00188-6]
- Kuiper, K. F.; Deino, Alan; Hilgen, F. J.; Krijgsman, Wout; Renne, P. R.; Wijbrans, J. R., 2008, Synchronizing rock clocks of earth history: *Science*, v. 320, no. 5875, p. 500–504. [https://doi.org/10.1126/science.1154339]
- Lanphere, M. A.; Baadsgaard, Halfdan, 2001, Precise K-Ar, $^{40}\text{Ar}/^{39}\text{Ar}$, Rb-Sr and U/Pb mineral ages from the 27.5 Ma Fish Canyon Tuff reference standard: *Chemical Geology*, v. 175, no. 3–4, p. 653–671. [https://doi.org/10.1016/S0009-2541(00)00291-6]
- Le Bas, M. J.; Le Maitre, R. W.; Streckeisen, A. L.; Zanettin, Bruno, 1986, A chemical classification of volcanic rocks based on the total alkali-silica diagram: *Journal of Petrology*, v. 27, no. 3, p. 745–750. [https://doi.org/10.1093/petrology/27.3.745]
- Lee, J. Y.; Marti, Kurt; Severinghaus, J. P.; Kawamura, Kenji; Yoo, Hee-Soo; Lee, J. B.; Kim, J. S., 2006, A redetermination of the isotopic abundances of atmospheric Ar: *Geochimica et Cosmochimica Acta*, v. 70, no. 17, p. 4507–4512. [https://doi.org/10.1016/j.gca.2006.06.1563]
- Lisiecki, L. E.; Raymo, M. E., 2005, A Pliocene-Pleistocene stack of 57 globally distributed benthic $\delta^{18}\text{O}$ records: *Paleoceanography*, v. 20, no. 1. [https://doi.org/10.1029/2004PA001071]
- Logan, R. L.; Walsh, T. J.; Stanton, B. W.; Sarikhan, I. Y., 2009, Geologic map of the Maytown 7.5-minute quadrangle, Thurston County, Washington: Washington Division of Geology and Earth Resources Geologic Map GM-72, 1 sheet, scale 1:24,000. [http://www.dnr.wa.gov/publications/ger_gm72_geol_map_maytown_24k.pdf]
- Ludwig, K. R., 2003, Isoplot 3.00: A geochronological toolkit for Microsoft Excel: Berkeley Geochronology Center, Berkeley, 70 p.
- Magsino, Sammantha; Sanger, Elizabeth; Walsh, T. J.; Palmer, S. P.; Blakely, R. J., 2003, The Olympia structure: Ramp or discontinuity? New gravity data provide more information [abstract]: *Geological Society of America Abstracts with Programs*, v. 35, no. 6, p. 479. [https://gsa.confex.com/gsa/2003AM/webprogram/Paper67057.html]
- McCaffrey, Robert; King, R. W.; Payne, S. J.; Lancaster, Matthew, 2013, Active tectonics of northwestern U.S. inferred from GPS-derived surface velocities: *Journal of Geophysical Research Solid Earth*, v. 118, no. 2, p. 709–723. [https://doi.org/10.1029/2012JB009473]
- Mickelson, K. A.; Jacobacci, K. E.; Contreras, T. A.; Biel, Alyssa; Slaughter, S. L., 2017, Landslide inventory, susceptibility, and exposure analysis of Pierce County, Washington: Washington Geological Survey Report of Investigation 39, 16 p. text, with 2 accompanying Esri file geodatabases and 1 Microsoft Excel file. [https://fortress.wa.gov/dnr/geologydata/publications/ger_ri39_pierce_county_landslide_inventory.zip]
- Min, Kyoungwon; Mundil, Roland; Renne, P. R.; Ludwig, K. R., 2000, A test for systematic errors in $^{40}\text{Ar}/^{39}\text{Ar}$ geochronology through comparison with U-Pb analysis of a 1.1-Ga rhyolite: *Geochimica et Cosmochimica Acta*, v. 64, no. 1, p. 73–98. [https://doi.org/10.1016/S0016-7037(99)00204-5]
- Miyashiro, Akiho, 1974, Volcanic rock series in island arcs and active continental margins: *American Journal of Science*, v. 274, no. 4, p. 321–355. [https://ajsonline.org/article/59682.pdf]
- Morelli, Carlo, editor, 1974, The International Gravity Standardization Net, 1971: International Association of Geodesy Special Publication no. 4, 194 p.
- Morrison, R. B., 1991, Introduction. In Morrison, R. B., editor, Quaternary nonglacial geology—Conterminous U.S.: Geological Society of America, Decade of North American Geology, The Geology of North America, v. K-2, p. 1–12. [https://doi.org/10.1130/DNAG-GNA-K2]
- Nelson, A. R.; Personius, S. F.; Sherrod, B. L.; Buck, Jason; Bradley, Lee-Ann; Henley, Gary, II; Liberty, L. M.; Kelsey, H. M.; Witter, R. C.; Koehler, R. D.; Schermer, E. R.; Nemser, E. S.; Cladouhos, T. T., 2008, Field and laboratory data from an earthquake history study of scarps in the hanging wall of the Tacoma Fault, Mason and Pierce Counties, Washington: U.S. Geological Survey Scientific Investigations Map 3060, 3 sheets, scale 1:30,000. [http://pubs.usgs.gov/sim/3060/]
- Noble, J. B.; Wallace, E. F., 1966, Geology and groundwater resources of Thurston County, Washington; Volume 2: Washington Division of Water Resources Water Supply Bulletin 10, v. 2, 141 p., 5 plates. [https://apps.ecology.wa.gov/publications/SummaryPages/WSB10b.html]
- Odum, J. K.; Stephenson, W. J.; Pratt, T. L.; Blakely, R. J., 2016, Shallow geophysical imaging of the Olympia anomaly: An enigmatic structure in the southern Puget Lowland, Washington State: *Geosphere*, v. 12, no. 5, p. 1617–1632. [https://doi.org/10.1130/GES01248.1]
- Paces, J. B.; Miller, J. D., Jr., 1993, Precise U-Pb ages of Duluth Complex and related mafic intrusions, northeastern Minnesota: Geochronological insights to physical, petrogenetic, paleomagnetic, and tectonomagmatic processes associated with the 1.1 Ga Midcontinent Rift System: *Journal of Geophysical Research Solid Earth*, v. 98, no. B8, p. 13,997–14,013. [https://doi.org/10.1029/93JB01159]
- Parker, B. L.; Goldstein, B. S.; Futornick, Z. O.; Pringle, P. T., 2008, Sedimentological evidence for an enriched glacial outburst flood in Thurston County, Washington [abstract]: *Geological Society of America Abstracts with Programs*, v. 40, no. 1, p. 70. [https://gsa.confex.com/gsa/2008CD/webprogram/Paper135405.html]
- Paton, Chad; Hellstrom, John; Paul, Bence; Woodhead, Jon; Hergt, Janet, 2011, Iolite: Freeware for the visualisation and processing of mass spectrometric data: *Journal of Analytical Atomic Spectrometry*, v. 26, p. 2508–2518. [https://doi.org/10.1039/C1JA10172B]
- Pease, M. H., Jr.; Hoover, Linn, Jr., 1957, Geology of the Doty-Minot Peak area, Washington: U.S. Geological Survey Oil and Gas Investigations Map 188, 1 sheet, scale 1:62,500. [https://ngmdb.usgs.gov/Prodesc/proddesc_5340.htm]
- Phillips, J. D.; Hansen, R. O.; Blakely, R. J., 2007, The use of curvature in potential-field interpretation: *Exploration Geophysics*, v. 38, no. 2, p. 111–119. [https://doi.org/10.1071/EG07014]
- Phillips, W. M.; Korosec, M. A.; Schasse, H. W.; Anderson, J. L.; Hagen, R. A., 1986, K-Ar ages of volcanic rocks in southwest Washington: Isochron/West, *Bulletin of Isotopic Geochronology*, v. 47, p. 18–24. [https://geoinfo.nmt.edu/publications/periodicals/isochronwest/47/iw_v47_p18.pdf]
- Phillips, W. M.; Walsh, T. J.; Hagen, R. A., 1989, Eocene transition from oceanic to arc volcanism, southwest Washington. In Muffler, L. J. P.; Weaver, C. S.; Blackwell, D. D., editors, Proceedings of workshop XLIV: Geological, geophysical, and tectonic setting of the Cascade Range: U.S. Geological Survey Open-File Report 89-178, p. 199–256. [https://doi.org/10.3133/ofr89178]
- Plouff, Donald, 2000, Field estimates of gravity terrain corrections and Y2K-compatible method to convert from gravity readings with multiple base stations to tide- and long-term drift-corrected observations: U.S. Geological Survey Open-File Report 2000-140, 35 p. [https://doi.org/10.3133/ofr00140]
- Polenz, Michael; Alldritt, Katelin; Hehemann, N. J.; Sarikhan, I. Y.; Logan, R. L., 2009, Geologic map of the Belfair 7.5-minute quadrangle, Mason, Kitsap, and Pierce Counties, Washington: Washington Division of Geology and Earth Resources Open File Report 2009-7, 1 sheet, scale 1:24,000. [https://www.dnr.wa.gov/publications/ger_ofr2009-7_geol_map_belfair_24k.pdf]

- Polenz, Michael; Petro, G. T.; Contreras, T. A.; Stone, K. A.; Legorreta Paulín, Gabriel; Cakir, Recep, 2013, Geologic map of the Seabeck and Poulsbo 7.5-minute quadrangles, Kitsap and Jefferson Counties, Washington: Washington Division of Geology and Earth Resources Map Series 2013-02, 1 sheet, scale 1:24,000, 39 p. text. [https://www.dnr.wa.gov/publications/ger_ms2013-02_geol_map_seabeck-poulsbo_24k.zip]
- Polenz, Michael; Favia, J. G.; Hubert, I. J.; Legorreta Paulín, Gabriel; Cakir, Recep, 2015, Geologic map of the Port Ludlow and southern half of the Hansville 7.5-minute quadrangles, Kitsap and Jefferson Counties, Washington: Washington Division of Geology and Earth Resources Map Series 2015-02, 1 sheet, scale 1:24,000, 40 p. text. [https://www.dnr.wa.gov/publications/ger_ms2015-02_geol_map_port_ludlow_hansville_24k.zip]
- Polenz, Michael; Allen, M. D.; Legorreta Paulín, Gabriel; Eungard, D. W.; Cakir, Recep; Scott, S. P.; Mahan, S. A., 2016, Geologic map of the Shelton Valley 7.5-minute quadrangle, Mason County, Washington: Washington Division of Geology and Earth Resources Map Series 2016-02, 1 sheet, scale 1:24,000, 45 p. text. [https://www.dnr.wa.gov/publications/ger_ms2016-02_geol_map_shelton_valley_24k.zip]
- Polenz, Michael; Vermeer, J. L.; Legorreta Paulín, Gabriel; Tepper, J. H.; Mahan, S. A.; Cakir, Recep, 2017, Geologic map of the Littlerock 7.5-minute quadrangle, Thurston County, Washington: Washington Geological Survey Map Series 2017-01, 1 sheet, scale 1:24,000, 36 p. text. [https://www.dnr.wa.gov/publications/ger_ms2017-01_geol_map_littlerock_24k.zip]
- Polenz, Michael; Ostrom, B. A.; Lau, T. R.; Sadowski, A. J.; Blanks-Bennett, A. L.; Cakir, Recep; Tepper, J. H.; Legorreta Paulín, Gabriel; Nesbitt, Elizabeth; DuFrane, S. A., 2018, Geologic map of the Violet Prairie 7.5-minute quadrangle, Thurston and Lewis Counties, Washington: Washington Geological Survey Map Series 2018-04, 1 sheet, scale 1:24,000, 41 p. text. [https://www.dnr.wa.gov/publications/ger_ms2018-04_geol_map_violet_prairie_24k.zip]
- Polenz, Michael; Toth, C. H.; Samson, Catherine; Sadowski, A. J.; Becerra, R. I.; Lau, T. R.; Anderson, M. L.; Nesbitt, E. A.; Tepper, J. H.; DuFrane, S. A.; Legorreta Paulín, Gabriel, 2019, Geologic map of the Rochester 7.5-minute quadrangle, Thurston and Lewis Counties, Washington: Washington Geological Survey Map Series 2019-02, 1 sheet, scale 1:24,000. [https://www.dnr.wa.gov/publications/ger_ms2019-02_geol_map_rochester_24k.zip]
- Polenz, Michael; Samson, Catherine; Reedy, Tabor; von Dassow, Wesley; Duckworth, C. W.; Lau, T. R.; Anderson, M. L.; Nesbitt, E. A.; Tepper, J. H.; DuFrane, S. A.; Legorreta Paulín, Gabriel, 2020, Geologic map of the Oakville and Rainbow Falls 7.5-minute quadrangles, Lewis, Thurston, and Grays Harbor Counties, Washington: Washington Geological Survey Map Series 2020-02, 1 sheet, scale 1:24,000, 19 p. text. [https://www.dnr.wa.gov/publications/ger_ms2020-02_geol_map_oakville_rainbow_falls_24k.zip]
- Polenz, Michael; Hladky, F. R.; Anderson, M. L.; Tepper, J. H.; Horst, A. E.; Miggins, D. P.; Legorreta Paulín, Gabriel, 2021, Geologic map of the Tenalquot Prairie and northern two-thirds of the Vail 7.5-minute quadrangles, Thurston and Pierce Counties, Washington: Washington Geological Survey Map Series 2021-02, 1 sheet, scale 1:24,000, 47 p. text. [https://www.dnr.wa.gov/publications/ger_ms2021-02_geol_map_tenalquot_prairie_northern_vail_24k.zip]
- Polenz, Michael; Hladky, F. R.; Anderson, M. L.; Alexander, K. A.; Tepper, J. H.; Miggins, D. P.; Legorreta Paulín, Gabriel, 2022, Geologic map of the McKenna and northern half of the Lake Lawrence 7.5-minute quadrangles, Thurston and Pierce Counties, Washington: Washington Geological Survey Map Series 2022-06, 1 sheet, scale 1:24,000, 35 p. text. [https://www.dnr.wa.gov/publications/ger_ms2022-06_geol_map_mckenna_northern_lake_lawrence_24k.zip]
- Polenz, Michael; Hladky, F. R.; Bauer, A. L.; Lau, T. R.; Tepper, J. H.; Nesbitt, E. A.; Legorreta Paulín, Gabriel, 2023, Geologic map of the Bald Hill 7.5-minute quadrangle, Thurston, Pierce, and Lewis Counties, Washington: Washington Geological Survey Map Series 2023-03, 1 sheet, scale 1:24,000, with 37 p. text. [https://www.dnr.wa.gov/publications/ger_ms2023-03_geol_map_bald_hill_24k.zip]
- Pratt, T. L.; Johnson, S. Y.; Potter, C. J.; Stephenson, W. J.; Finn, C. A., 1997, Seismic reflection images beneath Puget Sound, western Washington State: The Puget Lowland thrust sheet hypothesis: *Journal of Geophysical Research Solid Earth*, v. 102, no. B12, p. 27,469–27,489. [https://doi.org/10.1029/97JB01830]
- Pringle, P. T., 1990, The Nisqually landslide of September 1990: *Washington Geologic Newsletter*, v. 18, no. 4, p. 28–31. [https://www.dnr.wa.gov/Publications/ger_washington_geology_1990_v18_no4.pdf]
- Pringle, P. T.; Goldstein, B. S., 2002, Deposits, erosional features, and flow characteristics of the late-glacial Tanwax Creek–Ohop Creek Valley flood—A likely source for sediments composing the Mima Mounds, Puget Lowland, Washington [abstract]: *Geological Society of America Abstracts with Programs*, v. 34, no. 5, p. A-89. [https://gsa.confex.com/gsa/2002CD/webprogram/Paper35127.html]
- Pringle, P. T.; Goldstein, B. S.; Anderson, N. R., 2000, Tanwax Creek–Ohop Valley late-glacial flood—Evidence that discharge from an ice-dammed lake in the Carbon River Valley was augmented by a temporary landslide dam, Puget Lowland, Washington [abstract]. *In* Washington Department of Ecology; Washington Hydrologic Society; U.S. Geological Survey, Program and abstracts from the 3rd symposium on the hydrogeology of Washington State: Washington Department of Ecology, p. 85, Call Number: TD224 W2 W317h 2000
- Sadowski, A. J.; Keller, W. E.; Polenz, Michael; Lau, T. R.; Cakir, Recep; Nesbitt, Elizabeth; Tepper, J. H.; DuFrane, S. A.; Legorreta Paulín, Gabriel, 2018, Geologic map of the Centralia 7.5-minute quadrangle, Lewis County, Washington: Washington Geological Survey Map Series 2018-05, 1 sheet, scale 1:24,000, 43 p. text. [https://www.dnr.wa.gov/publications/ger_ms2018-05_geol_map_centralia_24k.zip]
- Sadowski, A. J.; Becerra, R. I.; Toth, C. H.; Polenz, Michael; Anderson, M. L.; Lau, T. R.; Nesbitt, E. A.; Tepper, J. H.; DuFrane, S. A., 2019, Geologic map of the Adna 7.5-minute quadrangle, Lewis County, Washington: Washington Geological Survey Map Series 2019-01, 1 sheet, scale 1:24,000. [https://www.dnr.wa.gov/publications/ger_ms2019-01_geol_map_adna_24k.zip]
- Savage, W. Z.; Morrissey, M. M.; Baum, R. L., 2000, Geotechnical properties for landslide-prone Seattle area glacial deposits: U.S. Geological Survey Open-File Report 2000-228, 5 p. [https://doi.org/10.3133/ofr00228]
- Schasse, H. W., compiler, 1987a, Geologic map of the Centralia quadrangle, Washington: Washington Division of Geology and Earth Resources Open File Report 87-11, 28 p., 1 plate, scale 1:100,000. [https://www.dnr.wa.gov/publications/ger_ofr87-11_geol_map_centralia_100k.zip]
- Schasse, Henry W., compiler, 1987b, Geologic map of the Mount Rainier quadrangle, Washington: Washington Division of Geology and Earth Resources Open File Report 87-16, 43 p., 1 plate, scale 1:100,000. [https://www.dnr.wa.gov/publications/ger_ofr87-16_geol_map_mountrainier_100k.zip]
- Sherrod, B. L., 2001, Evidence for earthquake-induced subsidence about 1100 yr ago in coastal marshes of southern Puget Sound, Washington: *Geological Society of America Bulletin*, v. 113, no. 10, p. 1299–1311. [https://doi.org/10.1130/0016-7606(2001)113%3C1299:EFEISA%3E2.0.CO;2]

- Sláma, Jiří; Košler, Jan; Condon, D. J.; Crowley, J. L.; Gerdes, Axel; Hanchar, J. M.; Horstwood, M. S. A.; Morris, G. A.; Nasdala, Lutz; Norberg, Nicholas; Schaltegger, Urs; Schoene, Blair; Tubrett, M. N.; Whitehouse, M. J., 2008, Plešovice zircon—A new natural reference material for U-Pb and Hf isotopic microanalysis: *Chemical Geology*, v. 249, no. 1–2, p. 1–35. [https://doi.org/10.1016/j.chemgeo.2007.11.005]
- Snively, P. D., Jr.; Brown, R. D., Jr.; Roberts, A. E.; Rau, W. W.; Schopf, J. M., 1958, *Geology and coal resources of the Centralia-Chehalis district*, Washington: U.S. Geological Survey Bulletin 1053, 159 p., 7 plates. [https://doi.org/10.3133/b1053]
- Snively, P. D., Jr.; Rau, W. W.; Hoover, Linn, Jr.; Roberts, A. E., 1959, McIntosh Formation, Centralia-Chehalis coal district, Washington. *In* Washington Division of Mines and Geology, Tertiary stratigraphic papers, southwestern Washington: Washington Division of Mines and Geology Reprint 3, 10 p. [https://www.dnr.wa.gov/publications/ger_reprint3_strat_papers_sw_wa.pdf]
- Snively, P. D., Jr.; Roberts, A. E.; Hoover, Linn, Jr.; Pease, M. H., Jr., 1951, *Geology of the eastern part of the Centralia-Chehalis coal district*, Lewis and Thurston Counties, Washington: U.S. Geological Survey Coal Map 8, 2 sheets, scale 1:31,680. [https://doi.org/10.3133/coal8]
- Stanley, W. D.; Johnson, S. Y.; Nuccio, V. F., 1994, Analysis of deep seismic reflection and other data from the southern Washington Cascades: U.S. Geological Survey Open-File Report 94-159, 179 p. [https://doi.org/10.3133/ofr94159]
- Stanley, W. D.; Johnson, S. Y.; Qamar, A. I.; Weaver, C. S.; Williams, J. M., 1996, Tectonics and seismicity of the southern Washington Cascade Range: *Bulletin of the Seismological Society of America*, v. 86, no. 1A, p. 1–18. [https://doi.org/10.1785/BSSA08601A0001]
- Steiger, R. H.; Jäger, Emilie, 1977, Subcommission on geochronology: Convention on the use of decay constant in geo- and cosmochronology: *Earth and Planetary Science Letters*, v. 36, no. 3, p. 359–362. [https://doi.org/10.1016/0012-821X(77)90060-7]
- Sun, S.; McDonough, W. F., 1989, Chemical and isotopic systematics of oceanic basalts: implications for mantle composition and processes: *Geological Society, London, Special Publications*, v. 42, no. 1, p. 313–345. [https://doi.org/10.1144/GSL.SP.1989.042.01.19]
- Swick, C. A., 1942, Pendulum gravity measurements and isostatic reductions: U.S. Coast and Geodetic Survey Special Publication 232, 82 p. [https://books.google.com/books?id=rHciAQAAIAAJ&ots=AwvqZWxbAD&lr=&pg=PA6#v=onepage&q&f=false]
- Tacoma-Pierce County Health Department, 2023, *Pierce County Water Quality* [webpage]: Tacoma-Pierce County Health Department. [accessed Mar. 16, 2023, at https://piercecowa.maps.arcgis.com/apps/webappviewer/index.html?id=ea09ff7335974c20b89590db2586bf84]
- Telford, W. M.; Geldart, L. P.; Sheriff, R. E., 1990, *Applied geophysics*, 2nd ed.: Cambridge University Press, 770 p. [https://books.google.com/books?hl=en&lr=&id=oRP5fZYjXMC&oi=fnd&pg=PR15&ots=CdXkOn0zje&sig=Dn85KlcXmJtC8N2O04KGg-hiTL#v=onepage&q&f=false]
- Troost, K. G., 2014, *Jokulhlaups from glacial Lake Puyallup*, Pierce County, Washington: Ice Age Floods Institute Puget Lobe Chapter Field Trip September 20, 2014, 38 p. [https://arks.princeton.edu/ark:/88435/dsp01pg15bh126]
- Troost, K. G., 2016, *Chronology, lithology and paleoenvironmental interpretation of the penultimate ice-sheet advance into the Puget Lowland*, Washington: University of Washington Doctor of Philosophy thesis, 239 p. [https://digital.lib.washington.edu/researchworks/handle/1773/38517]
- Troost, K. G.; Booth, D. B., 2008, *Geology of Seattle and the Seattle area*, Washington. *In* Baum, R. L.; Godt, J. W.; Highland, L. M., editors, *Landslides and engineering geology of the Seattle, Washington, area*: Geological Society of America Reviews in Engineering Geology, v. 20, p. 1–35. [https://doi.org/10.1130/2008.4020(01)]
- U.S. Geological Survey Geologic Names Committee, 2018, Divisions of geologic time—Major chronostratigraphic and geochronologic units: U.S. Geological Survey Fact Sheet 2018-3054, 2 p. [https://pubs.usgs.gov/fs/2018/3054/fs20183054.pdf]
- Van Wagoner, T. M.; Crosson, R. S.; Creager, K. C.; Medema, G. F.; Preston, L. A.; Symons, N. P.; Brocher, T. M., 2002, Crustal structure and relocated earthquakes in the Puget Lowland, Washington, from high-resolution seismic tomography: *Journal of Geophysical Research Solid Earth*, v. 107, no. B12. [https://doi.org/10.1029/2001JB000710]
- Walker, J. D.; Geissman, J. W., compilers, 2022, *Geologic time scale v. 6.0*: Geological Society of America, 1 p. [https://rock.geosociety.org/net/documents/gsa/timescale/timescl.pdf?v=2022]
- Walsh, T. J.; Korosec, M. A.; Phillips, W. M.; Logan, R. L.; Schasse, H. W., 1987, *Geologic map of Washington—Southwest quadrant*: Washington Division of Geology and Earth Resources Geologic Map GM-34, 2 sheets, scale 1:250,000, with 28 p. text. [http://www.dnr.wa.gov/publications/ger_gm34_geol_map_sw_wa_250k.pdf]
- Walsh, T. J.; Logan, R. L., 2005, *Geologic map of the East Olympia 7.5-minute quadrangle*, Thurston County, Washington: Washington Division of Geology and Earth Resources Geologic Map GM-56, 1 sheet, scale 1:24,000. [http://www.dnr.wa.gov/Publications/ger_gm56_geol_map_eastolympia_24k.pdf]
- Walters, K. L., 1965, Mashel Formation of southwestern Pierce County, Washington. *In* Cohee, G. V.; West, W. S., *Changes in stratigraphic nomenclature by the U.S. Geological Survey, 1964*: U.S. Geological Survey Bulletin 1224-A, p. 55–59. [https://doi.org/10.3133/b1224A]
- Walters, K. L.; Kimmel, G. E., 1968, Groundwater occurrence and stratigraphy of unconsolidated deposits, central Pierce County, Washington: Washington Department of Water Resources Water Supply Bulletin 22, 428 p., 3 plates. [https://fortress.wa.gov/ecy/publications/SummaryPages/WSB22.html]
- Washington Geological Survey, 2005, *Puget Lowlands 2005 project* [lidar data]: originally contracted by Clallam County, Washington Dept. of Natural Resources, and Washington State Dept. of Transportation. [accessed Apr. 16, 2023, at http://lidarportal.dnr.wa.gov]
- Washington Geological Survey, 2017, *Swwa Foothills 2017 project* [lidar data]: originally contracted by U.S. Geological Survey and Washington Dept. of Natural Resources. [accessed Apr. 16, 2023, at http://lidarportal.dnr.wa.gov]
- Washington Geological Survey, 2019, *Oil and gas wells—GIS data*: Washington Geological Survey Digital Data Series 21, version 3.4, previously released July 2016. [https://fortress.wa.gov/dnr/geologydata/publications/data_download/ger_portal_oil_gas.zip]
- Washington Geological Survey, 2020a, *Lewis East Sthelens 2020 project* [lidar data]: originally contracted by U.S. Forest Service. [accessed Apr. 16, 2023, at http://lidarportal.dnr.wa.gov]
- Washington Geological Survey, 2020b, *Pierce 2020 project* [lidar data]: originally contracted by Pierce County. [accessed Apr. 16, 2023, at http://lidarportal.dnr.wa.gov]
- Washington Geological Survey, 2022, *Thurston 2021 project* [lidar data]: originally contracted by Washington Dept. of Natural Resources. [accessed Apr. 16, 2023, at http://lidarportal.dnr.wa.gov]
- Washington Geological Survey, 2023, *Geophysics Database—GIS data*: Washington Geological Survey Digital Data Series 28, version 1.0, April 2023. [https://fortress.wa.gov/dnr/geologydata/publications/data_download/ger_portal_geophysics.zip]
- Weaver, C. E., 1912, A preliminary report on the Tertiary paleontology of western Washington: *Pacific Mining Journal*, v. 1, no. 5, p. 86–87.
- Weaver, C. E., 1937, *Tertiary stratigraphy of western Washington and northwestern Oregon*: University of Washington Publications in Geology, v. 4, 266 p. [http://babel.hathitrust.org/cgi/pt?id=ucl.b3666455;view=lup;seq=5]

- Wells, R. E.; McCaffrey, Robert, 2013, Steady rotation of the Cascade arc: *Geology*, v. 41, no. 9, p. 1027–1030. [<https://doi.org/10.1130/G34514.1>]
- Wells, Ray; Bukry, David; Friedman, Richard; Pyle, Doug; Duncan, Robert; Haeussler, Peter; Wooden, Joe, 2014, Geologic history of Siletzia, a large igneous province in the Oregon and Washington Coast Range: Correlation to the geomagnetic polarity time scale and implications for a long-lived Yellowstone hotspot: *Geosphere*, v. 10, no. 4, p. 692–719. [<https://doi.org/10.1130/GES01018.1>]
- Wiedenbeck, Michael; Allé, P.; Corfu, Fernando; Griffin, W. L.; Meier, Martin; Oberli, Felix; Von Quadt, Albrecht; Roddick, J. C.; Spiegel, W., 1995, Three natural zircon standards for U-Th-Pb, Lu-Hf, trace element and REE analyses: *Geostandards Newsletters*, v. 19, p. 1–23. [<https://doi.org/10.1111/j.1751-908X.1995.tb00147.x>]
- Williams, I. S., 1997, U-Th-Pb Geochronology by ion microprobe. *In* McKibben, M. A.; Shanks, W. C., III; Ridley, W. I., editors, *Applications of microanalytical techniques to understanding mineralizing processes: Reviews in Economic Geology*, v. 7, p. 1–35. [<https://doi.org/10.5382/Rev.07>]
- Willis, Bailey, 1898, Some coal fields of Puget Sound: U.S. Geological Survey Annual Report 18, Part 3, p. 393–436.
- Wilson, Marjorie, 1989, *Igneous petrogenesis: A global tectonic approach*: Unwin Hyman, 466 p. [<https://doi.org/10.1007/978-1-4020-6788-4>]
- Winter, John, 2010, *Principles of Igneous and Metamorphic Petrology*, 2nd Edition: Pearson, 720 p.

Appendix A. Geochronology

LUMINESCENCE DATING

Overview and Purpose

Luminescence dating estimates the time that has passed since sediment was deposited and buried. Following sediment deposition, environmental radiation causes electrons in minerals to jump into metastable, higher-energy electron traps. The technique assumes that this occurs at a predictable rate, such that older sediment contains proportionately more electrons in traps. The technique functions by measuring how much light electrons emit when released from traps. This is done by subjecting the sample to a pulse of activation energy that knocks the electrons out of their metastable traps; their return to a lower energy level emits light. The amount of light emitted is proportional to the time since deposition of the sample—meaning that more light is indicative of an older sample. OSL uses optical light to stimulate luminescence from quartz, while IRSL uses infrared light on K-feldspar. Exposure to daylight restores electrons from their energized states to more stable, lowest-energy states and resets the luminescence age to zero. Samples must therefore be collected by forcing an opaque collection tube into an outcrop and only analyzing the inner, totally dark part of the collected material.

Sample Collection and Preparation

We first removed at least 5 cm of sand from a sand exposure and then pounded a 4.2-cm inner diameter, 30.5-cm-long steel tube (1-5/8-inch diameter electrical conduit) into the in-place sand (preferably surrounded by least 30 cm of undisturbed sand on all sides). We retrieved the tube by digging out the surrounding material until we could remove and seal the tube without loss of sand from inside the tube. We sealed the sample tube with opaque metal foil (heater-duct tape) and rubber caps. We collected some of the surrounding host sand into a plastic zip-lock bag in case the lab needed a bulk dose rate measurement, and sand packed tightly into a completely filled, small, well-sealed glass or plastic vial (such as a 35-mm film canister) for a field moisture content assessment. The lab analyzed sand from the core of the tube, which had not been exposed to light during sampling.

Analytical Methods

Our sample was analyzed by Sebastien Huot (Illinois State Geological Survey), whose report (Data Supplement) describes the analytical methods.

Results

We collected and analyzed one sample of alluvial sand where the eastern map edge intersects a south-facing cliff along the shore of Alder Lake (GD11).

Table A1. Infrared-stimulated (IRSL) luminescence ages from the Eatonville 7.5-minute quadrangle. See Data Supplement for full analytical results.

Site ID	GD11	Luminescence age dates sand deposition 4 m below the top of a >6-m-thick fluvial section of sand (and some small pebble gravel) that is directly overlain by a 2–5-m-thick, compact diamicton that we field-interpreted as Mount Rainier-sourced lodgment till of the Hayden Creek Drift. We field-interpreted the fluvial section as low-energy channel deposits. It is unclear if sand deposition below the till was proglacial, and if so, what the distance from ice margin was. Sand is medium to pale gray, faintly greenish, weathers orange brown to pale yellow; compact; mostly fine-grained but poorly sorted, ranging from silt to coarse sand; rounded to angular, mostly subangular; mostly planar-bedded, ranging to cross bedded. Petrography suggests approximately 93% intermediate volcanic lithic fragments, 5% plagioclase, 1% pyroxene, and 1% quartz. The field setting is a southeast-facing cliff above the Alder Lake shore. We suspect shore erosion developed the cliff after Alder Dam was constructed in 1944. Sampled 8/2/2023, by M. Polenz, C. Lambert, and Lowell Dickson (DNR).
Field sample ID	EVm051b	
Map unit	Qpcph	
TRS location	Sec. 24, T15N R4E	
Latitude (degrees)	46.77586	
Longitude (degrees)	-122.25061	
Elevation (ft)	1,210	
Age (ka) ±2σ		105 ±242

U-PB DATING

Overview

U-Pb dating uses radioactive decay of uranium (multiple isotopes) to lead (also multiple isotopes) to estimate the crystallization age of uranium-bearing minerals. We sample rocks or sediment to assess the crystallization ages of zircons within the deposit, and thereby estimate the igneous rock crystallization age, or constrain the maximum possible age of sediment deposition; meaning that any sediment deposit must be younger than the zircons within it.

More than 100 zircons are usually analyzed from one sample of sediment or sedimentary rock; volcanic deposits may be analyzed with fewer zircons because most or all zircons are expected to have formed from the same magma body and therefore be of similar age. Each zircon yields a separate, individual crystal age. Because zircons of different ages within a detrital sample can have different geologic (and geographic) sources, inferences on sedimentary provenance can sometimes also be made from consideration of zircon age spectra in the context of other geologic constraints.

Sample Collection and Preparation

We generally collect about 2–10 kg of freshly exposed rock per sample, while avoiding contact with soil or other surface deposits that could introduce extraneous zircons; weathering and alteration do not usually affect the age of zircon and therefore pose no concern for this technique. We send our samples to ZirChron, LLC, for mineral separation using the following procedure:

Samples are pressure washed with water and then disaggregated using an Electro Pulse Disaggregator (EPD, Marx generator) at 1 Hz with discharges of ~250 kV for 15 minutes. Any clasts >500 µm are crushed in a crusher or pulverizer. Using stainless steel sieves, the fraction between 350 µm and 25 µm is retained and then processed using the Wilfley water table, Frantz paramagnetic separator, and a two-step (3.00 g/cm³ and 3.32 g/cm³) heavy liquid methylene iodide separation. Zircon grains from each sample are hand selected and mounted in epoxy, polished to expose the grain centers, and regions suitable for analysis are identified from optical imaging.

U-Pb Analytical Methods

The following text is reproduced from a technical writeup by the Washington State University Radiogenic Isotope and Geochronology Laboratory (RIGL) with minimal modification:

Zircon U-Pb ages are measured at the Radiogenic Isotope and Geochronology Lab (RIGL) at Washington State University using an Analyte G2 193 excimer laser ablation system coupled with a Thermo-Finnigan Element 2 single-collector inductively coupled plasma mass spectrometer. The laser parameters are 25-µm-diameter spot size, 10 Hz repetition rate, and fluence of ~5.0 J/cm². For the U-Pb measurement, we mostly followed the method of Chang and others (2006) and Gaschnig and others (2010), except for the use of a 193-nm laser system. A 10-second blank measurement of the He and Ar carrier gasses (laser off) before each analysis is followed by 250 scans across masses ²⁰²Hg, ²⁰⁴Pb+Hg, ²⁰⁶Pb, ²⁰⁷Pb, ²⁰⁸Pb, ²³²Th, ²³⁵U, and ²³⁸U during ~30-second laser ablation periods. Analyses of zircon unknowns, standards, and quality control zircon grains are interspersed with analyses of external calibration standards, typically with 10–12 unknowns bracketed by multiple analyses of two different zircon standards (Plešovice and FC-1). The Plešovice standard (337 Ma; Sláma and others, 2008) is used to calibrate the ²⁰⁶Pb/²³⁸U and ²⁰⁷Pb/²³⁵U ages, and the FC-1 standard (1,099 Ma; Paces and Miller, 1993) is used for calibration of ²⁰⁷Pb/²⁰⁶Pb ages owing to its high count rate for ²⁰⁷Pb (~2–4 times higher than that of Plešovice). Zircon 91500 (1,065 Ma; Wiedenbeck and others, 1995), Fish Canyon Tuff (~27.5 Ma; Lanphere and Baadsgaard, 2001), and Temora2 (417 Ma; Black and others, 2004) are used as quality control standards. Data are processed offline using the Iolite software (Paton and others, 2011). Common Pb correction is performed using the ²⁰⁷Pb method (Williams, 1997).

Results

We collected and analyzed six samples (age sites GD2–GD5, GD7, GD8). GD2 and GD3 are detrital zircon analyses from sediment in or near the Mashel Formation type section (unit **RMC_m**). The other four samples are volcanic rocks from the Eocene Northcraft Formation (units **Evt_n** and **Eli_n**). All ages are computed by the Washington State University Radiogenic Isotope and Geochronology Laboratory (RIGL) using the TuffZirc algorithm (Ludwig, 2003).

INTERPRETING OUR REPORTED AGES

Table A2 presents a single age statement for each sample. Readers should understand that this provides our interpretation of the best approach for the lab-reported age spectrum from that particular sample and its geologic context—but other interpretations are possible and can rarely be dismissed as wrong. Because the lab generates separate, individual ages for multiple crystals from each sample (Data Supplement), in order to report a single age statement, we necessarily pick and choose or synthesize. For instance, we can argue that, because all crystals formed before their source magma or lava was fully cooled, the single youngest crystal age should be reported. Alternatively we can argue that any individual crystal analysis may be inaccurate, and a single age statement should therefore be statistically developed from the different ages of multiple crystals (this is what the TuffZirc algorithm does.)

Table A2 therefore specifies when a reported age was computed using an algorithm such as TuffZirc—and may additionally note the youngest age reported by the lab for a single crystal.

AGES FROM DETRITAL SAMPLES

TuffZirc was developed to produce statistically robust age statements for zircon populations from igneous rocks—where all crystals formed more or less simultaneously while the melt cooled. In contrast, detrital samples usually incorporate crystals from multiple igneous events of different ages. Detrital age populations usually include “peaks” (clusters of similar ages), and some peaks may be from individual igneous events, but detrital peaks may also include ages from other events. Reliance on an age computed by an algorithm such as TuffZirc is therefore conceptually less robust in detrital samples than it is for igneous samples. When our interest is the age of the sampled deposit, detrital spectra therefore offer a stronger argument for accepting as most insightful the single youngest lab-reported crystal age (as opposed to an algorithm-generated peak age). In addition, even if the single youngest crystal age in a detrital spectrum is much younger than the youngest peak in the same spectrum, the deposit may still be much younger than the youngest crystal. The geologic interpretation of lab-reported U-Pb age populations, especially in detrital samples, is therefore quite separate from acceptance of the validity of the lab-reported analytical results. To honor that distinction, Table A2 reports our preferred interpretation of the age(s) implied by the lab-reported analytical results. In contrast, Table 1 reports what we think that age means for our geologic context—which is why detrital ages are reported as “# ±#” in Table A2 but as “<# ±#” in Table 1. In other words, detrital deposits are younger than the igneous crystals within them.

Table A2. $^{238}\text{U}/^{206}\text{Pb}$ ages of zircons from the Eatonville 7.5-minute quadrangle. See Data Supplement for full analytical results.

Site ID	GD2	Maximum depositional age computed using TuffZirc from a coherent group of 5 detrital zircon ages at the young end of a spectrum of 110 zircon ages. The youngest single grain (excluded by TuffZirc) yielded a 5.2 ± 0.3 Ma age. Lab: V. Valencia, Zirchron + RIGL. Sampled from sand in Mashel Formation type section along road cut above former Weyerhaeuser road, approximate elevation 650 ft—about 40 ft (12 m) below the top of the type section. Sampled 8/8/2023 by C. Lambert and M. Polenz.
Field sample ID	EVm099	
Map unit	RMC _m	
TRS location	Sec. 20, T16N R04E	
Latitude (degrees)	46.85134	
Longitude (degrees)	-122.33404	
Elevation (ft)	650	
Age (Ma) $\pm 2\sigma$		6.1 +0.2/-0.3
Site ID	GD3	Maximum depositional age computed using TuffZirc from a coherent group of 35 detrital zircon ages at the young end of a spectrum of 107 zircon ages. The youngest single grain (excluded by TuffZirc) yielded a 5.3 ± 0.7 Ma age. Lab: V. Valencia, Zirchron + RIGL. Sampled from northwestern channel edge of Mashel River about 260 m downvalley (south) of where a now-washed-out Weyerhaeuser road once marked the base of the Mashel Formation type section. Elevation about 495 ft—approximately 0–5 m downsection of the type section base. Sampled 8/8/2023 by C. Lambert and M. Polenz.
Field sample ID	EVm092	
Map unit	RMC _m	
TRS location	Sec. 29, T16N R04E	
Latitude (degrees)	46.84600	
Longitude (degrees)	-122.33230	
Elevation (ft)	495	
Age (Ma) $\pm 2\sigma$		6.0 +0.1/-0.2
Site ID	GD4	Zircon crystallization age computed using TuffZirc from a coherent group of 34 zircon ages in a single-peak spectrum of 50 zircon ages from rhyolite tuff. The youngest single grain (excluded by TuffZirc) yielded a 35.7 ± 1.2 Ma age. Lab: V. Valencia, Zirchron + RIGL. Sampled from a forest road cut 1.2 km west-southwest of Hugo Peak. Sampled 10/31/2023 by C. Lambert and M. Polenz.
Field sample ID	EVm353	
Map unit	Evt _n	
TRS location	Sec. 28, T16N R04E	
Latitude (degrees)	46.83530	
Longitude (degrees)	-122.31042	
Elevation (ft)	1195	
Age (Ma) $\pm 2\sigma$		37.5 ± 0.5

Table A2 continued.

Site ID	GD7	Zircon crystallization age computed using TuffZirc from a coherent group of 36 zircon ages in a single-peak spectrum of 46 zircon ages from rhyolite tuff. The youngest single grain (excluded by TuffZirc) yielded a 35.7 ± 0.7 Ma age. Lab: V. Valencia, Zirchron + RIGL. Sampled from an SR7 road cut near the east end of Alder Lake. Sampled 11/8/2023 by A. Bauer and T. Lau.
Field sample ID	EVm148	
Map unit	Evt _n	
TRS location	Sec. 10, T15N R04E	
Latitude (degrees)	46.80027	
Longitude (degrees)	-122.27799	
Elevation (ft)	1220	
Age (Ma) $\pm 2\sigma$		37.4 ± 0.5

Site ID	GD8	Zircon crystallization age computed using TuffZirc from a coherent group of 33 zircon ages in a spectrum of 42 zircon ages from pyroxene tonalite. The youngest single grain (excluded by TuffZirc) yielded a 35.6 ± 0.8 Ma age. Lab: V. Valencia, Zirchron + RIGL. Sampled from a dormant quarry about 1 km west of Alder Lake. Sampled by Michael Polenz 8/31/2023.
Field sample ID	EVm194	
Map unit	Ei _n	
TRS location	Sec. 17, T15N R04E	
Latitude (degrees)	46.79143	
Longitude (degrees)	-122.32986	
Elevation (ft)	1320	
Age (Ma) $\pm 2\sigma$		36.9 ± 0.5

Site ID	GD5	Zircon crystallization age computed using TuffZirc from a coherent group of 53 zircon ages in a single-peak spectrum of 58 zircon ages from rhyolite tuff. The youngest single grain (excluded by TuffZirc) yielded a 35.6 ± 1.3 Ma age. Lab: V. Valencia, Zirchron + RIGL. Sampled from an SR7 road cut 1.7 km southwest of Hugo Peak. Sampled 10/31/2023 by C. Lambert and M. Polenz.
Field sample ID	EVm258	
Map unit	Evt _n	
TRS location	Sec. 33, T16N R04E	
Latitude (degrees)	46.83206	
Longitude (degrees)	-122.30892	
Elevation (ft)	1085	
Age (Ma) $\pm 2\sigma$		37.9 ± 0.5

⁴⁰AR/³⁹AR DATING

Overview

Argon dating uses the radioactive decay of ⁴⁰K to ⁴⁰Ar to determine the age of potassium-bearing minerals and materials. We used argon dating to estimate the crystallization ages of the groundmass or crystallization ages of selected crystal fractions (such as plagioclase) in igneous rocks.

Sample Collection and Preparation

Samples for argon dating were collected from in-place volcanic or volcanoclastic rock. We prioritized relatively unweathered rock with few fractures, though such exposures are not abundant in the map area. Blocks of the outcrop were broken into smaller pieces to remove weathering rinds. We then placed about 1–3 kg of rock into a bag. Candidate sample sites were ranked based on many factors, including stratigraphic location, rock type, the desire for spatial coverage, and budgetary constraints. For analysis, we selected the freshest pieces and sent 1–2 kg of material to the lab.

Analytical Methods

The following section of text is reproduced from an analytical report provided by the Oregon State University Argon Geochronology Laboratory, with minimal modification:

Samples were crushed, sieved, washed, and dried using standard mineral separation techniques. Groundmass splits were obtained for the sample, rinsed with cold water, then dried in a drying oven at 55 °C. Once the samples were dried, they were sieved

Site ID	GD1	Age (Ma) ±2σ	Age type	Material	% total ³⁹ Ar included in age	Heating steps included in age	MSWD
Field sample ID	EVm022	34.59 ±0.19	mini-plateau	groundmass	17	9	2.49
Lab ID	24G01371	Mini-plateau age on porphyritic andesite groundmass dates eruption of lava. Error is internal; full external error ±1.80 m.y.; analytical error ±0.13 m.y. Lab: Dan Miggins (Oregon State University). Sampled in backyard of Eatonville Public Library. Sampled 7/31/2023 by C. Lambert and M. Polenz.					
Geochemical classification	Andesite						
Map unit	Eva _n						
TRS location	Sec. 14, T16N R04E						
Latitude (degrees)	46.86675						
Longitude (degrees)	-122.26909						
Elevation (ft)	820						

Appendix B. Geochemistry

OVERVIEW

We use major- and trace-element analyses to classify igneous rocks in the map area and to aid in their identification and correlation. Our 50 samples span a range of rock types from Eocene to Pliocene volcanism.

SAMPLE COLLECTION AND PREPARATION

We select samples for geochemical analysis from intrusive, volcanic, and volcanoclastic rocks. We use hammers, usually a small sledgehammer, to break off the freshest pieces. Where we are concerned about possible contamination from hammer streaks, we try to remove those, usually by using fragments of the same sample to scrape or break off any streaks. We generally submit between ~100 and ~200 g of the freshest available material for lab analysis, except where sample sizes are necessarily smaller, for example, among smaller pumice clasts.

ANALYTICAL METHODS

We reproduce the following abbreviated methods directly from documents provided by the ALS Geochemistry Laboratory in Vancouver, British Columbia; only general descriptions of methods are provided by ALS on their website:

Major element percentages are determined on a fused bead after acid digestion using Inductively Coupled Plasma-Atomic Emission Spectroscopy (ICP-AES) (ALS analysis code ME_ICP06). A prepared sample (0.1 g) is added to lithium metaborate/lithium tetraborate flux, mixed well, and fused in a furnace at 1,025°C. The resulting melt is then cooled and dissolved in an acid mixture containing nitric, hydrochloric, and hydrofluoric acids. This solution is then analyzed by ICP-AES. Results are corrected for spectral inter-element interferences.

Loss on Ignition (LOI) (ALS analysis code OA_GRA05) is determined using a 1 g sample, placed in an oven at 1,000°C for one hour, cooled, and then weighed again. The percent loss on ignition is calculated from the difference in weight before and after ignition.

Trace element concentrations are determined using Inductively Coupled Plasma-Mass Spectroscopy (ICP-MS) (ALS analysis code ME_MS81). Samples are prepared following the same lithium borate fusion and digestion procedure as applied in ICP-AES analyses, but are subjected to an additional lithium borate fusion and an acid digestion procedure prior to analysis on the ICP-MS.

RESULTS

We obtained results for 50 samples. Sample locations are shown on the Map Sheet (geochemistry sites G#s); analytical data are in the Data Supplement. These data, along with those similarly presented west of Eatonville by Polenz and others (2021, 2022, 2023) are the basis for our in-text statements and figures about geochemical content of our samples.

Appendix C. Geophysics

OVERVIEW AND PURPOSE

Lateral changes in isostatic gravity across a region result from density changes within rocks of the mid to upper crust. Gridding gravity measurements creates a map that outlines areas of high gravity and low gravity. Areas of high gravity indicate that high-density rocks (for example, many igneous and metamorphic rocks) are closer to the surface. Areas of low gravity indicate that less-dense material is near the surface, such as sediment within a basin. Gravity surveys are especially useful in delineating steeply dipping contacts between two rock bodies that have a large contrast in density. Gravity data, combined with measured rock densities, allow us to quantitatively test models of subsurface geology against our observations.

DESCRIPTION OF METHODS

Field methods and sampled locations

Measurements from 224 new gravity stations were collected using a Scintrex CG-6 meter (Serial # 19050174), and a LaCoste and Romberg G908 gravimeter and combined with measurements from Finn and others (1991), PACES (now defunct; data obtained from B. Drenth, U. S. Geological Survey, written commun., 2020), Contreras and others (2023), Polenz and others (2021, 2022, 2023), and Alex Steely, WGS, written commun., 2021). We established a new base station ‘EATV’ with ties to ‘OLYK’ (Polenz and others 2021, 2022, 2023) and Enumclaw ‘ECLW’ (Washington Geological Survey, 2023) to tie our data to the U.S. gravity network.

Gravity station spacing at roughly 2 km generates a basic grid over a large area. Where known structures exist or initial gravity data collection showed a significant gradient, station spacing is reduced to 1 km to provide greater resolution. Sixty seven new bedrock density samples and 509 new magnetic susceptibility measurements collected from exposed bedrock help to constrain our geophysical models.

Data reduction and processing

A Javad Triumph-2 differential GPS unit provided the horizontal and vertical position of each station. Proprietary Javad Justin software allows us to carefully edit data and post-process for differential correction using the National Oceanic and Atmospheric Administration and the National Geodetic Survey’s Continuously Operating Reference Stations (CORS) within 70 km of the study area. After processing, typical positional accuracy is 0.15 m in the vertical and horizontal. Suspect GPS elevations were replaced with lidar data where those appear to be good. We apply the gravimeter’s factory calibration constants to each gravity observation, augmented by correction factors obtained from the Mount Hamilton calibration loop east of San Jose, CA (Barnes and others, 1969), and Earth tide corrections to produce observed gravity values. The data reference the International Gravity Standardization Net of 1971 (Morelli, 1974) and the reference ellipsoid is the Geodetic Reference System of 1967 (International Union of Geodesy and Geophysics, 1971). The observed drift between base stations is assumed to be linearly distributed to each station and results in a maximum gravity reading error of 0.05 mGal.

Gravity data reduction formulas for the free-air anomaly are standard (for example, Telford and others, 1990; Swick, 1942) and applying Bouguer, Earth curvature, and terrain corrections out to 166.7 km from each station produces a complete Bouguer anomaly. Terrain corrections are a combination of a field-based component (to a radius of 68 m using the Hayford system; Plouff, 2000) and a computer-generated component (using 30-m USGS DEM digital grids). To assist in the interpretation of mid- to upper-crustal density contrasts, the complete Bouguer anomaly is further reduced to an isostatic anomaly by applying formulas that adjust for long-wavelength variations, such as those caused by the existence of a crustal root and (or) upper-mantle density contrasts. An Airy-Heiskanen model (Heiskanen and Vening-Meinesz, 1958) produces the isostatic correction, assuming a 25-km-thick crust at sea level and a crust-mantle density contrast of 400 kg/m³. All parts of the data-reduction process assume a reduction density of 2,670 kg/m³. Gravity readings and computed anomalies are in the Data Supplement.

Uncertainties in the gravity data are predominantly due to uncertainty in vertical position and the terrain corrections. Elevation data in this study have average uncertainties of 0.15 m (but range to a maximum of 1.5 m). This results in an average uncertainty from elevation of 0.03 mGal, up to a maximum of 0.30 mGal. The uncertainty associated with terrain corrections is generally only 5–10 percent of the actual correction. This results in an average terrain-correction uncertainty of 0.08–0.15 mGal but varies according to topography. Average uncertainty in steep and hilly regions is 0.12–0.23 mGal, whereas average uncertainty in flatter areas is 0.05–0.1 mGal. Based on this, gravity anomalies of 0.5–1 mGal and greater reflect interpretable density variations in the upper crust.

The minimum-curvature algorithms in the GIS software package Geosoft Oasis Montaj® version 2023.1.1 transform our point isostatic anomaly data into gridded surfaces. The maximum horizontal gradient (referred to as ‘max-spots’), is calculated using the curvature analysis methodology of Phillips and others (2007). Lines along which max spots cluster quantitatively locate

strong and linear geophysical boundaries that we interpret as boundaries between rocks in the subsurface that have substantial density differences.

Hand Sample Densities

We collected bedrock samples throughout the study area for laboratory analysis. We weighed samples using an A&D company limited FX-3000i WP analytical balance. We combined three measurements per sample to determine density: a dry weight in air, a submerged (water-saturated) weight, and a water-saturated weight in air. We used the saturated bulk density in our modeling as it best reflects subsurface conditions.

GEOMAGNETICS

Overview and Purpose

Magnetic surveys map local changes in the Earth's magnetic field due to local magnetic sources at high resolution. This method delineates contacts between geologic units of contrasting magnetic properties, particularly in the mid- to upper crust. Collecting a large number of magnetic profiles helps to precisely determine magnetic contacts and trace them across a map area. Individual profiles, coupled with magnetic susceptibility measurements of surficial rocks, are powerful geophysical constraints for 2D subsurface modeling.

Description of Method

Aeromagnetic data used in this study were acquired in 1995, 2016, and 2023 (Blakely and others, 1999, 2020, 2024) via low-flying aircraft with a stinger-mounted magnetometer. For the 1995 survey, north-south flight lines were spaced 0.4 km apart with east-west tie lines spaced at 8 km. For the 2016 and 2022 surveys, east-west flight lines were spaced 0.4 km apart with north-south tie lines spaced at 4 km. Aeromagnetic measurements were interpolated to a projected, rectilinear grid using a bi-directional gridding algorithm within the GIS software package Geosoft Oasis Montaj®. We use a 'reduced-to-pole' filter (Blakely, 1995) to correct inclination and declination (such that Inclination = 0 deg, and Declination = 0 deg). This correction centers anomalies over their sources for more precise map-view interpretation.

Hand Sample and Model Unit Properties

In addition to the rock density measurements described above (see *Gravity*), we measured magnetic susceptibility of some outcrops and (or) hand samples, using a KT10 Kappa Meter. We did not measure magnetic remanence and relied on our magnetic susceptibility measurements for determining model unit properties. Weathering tends to replace denser minerals with less dense weathering products and turn magnetite into less magnetic minerals like hematite. Therefore, all our measured rock densities and susceptibilities can be considered minimum values. Results from our measurements are presented in the Data Supplement. Table C1 presents average values from combining our measurements with measurements from previous work, in order to base our geophysical interpretations on a larger, more robust dataset. Lab measurements are presented separately from outcrop measurements because the latter tend to better represent the in-place magnetic susceptibility. Model unit properties are largely determined from the compiled averages of our measured samples, and are constrained by measured minimum/maximum values and compared with published rock property values (Telford and others, 1990). For some model units we combine lithologies but still derive model properties from measured values. Unconsolidated model unit properties, including undifferentiated Quaternary and Mashel Formation and older sediments, are derived from previous WGS modeling in the region (Contreras and others, 2023, Polenz and others 2021, 2022; Telford and others, 1990; Savage and others, 2000; and unpublished WGS records).

Results

We display the results from the new rock samples in the data supplement and combined averages of existing measurements with the density and magnetic susceptibility measurements in Table C1.

Table C1. Combined averages of geophysical properties including saturated bulk density and magnetic susceptibility from rock samples and outcrops in the south Puget Sound area (Polenz and others 2019, 2020, 2021, 2022, 2023).

Sample Type	Magnetic susceptibility (10^{-3} SI)				Saturated bulk density (kg/m^3)			Lithology
	Average susceptibility from lab samples	# of lab samples	Average susceptibility from outcrop measurements	# of outcrop measurements	Maximum measured susceptibility	Average measured density	Maximum measured density	
Miocene and Oligocene volcanics	21.69	25	12.99	108	35.25	2430	2650	Intrusive rocks and lava flows
Northcraft—all units (Ev_n)	17.83	327	16.37	834	73.4	2500	2900	Igneous rocks
Northcraft volcanics (Ev _n)	12.29	70	11.4	186	39.1	2380	2660	Volcaniclastic rocks (including tuff)
Northcraft rhyolite tuff (E _{vt})	1.48	18	0.55	49	7.7	2420	2590	Felsic lava flows and tuff
Northcraft dacite (E _{vd})	14.31	26	20.53	39	34	2480	2610	Felsic lava flows
Northcraft basalt and basaltic andesite combined (E _{va})	20.53	162	19.12	470	73.4	2550	2810	Intermediate lava flows
Northcraft—intrusive (E _{in})	30.09	23	17.85	75	68.1	2580	2830	Intrusive rocks
Eocene sediments (En)	0.24	12	0.21	27	0.39	2420	2640	Sedimentary rocks
Mashel (R _{MC})	2.04	4	4.52	49	44.7	*	*	Sedimentary deposits

* We were unable to measure the saturated bulk density due to the unlithified samples disintegrating in water.

QUANTITATIVE CROSS-SECTION MODELING

Overview

Quantitative 2D forward modeling of cross sections constrained by potential-field data provides insight into the geometry of units and structures that go beyond qualitative interpretations of map-view data. This technique helps provide the best possible interpretations of structure types (for example normal, reverse, or strike-slip faults), fault or contact dips in the upper crust (for example steep or shallow), and offset across faults on units with particularly strong physical property contrasts with surrounding rocks. This method also can identify blind faults that have little surface expression and are difficult to capture via surface geology observations.

Description of Method

GM-SYS software (part of Geosoft Oasis Montaj®) provides a platform for computing the sum effect on both the gravitational and geomagnetic fields of the Earth from a given 2D cross section of the sub-surface. This is a forward-modeling method, meaning that the operator hypothesizes which rock types are in the subsurface along with their location and geometry, and the GM-SYS program predicts the total fields that result from that particular model. The operator's responsibility is to refine the hypothesis until the predicted potential-fields match the data measured in the field and lab. A good match is when the calculated gravity and magnetics from our model inputs are within (0–0.25 mGal and 10–15 nT) from the observed gravity and magnetics.

In addition to the gravity and aeromagnetic data, surface geology constrains the model's near-surface geometry, and laboratory measurements of density and magnetic properties of hand samples from the surface (see *Hand Sample and Model Unit Properties*) and from the Willhoite well (Washington Geological Survey, 2019; Contreras and others, 2023) provide additional rock property constraints. Also essential is the knowledge of the operator and collaborators in the project about the geologic history, expected stratigraphy in the subsurface, and structural geometries that are physically possible based on standard geologic mapping and cross-section construction techniques.

Sometimes multiple hypotheses of subsurface geometry fit the gravity and magnetic data within the accepted error for those two data types. Therefore, care in the construction of models, and testing various hypotheses, can help define which parts of the subsurface model are well constrained.

In general, potential-field data provide strong constraints on the position and dip of simple, steeply dipping boundaries between rocks with strong differences in physical properties. However, potential-field data provide very poor constraints on horizontal boundaries or boundaries between rocks with little contrast in physical properties. Depths of subhorizontal stratigraphic boundaries

within sedimentary rocks are particularly suspect and never well-constrained without the addition of good quality well or reflection-seismic data. Depths of subhorizontal boundaries between units of strongly contrasting properties are resolvable depending on uncertainties in the physical properties of those units. Where geophysical properties are uncertain, changing modeled density and (or) magnetism values of the juxtaposed rocks may change the depth of a boundary.

In our modeling approach, the length of our model section extends far beyond the ends of the model shown in this report. This avoids edge effects due to truncated subsurface volumes. We first construct an initial simplified model, including uniform packages of sediment, sedimentary rock, metamorphic rock, and volcanic rock to fit the long-wavelength features in the gravity and magnetic data. Typically, fitting the long-wavelength features constrains the depth, contact orientations, and structures of basement units, but may include other deeply buried units. We then iteratively add detail in the stratigraphy and decrease the size of blocks, particularly near the surface, to fit shorter wavelength anomalies. During each iteration, we test options for rock properties and geometries of boundaries that are compatible with surface geology observations and measured rock-property constraints. Once repeated iterations provide similar data fit (that is, additional model modifications no longer improve data fit), we conclude that we have converged on a model with a good fit to the data.

Appendix D. Landsat Spectral Image Analysis

OVERVIEW AND PURPOSE

We analyzed multispectral satellite images to add insights into our geologic mapping where field data were sparse, or to help us identify areas for additional field work. Our multispectral analysis uses pixel responses at multiple electromagnetic wavelengths to obtain information about the materials within each pixel. We use our field observations to identify multispectral signatures that correlate to particular rock or sediment types and then use these to identify areas where the spectral data suggest otherwise unrecognized types of rocks or sediment for which we may want to seek additional field observations, or to infer surface lithologic information and help identify map units and (or) locate geologic map unit boundaries where field data are sparse.

DESCRIPTION OF METHOD

We combined:

- 30-m-resolution multispectral imagery from the U.S. Geological Survey-operated Operational Land Imager (OLI) mounted to the Landsat 8 (NASA) satellite.
- 100-m-resolution Thermal Infrared Sensor (TIRS) imagery, also from the Landsat 8 (NASA) satellite.
- A 30-m-resolution digital elevation model (DEM) from the Japanese Advanced Spaceborne Thermal Emission and Reflection Radiometer (ASTER) remote sensing instrument mounted to the NASA-launched Terra satellite.

Landsat 8 provides geospatial imagery in 11 bands of data ranging from ultra blue (0.435–0.451 μm wavelengths) to Thermal 2 (11.50–12.51 μm wavelengths). We used Landsat 8 OLI images collected in 2015 (all bands except Panchromatic, Cirrus, and TIRS images). We combined the Landsat images with DEM data, which Brown and others (2007) found improves separability between “classes” that represent lithologic categories identified by our analysis of the geospatial image data. We used ASTER 30 m DEM data (version 2) because that grid resolution matches the 30 m resolution of the Landsat 8 image data, which simplifies our image processing. We used ENVI 5.3 image analysis software to visualize, process, and analyze this geospatial imagery, including postprocessing for radiometric and atmospheric correction (to clean up the diffusion and scattering of light in the spectral images), and image enhancement as described by Ali and others (2012).

In a process referred to as supervised classification, we used spectral signatures from 1:24,000-scale geologic mapping just west of the current map area (Polenz and others, 2023) to define groupings (classes) of spectral signatures such as bedrock, basalt, peat, sand, clay, and water—as described, for instance, by Kettles and others (2000). We did this using the Maximum Likelihood classification algorithm in ENVI, which calculates the probability that a given pixel belongs to a specific class by assuming that the statistics for each class in each band are normally distributed. We then used locations where we had field observations (training sites) to iteratively refine matches between spectral signatures and classes by redefining classes where needed, and by progressively subdividing classes that yielded varied spectral signatures and therefore lacked distinction relative to other categories, as described by Brown and others (2007). We processed the classified data into both images and polygons to provide flexibility in displaying the results. The images are visually messier but more nuanced whereas the polygons allow more display options, for instance by displaying only selected classes.

Results

We produced two analyses, one in which our classes attempted to identify lithologies, and a second in which they attempted to identify map units. Although the validity of the resulting classes and polygons seems mostly poor, we could observe some interesting and potentially useful patterns. For instance, a transition from the “lithologic” class “clay/volcanic/basalt” upslope to volcanic rocks (“basalt” and “andesite”) tends to approximate our alpine ice limit lines, which we based on relatively few alpine drift outcrops that establish lower bounds for the alpine ice limit. The correspondence is mostly within 100 ft elevation. However, the Vashon ice limit lacked a similar pattern, and the main takeaway is that in our densely vegetated western Washington map area, the geospatial classification data are no substitute for field mapping and should not be over-interpreted—as also suggested by analyses of less vegetated areas (for instance, Kettles and others, 2000; Brown and others, 2007). We used them to help target some of our field data collection and to inform other-wise poorly constrained decisions where field data are sparse.